# TRIBOLOGICAL STUDIES OF WATER-BASED MUD

# AND

# SELF-WELDING BEHAVIOUR

A Dissertation

by

YONG ZHENG

Submitted to the Office of Graduate and Professional Studies of
Texas A&M University
in partial fulfillment of the requirements for the degree of

DOCTOR OF PHILOSOPHY

| | |
|---|---|
| Chair of Committee, | Andreas A. Polycarpou |
| Committee Members, | M. Cynthia Hipwell |
| | Jonathan R. Felts |
| | Mohammad Naraghi |
| Head of Department, | Andreas A. Polycarpou |

May 2020

Major Subject: Mechanical Engineering

## ABSTRACT

Comprehensive evaluation on the influence of select commercial friction-modifying additives on the tribological performance of water-based mud will enable more widespread usage of water-based mud (WBM) with confidence as a replacement for conventional oil-based mud (OBM). OBM is well known for a wide range of concern-raising issues/disadvantages, for oil & gas exploration and production drilling activities, especially adverse environmental effects. During the drilling process, the drill bit and stationary pipe wall are in contact, and under certain conditions, may experience severe metal-on-metal friction and reach extremely high surface temperature within very short period of time due to excessive heat generation, which simultaneously expedites vaporization of drilling fluid leading to boundary or starved lubrication conditions. The high surface temperature combined with the high pressure inside the wellbore, together imposes a risk of seizure between the contacting parts, which, essentially is a form of self-welding/diffusing bonding due to element migration. Similarly, the extreme conditions under high-pressure and high-temperature (HPHT) in nuclear reactors also renders the mechanical system subject to this phenomenon. Whenever seizure or self-welding occurs, the whole system, for both drilling system and nuclear reactors, will be forced to experience overhaul due to system failure, as a result of paralyzed operability. This study is dedicated to a systematic investigation on the tribological performance improvement of WBM focused on its potential as a promising replacement for OBM with the aid of select commercial friction-modifying additives, and the tendency and behavior of self-welding between metallic components of drilling systems and nuclear reactors, respectively. Various state of the art instruments for material characterization were utilized to aid in understanding the underlying mechanisms of the phenomena observed and test data obtained. The test data shows that with the influence of certain additives, the tribological performance of WBMs

could be brought to a level where they are as good as, or even outperform conventional OBM for oil and gas drilling applications. Work on the self-welding behavior of nickel alloy shows that even in the absence of reducing (air) medium but only inert atmosphere, self-welding phenomenon does occur and could demonstrate significantly high bonding strength, which is of critical importance to the operability and reliability of nuclear reactors and other high-temperature applications.

## DEDICATION

*To my wife, Qingxia Wang, for her love, support, encouragement and sacrifice*

*To my daughters, Victoria and Charlotte, for coming to me as my angels*

*To my father and mother, Hanqiao Zheng and Meixian Chen, for their love, guidance, and support*

## ACKNOWLEDGEMENTS

I would like to thank my committee chair, Dr. Andreas A. Polycarpou, my committee members, Dr. M. Cynthia Hipwell, Dr. Jonathan R. Felts, and Dr. Mohammad Naraghi, for their guidance and support throughout the course of this research.

I also would like to thank Dr. Ahmad Amiri, for his expertise, guidance and advice on the chemical characterization and analysis.

Thanks also go to my friends and colleagues and the department faculty and staff for making my time at Texas A&M University a great, valuable and unforgettable experience.

Finally, thanks to my mother and father for their endless love, and to my wife Qingxia Wang for her love, support and sacrifice.

## CONTRIBUTORS AND FUNDING SOURCES

### Contributors

This work was supervised by a dissertation committee consisting of Professor Andreas A. Polycarpou, Professor M. Cynthia Hipwell, and Professor Jonathan R. Felts of the Department of Mechanical Engineering and Professor Mohammad Naraghi of the Department of Aerospace Engineering.

The XPS analysis for Chapter 4 was provided by Dr. Ahmad Amiri. The SEM images and EDS element mapping images in Chapter 6 and Chapter 7 were conducted with the help and guidance from Dr. Ahmad Amiri.

All the analysis and interpretations for the SEM/EDS images was conducted by the student independently. All other work conducted for the dissertation was completed by the student independently.

### Funding Sources

Graduate study was supported by a research assistantship and two fellowship from Texas A&M University.

## NOMENCLATURE

| | |
|---|---|
| WBM | Water-Based Mud |
| OBM | Oil-Based Mud |
| HPHT | High-Pressure High-Temperature |
| COF | Coefficient of Friction |
| ERD | Extended-Reach Drilling |
| API | American Petroleum Institute |
| SBM | Synthetic-Based Mud |
| SFR | Sodium-Cooled Fast Reactor |
| SCWR | Supercritical Water Reactor |
| LFR | Lead-Cooled Fast Reactor |
| MSR | Molten Salt Reactor |
| GFR | Gas-Cooled Fast Reactor |
| DFR | Dual Fluid Reactor |
| VHTR | Very-High-Temperature Reactor |
| LCM | Lost-Circulation Material |
| UHPT | Ultra-High Pressure Tribometer |

## TABLE OF CONTENTS

## LIST OF FIGURES

## LIST OF TABLES

# CHAPTER 1

# INTRODUCTION

Since the successful establishment of the first oil well in North America (Oil Springs, Ontario, Canada) in 1858 and the following discovery of oil in the United States at Oil Creek Pennsylvania in 1859, there has been a continuous increasing demand in energy needs. Over a century of conventional explorations has reduced the availability of natural energy resources in land to a level of scarcity, pushing oil & gas industry to extend their exploration and production activities from onshore to offshore sites. More importantly, the discovery of shale gas and oil, enabled huge increases in oil and gas production. However, these technologies required stringent operating conditions, including extreme pressures and temperatures. To this end, the oil & gas industry has turned to Extended-Reach Drilling (ERD) technique, which has been heavily relying on oil-based mud (OBM) lubricant to improve the drilling efficiency, and protect the drill bit and well wall pipes from potential failures due to excessive heat, seizure, caused by material wear and elemental diffusion during the drilling process. OBM is a type of mud where the base fluid is typically a petroleum-based product; this oil base can be diesel, kerosene, fuel oil, selected crude oil or mineral oil [1]. Its advantages include increased lubricity, enhanced shale inhibition, and greater cleaning abilities. It can also withstand greater heat without breaking down due to its better thermal stability. Figure 1 [2] shows a schematic of the forces acting on the drill string at different stages of ERD wells. To further improve the drilling efficiency with OBM as the major lubricant, various commercial additives of different categories, but all with targeted functions, such as anti-friction, anti-wear and anti-corrosion have been studied and introduced into multiple types of OBM systems.

However, despite the effectiveness in lubricating and protecting the rotating drill bit and stationary wall-pipe from excessive friction and wear, even with the aid of selected additives, OBM by nature comes with several inherent disadvantages. These include relatively high expense, excessive energy loss due to its high viscosity, disabling analysis of oil in cuttings due to its indistinguishability from original oil, contamination of oil samples in cuttings for geochemical analysis, masking accurate determination of API (American Petroleum Institute) gravity, contamination of areas of freshwater aquifers, permanent environmental contamination due to inappropriate disposal of cuttings, all of which aggravate significantly and become more concern-raising as the exploration and production sites shift from in land to offshore.

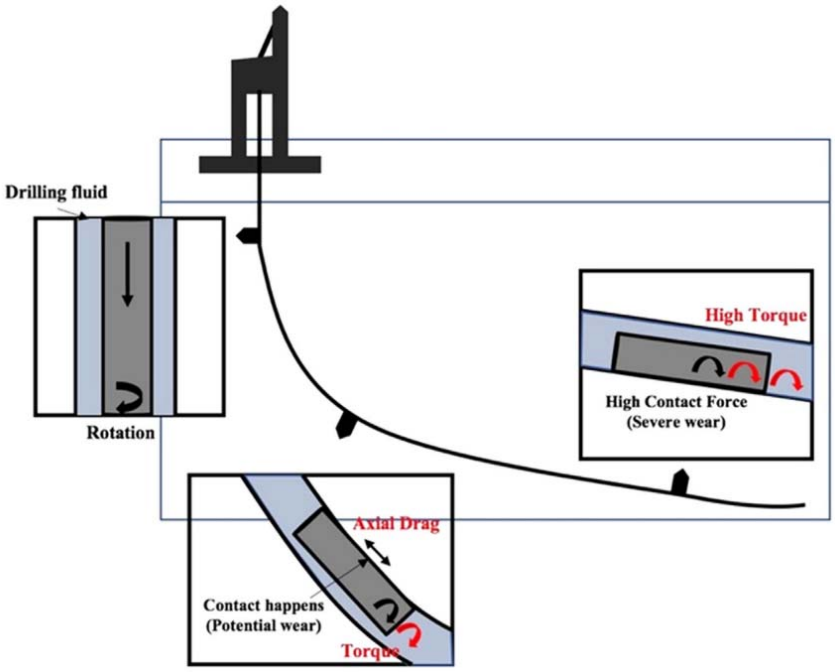


Figure 1. Schematic of the forces acting on the drill string at different stages of ERD. Adapted from [2].

In efforts to address the above mentioned concern-raising issues, and disadvantages of OBM and seek promising replacement candidate for OBM, the oil & gas industry has been considering and already using alternative muds for drilling activities, among which are mainly synthetic-based mud (SBM) and water-based mud (WBM). SBM is a mud where the base fluid is a synthetic oil, having the properties of an oil-based mud but much less toxicity of the fluid fumes than OBM. However, SBM still poses the same environmental damage and analysis obstruction problems as OBM, just to a less severe extent. On the other hand, WBM is a homogeneous blend of water with clays and other chemicals, resembling something between "chocolate milk" and a "malt," depending on its viscosity. One most commonly included clay is bentonite. Many other chemicals, i.e., potassium chloride, sodium chloride, polymers and functional groups can be added to a WBM system to realize specific purposes such as weight control, viscosity control, shale stability, increased drilling rate of penetration, better thermal stability, and better cooling and lubrication. However, research on the tribological performance of WBM with an emphasis on friction, wear and corrosion has been scarce, rendering highly limited availability of comprehensive evaluation and analysis for the tribological performance of WBM systems and their potential to be comparable to or even outperform OBM systems with and without the aid of additives. Hence the feasibility of fully replacing OBM with WBM has been quite ambiguous and uncertain, and WBM systems are only used in limited non aggressive applications, such as vertical wells.

Under extremely challenging lubrication conditions, i.e., boundary lubrication and dry film lubrication under high load, the temperature in the vicinity of the interface drastically increases as the applied load increases, and seizure occurs between contacting or sliding components when the interface reaches a critical temperature [3–8], which could further lead to 'self-welding' between the two counter parts due to adhesion. Self-welding, diffusion welding, and adhesion welding all

refer to a same phenomenon that in a strongly reducing medium and at elevated temperatures, connections take place between the contacting surfaces of components subject to a load that is perpendicular to the contacting surfaces. Once self-welded, it can be extremely hard to separate the bonded components, rendering the device inoperable. It is assumed that the cleaning effect of such reducing environment completely cleans the metal surfaces and thus removes potential barriers for diffusion to take place [9].

Similar to the HPHT conditions experienced by tribopairs during relative motion, immobile separate metallic parts at a relatively high temperature, i.e. ~70% of the material's melting point, also have the tendency to experience the above mentioned seizure due to diffusive adhesion at the contacting surfaces when the applied load (contact pressure) reaches a critical value and beyond, especially if the duration for this surface contact under HPHT conditions is sufficiently long. In this scenario, it is typically referred to as "self-welding," which has the potential to severely hamper or even completely paralyze the operability of the involved components and even the whole system.

For nuclear reactors, all the components and systems operate at extremely high temperatures, e.g., 500 °C for sodium-cooled fast reactors (SFR), 510-625 °C for supercritical water reactors (SCWR), 480-800 °C for lead-cooled fast reactors (LFR), 700-800 °C for molten salt reactors (MSR), 850 °C for gas-cooled fast reactors (GFR), 1000 °C for dual fluid reactors (DFR), 900-1000°C for very-high-temperature reactors (VHTR). Together with inherent large load as nuclear reactors typically highly relies on special heavy alloys for its components for the purpose of anti-oxidization and anti-corrosion, as well as the long duration of surface contacting between components within an operation cycle, all the conditions (high temperature, high load and long duration) required for self-welding to occur are in positon. Disabled operability of components/

systems in nuclear reactors can result in disastrous consequences, hence a comprehensive investigation and analysis on the self-welding behavior of nickel alloys for nuclear reactor applications is of significant importance. Similar system failure due to inoperability of counteracting parts is also commonly encountered during the drilling processes in oil & gas industry, as a consequence of seizure between the sliding tribo materials due to excessive heat generated by metal-on-metal friction.

### 1.1 Objectives and Tasks

The first objective of this study is to comprehensively investigate and analyze the tribological performance of various WBM systems for ERD applications (with and without the influence of select friction-modifying additives of different categories). Such studies will reveal the mechanisms through which their performance in friction, wear and corrosion is favorably or adversely affected, compared with a reference OBM system, with emphasis on the feasibility for WBM to be considered as a competitive and promising replacement drilling fluid for OBM. Further, evaluation is performed among multiple different commercial water-based mud systems regarding their tribological performance, under the influence of select friction-modifying additives, elevated hardness of the tribo materials, and synergistic effects of additives and elevated hardness. As part of the efforts seeking promising performance-boosting additives for WBM, a series of graphene is also evaluated regarding its influence on the tribological performance of WBM. Under certain circumstances, i.e., excessive heat generation and subsequent rapid vaporization of local drilling fluid due to metal-on-metal contact, the rotating drill bit and stationary pipe may experience seizure/self-welding with each other, therefore seizure behavior of tribopairs is also investigated in this study.

The second objective of this study is to evaluate the self-welding behavior of nickel alloys Inconel 617® and 800 HT® under the influence of multiple factors (surface roughness, contact pressure, aging period and atmosphere and analyze the tested samples for potential relationships among these varying parameters and the self-welding tendency and bonding strength.

To achieve these objectives, the proposed tasks are as follows:

a) Perform tribological tests with multiple WBM systems, with and without the influence of different select friction modifying additives;
b) Perform tribological tests with a reference OBM system, with and without the influence of the same additives used in a);
c) Analyze the tribological performance of WBM systems and their additive-altered versions, with focus on friction, wear, and corrosion;
d) Analyze the tribological performance of the reference OBM system and its additive-altered versions, with a focus on friction, wear, and corrosion;
e) Perform topography and chemical analysis of the tested samples obtained through a) and b) to understand the mechanisms through which the tribological performance of the WBM systems, reference OBM system, and their additive-altered versions are improved or adversely affected, using optical microscopy, 2D/3D profilometry, scanning electron microscopy (SEM), energy-dispersive X-ray spectroscopy (EDS) and X-ray photoelectron spectroscopy (XPS);
f) Evaluate the tendency of seizure/self-welding between tribopairs for drilling activities, albeit low;
g) Perform self-welding tests with nickel alloys at high temperatures (950 °C for Inconel 617®, 750 °C for 800 HT®), under the influence of varying surface roughness, varying normal load

(contact pressure), varying aging period (1 hour, 50 hours, 100 hours) in different atmosphere, i.e., helium with controlled impurities of oxygen and ambient air; and

h) Analyze the tested samples obtained through g) for oxidization, self-welding tendency, bonding strength, effective adhesion area and the relationships among them, using optical microscopy, 2D/3D profilometry, scanning electron microscopy (SEM), Energy-dispersive X-ray Spectroscopy (EDS) and an in-situ tensile measurements.

### 1.2 Flowchart of Approach

Figure 2 shows a flowchart summarizing an approach followed for this study, it provides an overview of materials, test samples, parameters under study and methods for experimental evaluations, and mechanical/ chemical characterization techniques utilized for this study.

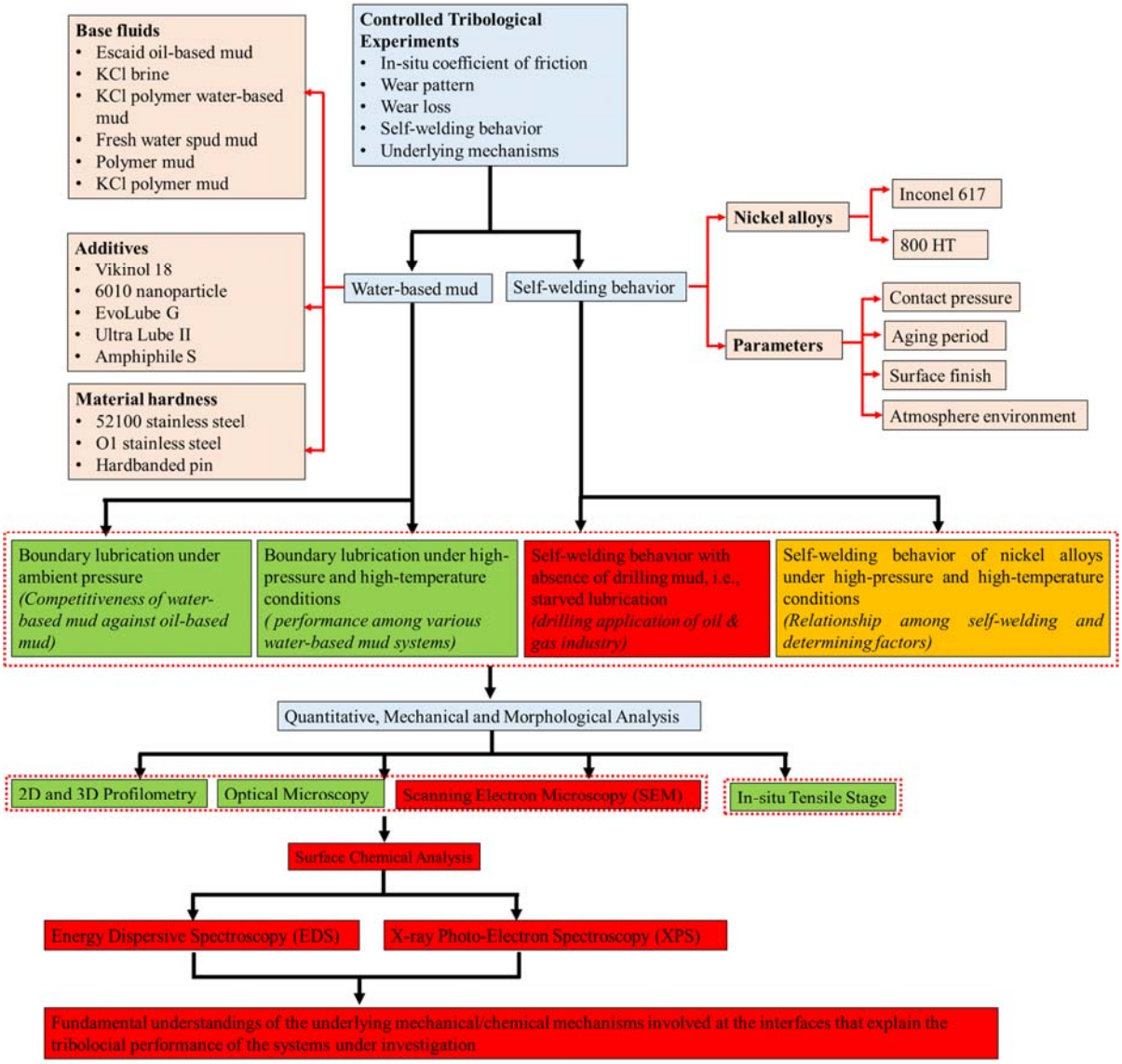


Figure 2. Flowchart of research approach for current study.

# CHAPTER 2

# LITERATURE REVIEW

## 2.1 Tribological Performance of Drilling Fluids

The depletion of conventional oil reserves has pushed the oil and gas industry to develop non-conventional oil recovery techniques such as extended-reach drilling (ERD), which enables optimization of field development through the reduction of drilling sites and structures and provides access to otherwise unavailable reserves [10]. This is achieved by deep and directional drilling, including wells with tangent angles of up to 82$^{o}$ that pose engineering challenges such as extreme frictional torque and drag, and hole cleaning [11]. Frictional torque proportionally translates to the amount of energy needed in the drilling process, thus its reduction is desirable to save cost. This can be achieved through friction reduction which depends heavily on mud lubricity, which is one of the most important technologies critical to the success of ERD [12].

Drilling mud, also known as drilling fluid, is a colloidal suspension made by mixing base fluid, additives, weighting agent such as bentonite clay, and lost-circulation material (LCM). Some of its main functions are to (1) carry cuttings from the hole and permit their separation at the surface, (2) cool and clean the drill bit, (3) reduce friction between the drill pipe and wellbore or casing, (4) maintain the stability of the wellbore, (5) prevent the inflow of fluids from the wellbore, (6) form a thin, low-permeable filter cake, (7) be non-damaging to the producing formation, (8) be non-hazardous to the environment and personnel [13,14]. At any time in the process of drilling a well, one or more of these functions may take precedence over the others. In the case of extended-reach and horizontal drilling, hole cleaning and wellbore integrity maintenance are generally considered the most important functions [15]. Additionally, there are various types of drilling

fluids such as oil-based fluids, synthetic based mud drill-in fluids, and water-based fluids which are all designed and used for specific well conditions. The three key factors that drive the selection process of drilling fluids are cost, tribological performance (friction, wear, corrosion), and environmental impact [16].

Among the different drilling fluid types, SBM is known to have excellent lubricity, non-polluting, and minimally toxic, making it preferable than oil-based fluid for ERD [17]. The performance of the drilling mud can then be improved further to meet different criteria using lubricant additives for different target effects. The roles of these lubricant additives are (1) to enhance existing base mud properties with antioxidants, corrosion inhibitors, anti-foam agents, and demulsifying agents, (2) to suppress undesirable base oil properties with pour-point depressants, and viscosity index (VI) improvers, and (3) to impart new properties to base oils with extreme pressure (EP) additives, detergents, friction modifiers and anti-wear agents [18]. Friction modifier additives are especially important in reducing friction, and are classified into four major categories, i.e., organic friction modifiers (OFM), organo-molybdenum friction modifiers, functionalized polymers, and nanoparticles, each of which has different mechanical/chemical lubricating mechanisms such as forming protective tribofilms, acting as molecular bearings, and molecular adsorption [19].

Historically, OFMs were fatty acids which can bring in corrosive damages to metallic surfaces, and later replaced by amphiphiles such as amides, amines, and ester, or more complex organo-acid-based compounds that enable the formation of insoluble metal salt passivating layers [20–25]. The chemical reaction occurring between lubricant/environment and the surfaces under boundary conditions are known as tribochemistry. However, the precise nature of the reaction was not well understood [26]. Although the precise chemical structures of the additives that are used in this study are unknown, they are known to have one or more functional head groups at one end such

as amides and amphiphiles [19]. Other additives with functional head groups such as carboxylic acid and amine are generally more effective lubricants than alcohol, ester, nitrile or halide groups on ferrous substrates [19,27–29].

### 2.1.1 Tribological Performance of OBM

In 1940, Beeck et al. evaluated the effect of long-chain polar compounds on the coefficient of friction (COF) of white oil under boundary conditions using the Boerlage four-ball friction apparatus, for various lubricants as a function of relative velocity [7]. The authors found that the mechanism through which long-chain polar compounds reduced COF was primarily inducing wedging of oil under the surface (oil drag) while not providing direct protection to the surface. Wear prevention typically involves mechanical or chemical polishing action, through which the load supporting area becomes larger, hence resulting in decreased local pressure and temperature. For instance, additives with compounds containing phosphorous, chlorous acid, glycols, amine groups, or other elements of group V of the periodic system are found to react with the surfaces of tribopairs to form a metal phosphide or chloride on the counteracting interface in the form of films. These tribofilms have much lower melting point, and serve as a boundary lubrication films between the two counteracting surfaces, as interface temperature increases due to friction [8,30]. Beeck et al. [8] evaluated the wear performance of metal-plated steel balls, adding 1.5% tripheyl phosrine and triphenyl arsine in white oil, which resulted in wear prevention factors of 7.2 and 12.2 respectively. Further adding 1% of a long chain polar compound to the above chemical anti-wear agents doubled the wear prevention factor delivered by polishing agents, rendering a wear prevention factor as high as 17.6.

In 1951, Menter et al. [31] studied the influence of temperature on the structure and orientation of fatty acid films and soap films adsorbed on metal surfaces. At room temperature, the authors found that orientation of the first monolayer mainly aligned with the hydrocarbon chains perpendicular to the surface. Increase in temperature imposed a disorientation effect over the film, which is reversible through cooling. Also, when the chain length is below a certain value, the orientation would also become poorer.

For boundary lubrications of metals, the dominant factor determining friction is the nature of the chemical composition of the lubricant and the underlying surfaces, where the latter could be altered by the former through physically and/or chemically. On the other hand, bulk viscosity plays a negligible role [32]. Polar compounds, such as long chain alcohols, esters and fatty acids are all effective additives in boundary lubrication. These compounds are physically adsorbed by their polar group to the metal, and oriented to form a complete monolayer, which prevents direct metallic contact, and that the frictional resistance is due entirely to these adsorbed films. However, these boundary films, are easy to be penetrated due to local adhesion and welding between the metal interfaces, and hence not able to provide complete protection to the surfaces. Further, physically adsorbed films are not enough, and the most effective lubrication is only obtained when the fatty acid has reacted chemically with the surface to form the appropriate tribofilm.

For alcohols and pure paraffins, the disorientation and its reversion occurs at the bulk melting point of the lubricant and independent of the underlying metal. For hydrocarbon films, the temperature affects the system's friction performance through diminishing the lateral adhesion between the molecules in the boundary film as the interface temperature increases to the melting point [32].

For fatty acids, the influence of temperature on the friction shows a transition effect, at a temperature much higher than that of the bulk melting point of the fatty acid. The transition usually

results in increased damage and wear to the contacting surfaces, which corresponds to melting or softening of the film formed on the metal surface due to reaction. However, this transition effect is also reversible upon cooling, showing reduction of COF back to its original value. Accordingly, the surface damage gets "healed" as the tribofilm reforms on the surfaces.

In 1972, Hoyt [33] peroformed a detailed study on the influence of additives on fluid friciton. The author concluded that introduction of polymer could reduce the friction resistance by up to 75% when compared with the base solution, which ascribed to the polymer properties, hydrodynamics, polymer chemistry and rheology.

Sodium carboxymethylcellulose (CMC) is the first water-soluable friction-reducing material evaluated in the literature, which requires relative high concentrations than other polymers for the same percentage of reduction in friction. Guar, a complex polysaccharide derived from plants, has a COF lower than water. It is widely applied as a suspending agent for sand in drilling muds because of its low cost and that its moleucles tend to prevent degradation due to high shear forces. Polyethylene oxide is also extremely effective friction-reducting polymer that is soluable in water. It was observed to reduce COF by up to 40% with a concentration of 0.5 ppm. With a 25 ppm concentraiton, Fabula [34] obtained a 75% reducetion in COF in a 1.02 cm diameter pipe at a high Reynolds number of $10^5$. In 1966, Hoyt [33,35] found that introducing polyethylene oxide into sea water and other fluids (dextran, saline, and plasma) all resulted in significant reduction in COF. With poor solvent like water, Pruitt et al. [36] showed that a certain concentration of halide such as $K_2SO_4$ aids in the friction-reduction as well. Polyacrylamide is also effective in reducing friction in water, it has a better soluability than polyethylene oxide.

### 2.1.2 Tribological Performance of WBM

WBM has been applied more widely for drilling applications due to similar advantages that it shares with water-based cutting fluid, i.e., low pollution, long durability and energy-saving potential involved [37].

As potential replacement for OBM widely used in high-angle well drilling, WBM systems can be classified as polymer muds, salt/polymer muds or cationic muds, all of which have been widely used in horizontal and extended-reach drilling [38]. For drilling of wellbores with no unstable shales, polymer muds such as fresh-water, polymer mud systems are known for being highly cost-effective. Thus, when unstable shale is absent, the hole could be cleaned effectively with a sufficiently high annular velocity. For wellbores where stability is a concern, polymer muds are usually supplemented with certain concentrations of salt or halide, such as sodium chloride, potassium chloride, etc. A cationic drilling fluid is featured for a predominantly cationic chemical nature, introduction of any additives that are anionic will result in drastic changes to its original properties, and it is well known for poor fluid loss control [38].

An inherent concern of WBM is that its pure version is not as good as pure OBM, as far as its tribological performance. However, with the aid of selected additives, the wear and friction properties can be significantly improved, and thus enabling WBM to be a potential replacement for OBM.

There are multiple categories of additives that can be introduced in WBM systems, including: a) synthetic materials polyethers (polyalkylene glycols, polyalkylene glycol esters, and polyalkyl glycolethers) [39], b) halide solutions or water-soluble chemicals containing active elements like chlorine (Cl) sulfur (S), phosphorus (P) and nitrogen (N), and c) nano-sized particles. The first two categories are especially effective for ferrous-based equipment, since they are easy to react with

metal and form tribofilms by the process of molecule adsorption, deposition and tribochemical reaction [40].

The anti-wear and friction-reducing performance can be ascribed to the formation of films on the metal surface, and the mechanism of the process of molecules adsorption, new compounds production through tribochemical reactions, film formation and destruction [41]. For instance, phosphorus exists in the form of adsorbed molecule, phosphate or polyphosphate, and sulfur in the form of alkyldisulfide, sulfide and sulfate, chlorine in the form of ferrous chloride ($FeCl_2$) [4–6,42]. Plaza et al. [43] synthesized some polyoxyethylene dithiophosphate derivatives, and found that these compounds showed very good load-carrying performance, and strongly reduced friction coefficients in both OBM and WBM [43,44]. Alvi et al. [45] tested the influence of nanoparticles on the tribological performance, with Boron Nitride microparticles dispersed in a solution of CMC and $Fe_2O_3$ nanoparticles dispersed in Xanthan gum solution in water. The results showed that the addition of 0.0095 wt. % BN and $Fe_2O_3$ reduced the mechanical friction coefficients of the laboratory drilling fluids by 37 %, and 43 %, respectively.

On the other hand, nanocomposite materials based on graphene with excellent mechanical and friction-resisting properties have attracted more and more attention for research & development of applications in a wide range of scenarios [46], among which, drilling process in oil & gas industry is a typical example where the outstanding lubricating performance of graphene-based agents could be of significant value.

In 2012, Choudhary et al. [47] reported the potential of graphene-based additives in improving the lubricating performance of organic solvents. Compared to pure hexadecane, adding an optimized dose of 0.06 mg $mL^{-1}$ Octadecylamine functionalized graphene reduced the friction and wear by 26% and 9%, respectively,. The authors concluded that the enhancement in lubricity could be

attributed to uninterrupted supplies of graphene nanosheets under the rubbing surfaces, where they prevent direct contact between the counteracting surfaces. In 2015, Elomaa et al. [48] evaluated the effect of graphene oxide (GO) on water lubrication performance, using tribopairs of diamond-like carbon vs. stainless steel. Under a normal load of 10 N, adding 1 wt. % of GO reduced the COF by 57% when compared with pure water, from 0.14 to 0.06. Morphology analysis also showed that the corrosive effect was reduced in the presence of GO additive. The authors confirmed that main tribological mechanism of GO additives in water was the embedding of GO sheets on the counter ball surface forming a lubricating layer and binding water molecules into the contact. Other studies have also proved that graphene-based additives with an optimized concentration could also significantly improve the tribological performance of oil-based lubricants [49–51].

### 2.2 Self-welding Behavior of Nickel Alloys

When two surfaces are mated and come into close contact, especially when under high load, strong interatomic forces and weak intermolecular forces of attraction come into play, which promote intense adhesion in a sequence of three stages: 1) contacting surfaces deforms due to loading; 2) the effective contacting area increases and hence activating the surfaces; and 3) volumetric diffusion of atoms occurs, followed by recrystallization. Such effects can occur in many tribological contacts, especially under higher contact pressures and temperatures. In many cases, the effect if isolated in a few local asperities and does not have a detrimental catastrophic effect. When its influence is more significant, scuffing and galling may occur which could be catastrophic. In ERD applications, such local phenomena may occur, especially in the absence of effective lubrication, and some basic experiments are performed in this work to measure the extent of damage under ERD-relevant conditions.

Another application where self-welding is likely a major issue is under extremely high temperature nuclear reactor applications. Components in nuclear reactors, i.e., earings and couplings, operating in a sodium-cooled reactor are subjected to the additional hazard of galling or self-welding. High temperature liquid sodium removes all traces of film, grease, and oxide from metal surfaces, leaving the surface in a very active/nascent condition, which induces adhesion between two mating material surfaces by providing optimum conditions for inter-diffusion or self-welding and galling [9].

In 1959, Leeser et al. [9] performed static load tests to determine the adhesion tendency of various bearing-couple materials when subjected to slow speeds and moderate bearing loads in different environments, including liquid sodium, argon and nitrogen gas. Similar experiments were performed but introducing an intermittent small-angle twist while the bearing-couple was under static load. The authors found that: a) harder material combinations generally showed better wear and resistance to self-welding than did softer materials; b) the resistance to self-welding was dependent on the design and the load application. The authors ascribed the absence of appreciable tendency for direct adhesion during the static load tests to the insufficiency in parameters including temperature, contact duration, and suggested that the duration for which the mated surfaces were under applied load could be a critical factor in occurrence of self-welding.

Diffusion welding is a process very similar to self-welding. In diffusion welding, metals are joined by causing the coalescence of the mating surfaces through the application of pressure at elevated temperature; this is usually done in a protective atmosphere. The temperatures used are substantially below the melting point of the lowest melting base metal in the assembly but high enough to permit diffusional processes to occur. The applied pressure is sufficient to assure intimate interfacial contact, but it is not sufficient for macroscopic deformation of the parts.

In 1967, King et al. [52] joined specimens by induction heating under a compressive load in vacuum environment at various temperatures, pressures, and dwell times. Based on the experimental results, the authors found that temperature exerted the greatest influence of the joining process. Both deformational and diffusional processes are accelerated by increasing temperature; this results in more rapid and complete growth of the contact area and faster void shrinkage. The influence of contact pressure exerted was of less importance, as long as a critical value was available to assure extensive initial deformation of the contacting surface asperities. The duration needed was not an independent variable but a function of the applied pressure and temperature. Diffusion across the interface occurs after the joint is made, and it cannot contribute to the joint formation. The fundamental force which causes the surfaces to join is the interatomic attractive force which causes a metal to be a solid. The nature of metallic interatomic bonding is such that if two hypothetical pieces with atomically flat and clean surfaces were placed in intimate contact, they would join together (cohesion and adhesion).

In 1970, Bendorf [53] carried out static load tests in sodium on structural materials to investigate the self-welding tendency of various materials including: austenitic materials, a stabilized ferritic steel, a nickel base alloy, as well as several hard facing and hard metal alloys. The temperatures involved were 580 and 700 °C, compressive load was up to 5 kp/mm$^2$ (49.03 MPa), with a duration up to 168 hours and oxygen content controlled at 20 ppm. As the test specimens were mainly structural materials that are subjected to a static load and not to movements under load, the author introduced an adhesion coefficient,

$$H = \frac{adhesion}{contact\ force} \tag{1}$$

Tests results showed the absence of self-welding for nickel-base alloy Inconel 718 but strong tendency for titanium carbide alloy. Analysis of the surfaces for samples which experienced self-

welding all exhibited sticking crystals of the counter material. The metal bridges which occurred on the interfaces seem to have been caused by strong plastic deformation and subsequent recrystallization in this region.

This confirms that the strengths of the welds occurring at the interface are higher than that of the base materials, which is possible according to the theory described in [54]: It assumes that only single aforementioned roughness contact each other and are plastically deformed by a correspondingly high load, above a certain threshold of stress until the contact area is sufficient to carry the load. It is then possible that plastic deformation distorts the grains and causes them to slide on top of each other forming new, permanent positions without producing a rupture in the base material. At these points, presumably strong welds occur which may attain or even exceed the strength of the base material. The author came to a conclusion that an adhesion coefficient above unity indicates very strong self-welding strength, and that the influence of time needs to be investigated in correlation with temperature.

In 1976, Huber et al. [55] carried out experimental investigations to further determine the separate influence of individual parameters responsible for self-welding, in terms of environmental temperature, contact pressure, time, contact area and surface finish. The test materials were Inconel 718 and Stellite 6 (cobalt base alloy), both were then to be used for the SNR 300 fuel element spacer pads. The authors found that the breakaway force was nearly proportional to the contact pressure. The influence of time and temperature on the breakaway forces for self-welded samples were both exerted in an indirect way, with the time related to the creep properties of the respective pairing materials, while temperature via the temperature-dependent strength properties of the pairing materials. Flushing for the same duration but at different temperatures results in different

self-welding behavior. Self-welding must always be anticipated under conditions leading to oxide-free metallic surfaces.

In 1984, Yokota et al. [56] studied self-welding behavior of FBR structural materials, i.e., Type 304, Type 321, Inconel 718 and 2¼ Cr-1Mo, with focus on the dependence on contact pressure, contact period, and environmental temperature (under sodium conditions). The authors found that the mating pairs composed of the same materials showed easier bonding or self-welding than those composed of different kinds of materials, and each type of the tested materials showed the same self-welding coefficient, and the measured shear stresses for the breakaway of bonded sample pairs were all proportional to the contact pressures. Further, the authors found that the welding coefficient was also proportional to the square root of the contacting period (aging period), which increased at elevated sodium temperature.

In 1993, Chander et al. [57] studied the self-welding behavior of austenitic stainless steel, hard chrome plating and Stellite-6 with a focus on the effect of surface finish regarding applications in FBRs in liquid sodium at 530 °C with a load pressure of 10, 40 MPa for a duration of 500 and 1000 hours. Results showed no signs of self-welding for stainless steel sample pairs, but a trend that surface roughness appeared to be more resistant to self-welding than smooth surfaces. The authors also suggested that elemental transfer might have promoting effect on self-welding.

In 2006, Wright [58] performed a summarized study of aging and environmental effects on Inconel 617®, which is the primary candidate alloy for the heat exchanger, the most critical metallic component of the Next Generation Nuclear Plant (NGNP). Under the NGNP materials program investigated the environmental effect of impurities in helium on Inconel 617® at elevated temperatures in terms of fusion welding/self-welding. Results indicated that aging under load

would result in considerable redistribution of carbides to the grain boundaries which experience tensile loading for certain temperatures and applied stress values.

In 2008, Li et al. [59] described the microstructure and mechanical properties of Inconel 617® for high temperature conditions. The authors found that though suggested as the most suitable material for heat exchanger operating in high temperature high pressure nuclear reactors, Inconel 617® still showed the tendency of self-welding.

# CHAPTER 3

# INSTRUMENTATION, METHODS AND MATERIALS

## 3.1 Equipment and Experimental Procedure

### 3.1.1 Falex Four-Ball Tester

A Falex 4-ball machine conforming to different ASTM standards was used to measure and compare the effectiveness in terms of friction and wear reduction of base fluids in the presence of four different commercial additives. Figure 3 shows schematics of the experimental setup. The bottom stationary balls are clamped inside a reservoir integrated with heating elements and filled with a lubricant, while the top ball is held stationary by a collet in the vertical direction, and rotates about the Z-axis as driven by a top shaft.

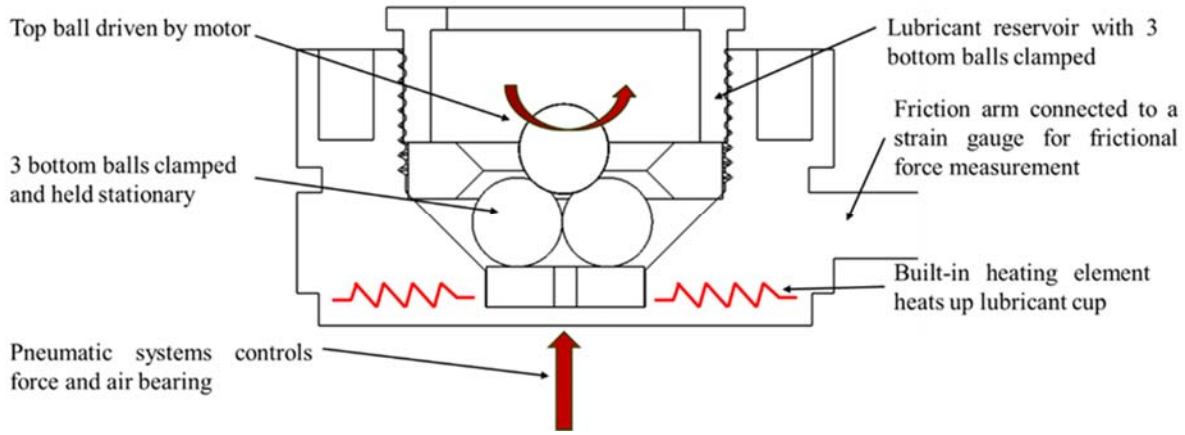


Figure 3. Schematics of Four-Ball tester.

The reservoir with bottom balls clamped stationary is positioned on top of and locked to a heating plate through a built-in groove, enabling synchronous and non-hysteretic motion between the reservoir and the heating plate. This heating plate allows elevating the temperature of the reservoir to a desired value, up to 200 °C. An embedded thermocouple measures the real-time temperature

of the lubricant inside the reservoir and provides feedback to the data-acquisition program in a closed control loop to maintain the desired lubricant temperature. A pneumatic loading mechanism pushes the lubricant reservoir up against the top ball, exerting a desired normal load. As the motor drives the top ball through a shaft to rotate and slide against the bottom stationary balls, a torque is exerted to the lubricant reservoir, which is accordingly forced to spin. An air bearing underneath the heating plate allows free rotation of the reservoir-heating plate sub-assembly, while a friction arm extending from the lubricant reservoir and connected to a strain gauge restrains the reservoir-heating plate sub-assembly to rotate. The tendency to rotate due to the torque exerted to the lubricant reservoir and the restraint of motion by the strain gauge enables the measurement of real-time frictional force. All the test conditions are set according to ASTM D5183 standard, with the rotational speed reduced from 1200 to 400 rpm. This lower speed allows a linear sliding speed which best replicates the boundary lubrication scenario in the field [2]. For each experiment, a new batch of four SAE E52100 steel balls with a diameter of 12.7 mm are used, as prescribed by the standard.

Table 1 shows the ASTM D5183 standard applied for the tribological wear tests; it is slightly modified to better resemble the boundary lubrication conditions in oil & gas drilling applications.

**Table 1. Modified ASTM D5183 to resemble drilling condition. Adapted from** [60]**.**

| **Test Parameters** | **Modified Setting** | **Original Standard Setting** |
|---|---|---|
| Load | 15 ± 0.2 kg | 40 ± 0.2 kg |
| Speed | 400 ± 10 rpm | 1200 ± 10 rpm |
| Temperature | 75 ± 2°C | 75 ± 2°C |
| Duration | 60 minutes | 60 minutes |

Two types of tribological experiments, constant load wear experiments, and Stribeck-type experiments, were carried out to measure the tribological performance of the operating fluids with and without additives. Each experiment was repeated twice to ensure repeatability. In the wear experiments, the normal load and sliding speed were kept constant at 147.15 N (15 kgf) and 400 ± 10 rpm, respectively. The duration of each test was one hour, corresponding to a sliding distance of 551 m. During the experiments, the in-situ friction coefficient was measured. The wear and steady-state wear coefficient were also measured and calculated after completing each experiment. In Stribeck curve type experiments, as shown in Figure 4, the 4-ball machine starts from 200 rpm, and then ramps up with a step of 200 rpm every 0.2 minutes, reaching 1200 rpm (0.459 m/s) at *t* =1 minute. In total, 6 different rotational speeds of 1200, 800, 400, 100, 50, and 10 rpm were used, which correspond to a linear velocity range of 0.004 - 0.459 m/s. For all the rotational speeds, the 4-ball machine runs for 10 minutes. During the whole experimental procedure, the fluid temperature is maintained at 75 °C under a normal load of 147.15 N (15 kgf).

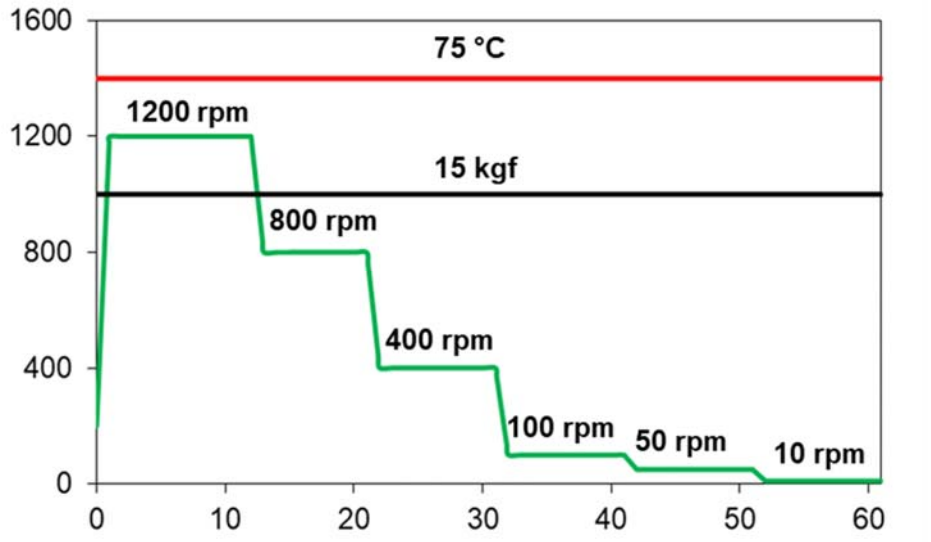

Figure 4. Test protocol for Stribeck curve analysis applied using 4-ball tester.

### 3.1.2 Ultra-High Pressure Tribometer (UHPT) and Test Configuration

A specialized tribometer designed for ultra-high pressure conditions is shown in Figure 5. It was modified to test ERD-based conditions, and is capable of tribological testing under a normal load up to 1120 N (250 lbf) through a closed-loop control system. Tribological tests are performed inside a closed atmosphere environment with a preset chamber pressure up to 13.8 MPa (2000 psi), which enables simulation for high pressure environment in down hole conditions (up to 1380 m sea water pressure) [61]. In detail, as shown in Figure 5 (a), the UHPT has a high-pressure chamber. With the aid of a heating element embedded under the secondary chamber, the UHPT is capable to perform experiments at high temperatures up to 250 °C for submerged lubrication conditions, as shown in Figure 5 (b–d). Figure 5 (d) shows a cross-section schematic of the secondary chamber, showing the pin-on-disk experimental configuration.

Experimental tests for OBM and WBM under the influence of select additives were performed in a pin-on-disk configuration. A disk with 50.8 mm (2 in) diameter and 9.5 mm (0.375 in) thickness was machined out of O1 tool and polished to a surface roughness of ~0.3 μm. The disk holder is secured to the top rotating shaft. A self-aligning pin holder that contains a sample pin and the suspension reservoir. A custom-designed cover on top of the secondary chamber helps prevent splashing of the drilling fluid from the secondary chamber due to high speed rotation. The hood inside the secondary chamber decreases the exposed area of the drilling fluid, and thus reduces the evaporation of the fluid at high temperatures. In-situ frictional force, real-time normal load, and near contact temperature are all recorded and the former used for COF calculation [61].

Figure 6 shows the test protocol used for the wear tests with UHPT. Wear tests were carried out to measure the tribological performance of the operating fluids with and without the effect of Amphiphile S at constant sliding speeds under varying normal load. Each experiment was repeated

twice to ensure repeatability. Figure 6 shows the experimental protocol applied for experiments with UHPT to investigate the tribological performance of the aqueous muds with and without the presence of loaded Amphiphile S for drilling applications. Each experiment is composed of four separate stages, and each stage lasts for 10 minutes with a constant rotating speed of 50 rev/min, which corresponds to a sliding speed of 0.095 m/s and a total sliding distance of 228 m for a 4-stage experiment. The running-in stages starts with a nil normal load but quickly ramps up to 44 N at 75 °C, the purpose for this stage as the beginning of the test is to obtain a stable surface condition and fully mix the drilling fluid and stabilize the fluid temperature. Between each experimental stage, the disk was stopped and disengaged from the pin. Stage 2 experiments start at 75 °C with a normal load of 22 N, after 5 minutes of running, the normal load ramps up to 200 N at a constant acceleration rate. The only difference between stage 2 and stage 3 is that the temperature of drilling fluid is maintained at 125 °C during stage 3 instead of 75 °C in stage 2. For stage 4, the reservoir temperature is maintained at 150 °C. The normal load starts at 22 N and maintain for 3 minutes, then it increases with an incremental of 89 N, reaching at 111, 200, 289 and 378 N, respectively. During the load ramping process from 111 ~ 289 N, each load is maintained for 1 minutes to obtain steady COF measurement. Then the normal load is maintained at 378 N for another 3 minutes. The stabilized COF under each normal load is obtained via averaging the real time COF measured. Note that all the experiments were conducted at least twice, and each repetition involves a new set of samples (pin, disk, and base/drilling fluid). To simulate the high pressure downhole, as well as to help prevent potential drilling fluid vaporization, each 4-stage experiment was carried out inside a closed Nitrogen ($N_2$) atmosphere, with the chamber pressure maintained at 35 atmosphere (absolute) during the whole process.

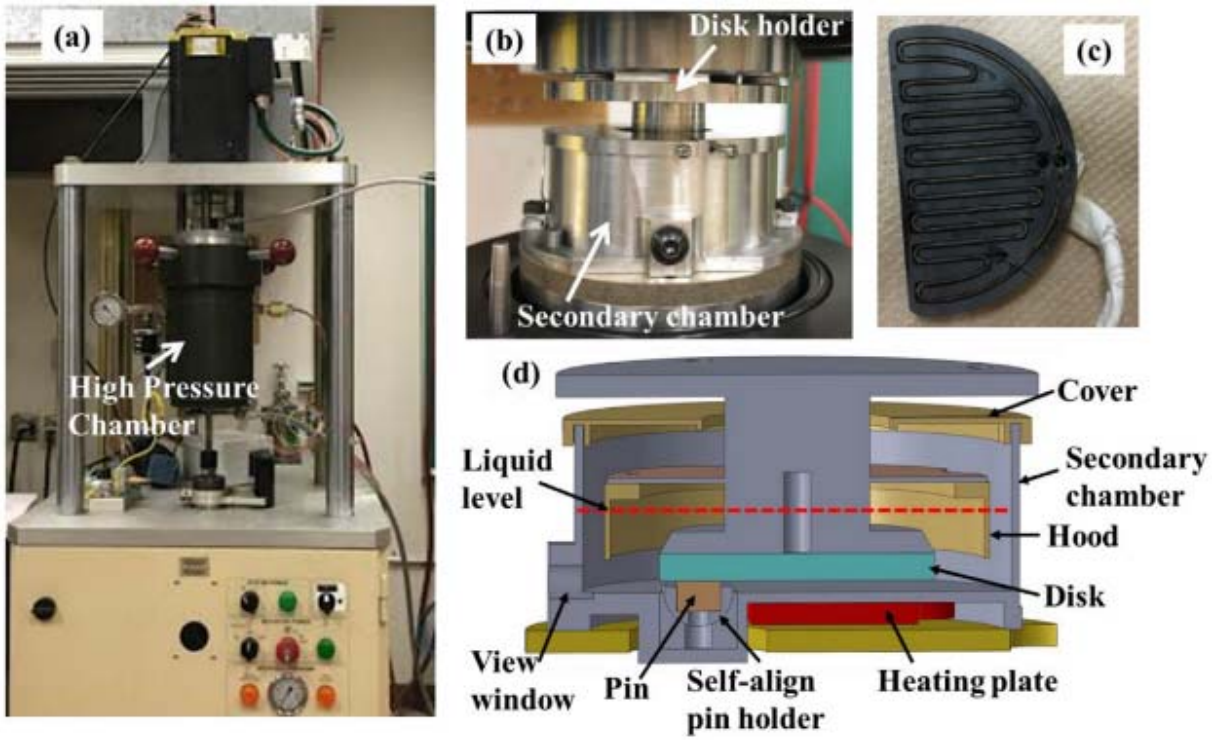


Figure 5. Ultra-high pressure tribometer (UHPT): (a) photograph of the overall system; (b) disk holder and secondary chamber; (c) heat element embed under the secondary chamber; (d) schematics of the secondary chamber. Adapted from [61].

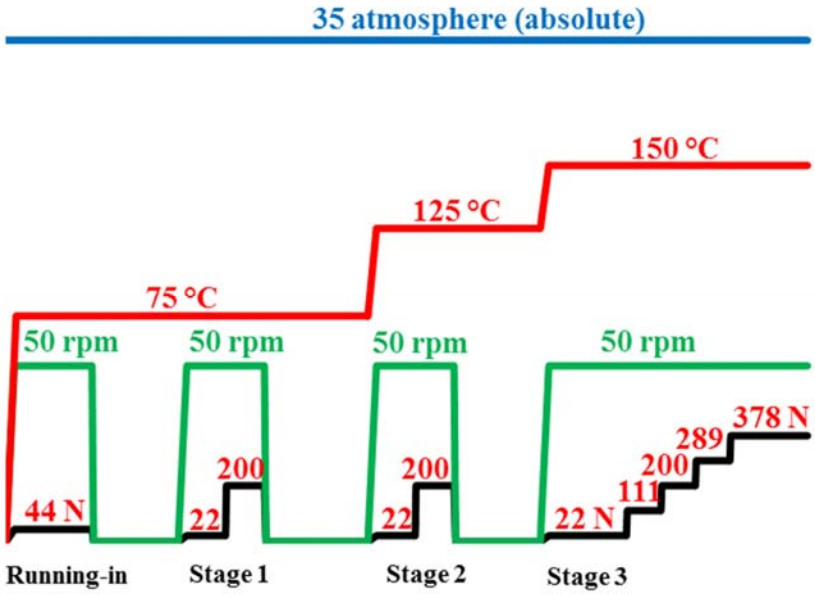


Figure 6. Complex test protocol for wear tests under high-pressure high-temperature conditions using the UHPT.

### 3.1.3 Controlled Atmospheric Muffle Furnace

A controlled atmospheric furnace shown in Figure 7 was used for the self-welding experiments. It has a chamber with high quality alumina fiber insulation and SiC heating elements, a double walled steel internal housing further minimizes heat loss to exterior surface. Its leakage-certified sealing ensures the proper atmosphere environment with accurate controlled temperature through with a built-in 28-segment PID digital temperature controller [62]. Furnace operation is controlled by Shimaden (Japan) 40-segment digital controller with built-in RS485 digital communications port and USB adaptor, allowing the user to connect to a PC for remote control and monitoring of the furnace. An atmospheric furnace provides the perfect environment for self-welding aging of nickel alloy covered in this study, providing the temperatures and atmospheres required [62]. Table 2 lists the test conditions for self-welding behavior of Inconel 617® and 800 HT®.

**Table 2. Test conditions for self-welding behavior of Inconel 617® and 800 HT®.**

| Sample | Apparent contact pressure [MPa] | Atmosphere | Temperature | Aging duration [hour] |
|---|---|---|---|---|
| Inconel 617® | 0.166, 0.248, 0.341 | Helium, Air | 950 °C | 50, 100 |
| 800 HT® | 0.166, 0.248, 0.341 | Helium, Air | 750 °C | 50, 100 |

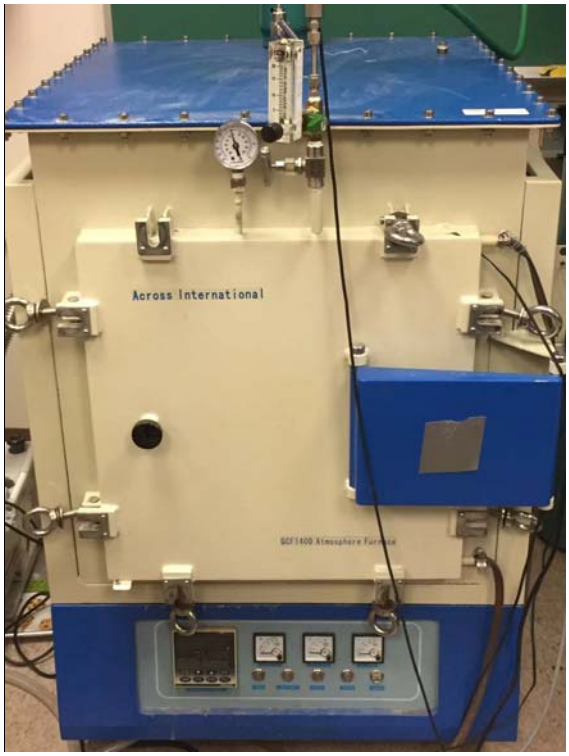

Figure 7. Controlled Atmospheric Furnace.

### 3.1.4 In-Situ Mechanical Tensile Stage

Figure 8 shows a photograph of a tensile/compression stage that is used to measure the bonding strength of self-welded mating pairs of Inconel 617® and 800 HT®, and it is capable to apply a load ranging from 10 μN ~10,000 N. With a preset increment (0.1 to 20 μm/s), the shear stress applied in the plane parallel to the contacting surfaces pulls the two samples away from each other until breakaway occurs. The real-time applied load is continuously monitored and recorded, the value at the point of the breakaway is noted as the bonding strength for the self-welded sample pair. The tensile stage is able to measure samples with dimensions up to 60 x 10 x 5 (mm).

Figure 8. In-situ mechanical tensile stage for bonding strength measurements.

## 3.2 Materials and Preparation

### 3.2.1 Materials for Tests with Falex 4-Ball Tester

The drilling fluids tested are Escaid oil-Based mud (OBM), potassium chloride polymer water-based mud (KCl polymer WBM) and potassium chloride solution (KCl brine). Note that the base stock for OBM and KCl polymer WBM are Escaid 110$^{TM}$ and KCl brine, respectively. For simplicity, in the following chapters, KCl polymer WBM will be referred to as WBM.

OBM, WBM, and KCl brine (40 grams of potassium chloride per 100 ml of distilled water) conventional base fluids are employed in this study. Four additives, namely Vikinol® 18 (Arkema), 6010® (Palmer International), EvoLube® G (Newpark Resources) and Ultra Lube® II (Integrity Industries) are well-known commercial additives that are commonly added into working fluids for reducing friction and wear. However, there is no comprehensive study investigating the effect of each additive on different base fluids, which is undertaken in this study.

Vikinol® 18 is a dihydroxy alkane with a carbon-based chain including 18 carbon atoms (C18) and hydroxyl terminal groups. It possesses good solubility in organic solvents and oils. It is used in different applications as viscosity modifier, acid scavenger, or even base oil. It is more polar than the corresponding mono-alcohols and has a stronger tendency to form hydrogen bonds. It also has

additional benefits including higher melting and boiling points than mono-alcohols, good adherence to the metal surface due to a chemical structure of hydrophobic hydrocarbon tail with a double polar head group; the polar head end adsorbs on the metal surfaces and the hydrophobic tail assists in the formation of a lubricant layer [63].

The 6010® is a black friction particle extracted from polymer of cashew-nutshell-liquid. It plays a functional role in stabilizing the COF, reducing wear, minimizing noise, and vibration [64]. The size of the nanoparticles allows easy entry into the boundary lubricant film and form a third body layer separating the sliding surfaces.

The EvoLube® G is a drilling performance enhancer and an effective lubricant blend. It is in the form of yellow to dark amber liquid. It is widely used as an effective additive in horizontal drilling applications where it minimizes torque and drag, thereby enhancing transmission energy to the bit, and increasing rate of penetration [65]. Further, it reduces stick-slip, thereby increasing drilling efficiency and reducing drill string damage. It is ideal for high-temperature applications due to good thermal stability up to 400 °F (204°C) [65]. Additionally, EvoLube® G reduces stick-slip, and hence increases drilling efficiency and reduces drill string damage [65]. It includes carboxyl head group (fatty acid) of petroleum distillates and hydrotreated light and 2, 2, 4-trimethylpentane-1, 3 diol monoisobutyrate (propanoic acid).

The Ultra Lube® II is an amide-based, environmentally safe, and non-flammable lubricant concentrate specifically developed for highly deviated or horizontal drilling applications, for both land and offshore use. It has a high affinity for metal surfaces, and will adhere to the drill pipe and drill collars. It eliminates torque and drag, prevents differential sticking, and protects the drill pipe from corrosion [66].

The above-mentioned commercial additives have drawn attention from researchers for their performance-improving potential for both OBMs and WBMs. They offer the promise of improved tribological properties, although not all of them have been comparatively studied [67,68].

The test samples used in the 4-Ball tester are made of SAE 52100 alloy steel balls, whose high iron content and low cost closely resemble the materials for drilling tools, which is typically stainless steel or aluminum alloy. Table 3 lists its detailed composition.

**Table 3. Alloying Material of 52100 Alloy Steel.**

| Composition | Weight % | Composition | Weight % | Composition | Weight % |
|---|---|---|---|---|---|
| Aluminum | 0-0.050 | Copper | 0-0.30 | Oxygen | 0-0.0015 |
| Iron | 95.75-97.37 | Manganese | 0.25-0.45 | Phosphorus | 0.025 Max. |
| Carbon | 0.93-1.10 | Molybdenum | 0-0.10 | Silicon | 0.15-0.35 |
| Chromium | 1.30-1.60 | Nickel | 0-0.25 | Sulfur | 0.25 Max. |

Figure 9 (a) shows the Escaid 110TM, which is a low viscosity hydrocarbon derived base fluid with low aromatics/ environmental toxicity. It is also commonly referred to as petroleum distillates (hydrotreated light) or base fluid (BF) and will be mixed with other ingredients to make drilling fluid with specific properties depending on the well/ application. Figure 9 (b) shows the OBM obtained from the production field, with its compositions summarized in Table 4. Figure 9 (c) and Figure 9 (d) show photographs of KCl brine and KCl polymer water-based mud, respectively.

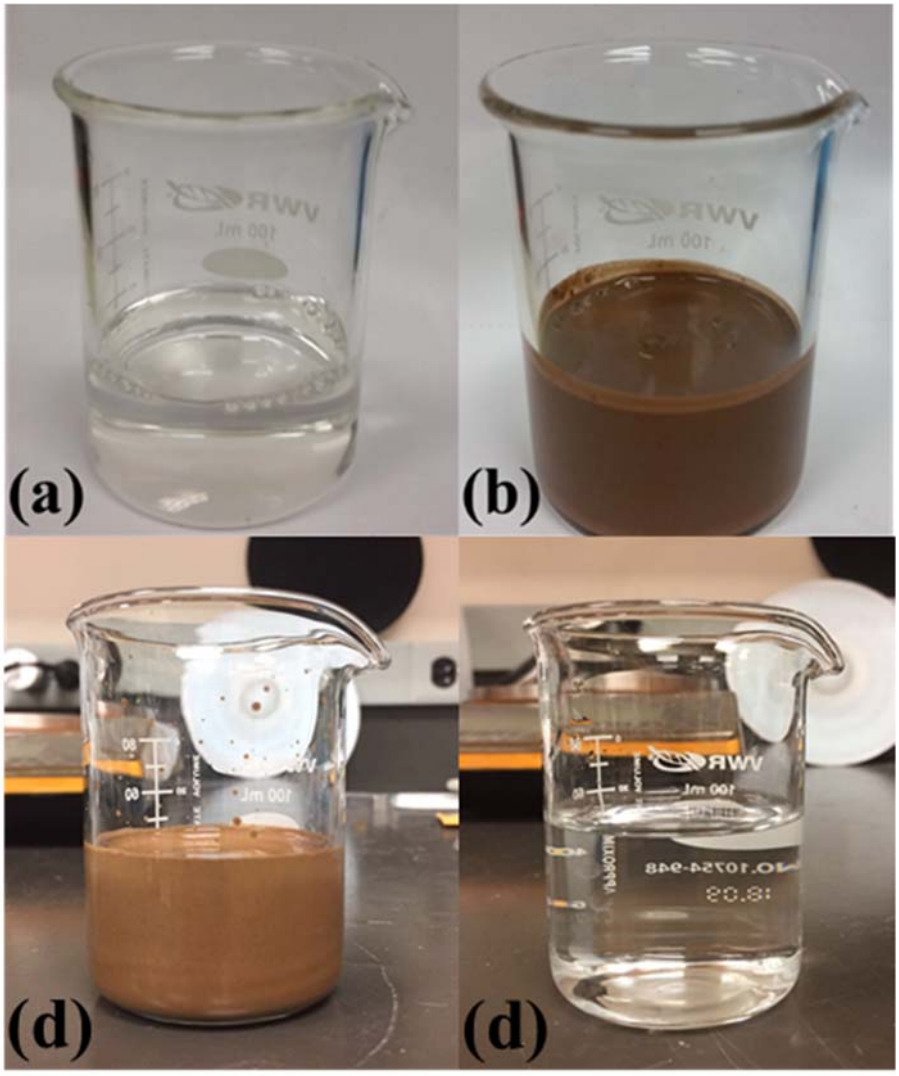

Figure 9. Oil-based drilling fluids: (a) Escaid 110$^{TM}$; (b) OBM; (c) KCl brine; (d) KCl polymer water-based mud.

**Table 4. Composition of OBM from oil field. Adapted from** [61]**.**

| Composition | Weight % |
|---|---|
| Barite | 30 – 60 |
| Petroleum Distillates, Base Fluid (BF) | 10 – 30 |
| Calcium Carbonate | 5 – 10 |
| Calcium Chloride | 1 – 5 |
| Silica, Crystalline, quartz | 1 – 5 |
| Mica | 1 – 5 |

KCl brine is a potassium chloride mixed with distilled water with a concentration of 40 g/100 ml. KCl polymer WBM is an environmentally-friendly alternative for OBM systems to provide high penetration rates, lubricity, wellbore inhibition, and production zone protection, with its composition shown in

Table 5. It is composed of significant Barium sulfate and limestone/ barite for increased viscosity, Bentonite is used for cooling the cutting tools, removing cuttings, and to help prevent blowouts [69]. Potassium chloride (KCl) dissolved in water releases $K^+$ ions to attach to clay surfaces and lend stability to shale formation that is exposed to drilling fluids by the bit and help hold the cuttings together from dispersing into finer particles. Major ingredients in KCl polymer WBM include Sodium Hydroxide (commonly known as caustic soda) to maintain stable pH towards alkalinity [70], Kaolin for improved flow properties and density [71], Sodium Carbonate (also known as soda ash) to treat calcium ion contamination in freshwater and seawater muds from causing clay flocculation and polymer precipitation and lower pH [70] and Quartz. Other ingredients in KCl polymer WBM include non-solid compositions of petroleum distillates (hydrotreated light), 2-Ethyhexanol, ester alcohol, and water.

**Table 5. Solid composition of KCl polymer water-based mud. Adapted from** [72]**.**

| WBM Composition | Weight % |
|---|---|
| Barium sulfate | 15 – 40 |
| Potassium Chloride | 15 – 40 |
| Bentonite | 1 – 5 |
| Limestone | 1 – 5 |
| Kaolin | 1 – 5 |
| Sodium Hydroxide | 1 – 5 |
| Quartz | 1 – 5 |
| Sodium Carbonate | 1 – 5 |

Four commercially available friction-modifying additives were evaluated for their influence on the tirbological performance of the four base fluids. These are Vikinol® 18 (white waxy solid), 6010® (black power of nano-size), EvoLube® G (yellow to dark amber liquid) and Ultra Lube® II (clear brown liquid).

Vikinol® 18 is a dihydroxy alkane with a carbon-based chain including 18 carbon atoms (C18) and hydroxyl terminal groups. It possesses remarkable solubility in organic solvents and oils. It is used in different applications as viscosity modifiers, acid scavenger, or even base oil. It is more polar than the corresponding mono alcohols and has a stronger tendency to form hydrogen bonds. It also has additional benefits including a higher melting point and boiling point than mono-alcohols, good adherence to the metal surface due to a chemical structure of a hydrophobic hydrocarbon tail with a double polar head group, the polar head end adsorbs on metal surfaces and the hydrophobic tail assists in the formation of a lubricant layer [63]. Figure 10 shows the chemical structure of Vikinol® 18.

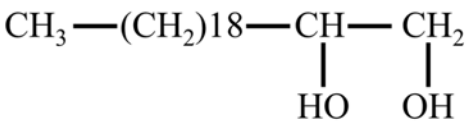


Figure 10. Chemical structure of Vikinol® 18.

6010® is a black friction particle extracted from polymer of cashew-nutshell-liquid. It plays a functional role in stabilizing the coefficient of friction, reducing wear, minimizing noise, vibration [64].

EvoLube® G is an effective performance enhancer for all WBM systems and is ideal for high-temperature applications due to its greater than 400 °F (204 °C) thermal stability, minimizes torque

and drag, thereby enhancing transmission energy to the bit and increasing rate of penetration (ROP) for horizontal drilling applications. It is particularly effective when used in systems formulated with low clay content or in clay-free formulations, such as the KCl polymer WBM. Additionally, EvoLube® G reduces stick-slip, thereby increasing drilling efficiency and reducing drill string damage [65]. It includes carboxyl head group (fatty acid) of petroleum distillates and hydrotreated light and 2, 2, 4-trimethylpentane-1, 3 diol monoisobutyrate (propanoic acid), whose chemical structure is shown on Figure 11.

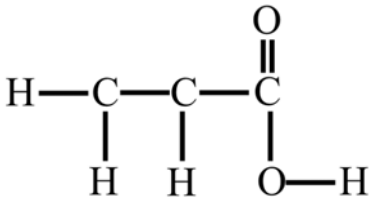

Figure 11. Chemical structure of propanoic acid.

Ultra Lube® II is an amide-based, environmentally safe, and non-flammable lubricant concentrate specifically developed for highly deviated or horizontal drilling applications for both land and offshore use. It has a high affinity for metal surfaces, and will adhere tenaciously to drill pipe and drill collars. It eliminates torque and drag, prevents differential sticking, and protects the drill pipe from corrosion [66]. Amide itself has three varieties. Structure of the head groups are shown in Figure 12.

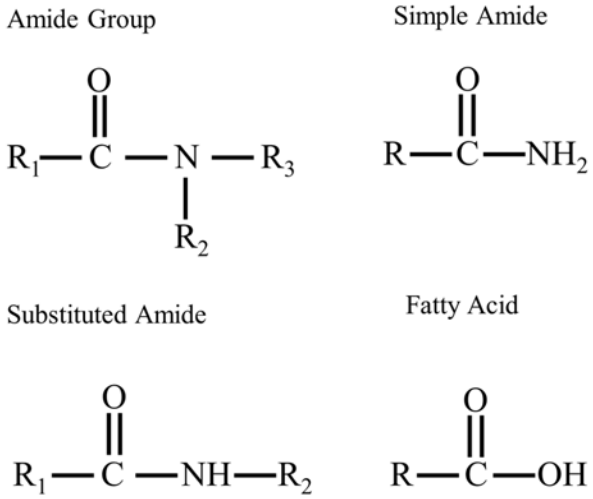

Figure 12. Chemical structure of various amide groups and carboxylic acid. Adapted from [73].

All above-mentioned commercial additives have drawn attention from researchers for their performance-improving potential for both oil-based and water-based drilling fluids, offering promising candidates with alternating tribological properties, although at this moment not all of them have been studied [67,68].

The desired amount of the additive, 2.61 (Vikinol® 18), 2.72 (6010®), 3.12 (EvoLube® G) and 2.69 (Ultra Lube® II) grams per 100 ml of base fluid, was added to the base drilling fluid in a beaker, which corresponds to a volume fraction of 3% (typical to what is used in the field). Each sample was then stirred at a constant speed of 600 rpm for 60 minutes to produce a homogenous suspension/ solution. The temperature of the beaker was heated up to 75 °C and then maintained at the same temperature during additive loading procedure. Figure 13 shows the solubility of each additive, loaded in distilled water and base oil for OBM, before and after full mixing.


Figure 13. Solvability of additives in distilled water and base oil of OBM: (a) Distilled water with additives before mixing; (b) Distilled water with additives after mixing; (c) Base oil loaded with additives before mixing; (d) Base oil with additives after mixing. In all figures, the additives are Vikinol® 18, 6010®, EvoLube® G and Ultra Lube® II, from left to right.

**Preparation of additives-added muds**

The desired amount of the additive, namely, 2.61 (Vikinol® 18), 2.72 (6010®), 3.12 (EvoLube® G) and 2.69 (Ultra Lube® II) grams per 100 ml of base fluid, was added to the base drilling fluid in a beaker, which corresponds to a volume fraction of 3%. Each sample was then stirred at a constant speed of 600 rpm for 60 minutes to produce a homogenous suspension/solution. The temperature of the beaker was heated to 75 °C and then maintained at the same temperature during the addition of the additives. Figure S1 shows the solubility of each additive, added in distilled water and base oil for OBM, before and after full mixing.

Once a test was completed, further examination and analysis of the tested samples was performed, using microscopy, wear track profiling, and surface and tribochemical analyses, using scanning electron microscopy, equipped with an energy dispersive X-ray spectroscopy (SEM-EDS) (JEOL JSM-7500F)**,** and X-ray photoelectron spectroscopy (XPS) (Omicron system with Argus detector). Besides the above-mentioned 4 commercial friction modifying additives, two types of graphene oxides were also introduced into the base fluids for evaluation of their influence on the tribological

performance of drilling mud systems. Table 6 and Table 7 lists the composition, thermophysical and morphological properties of the graphene oxides tested.

Considering the two-dimensional hexagonal lattice typical with graphene, a structure that has been widely applied as a general guidance in lubricant Amphiphile Selection, a commercial graphene product is also investigated for its potential in improving the tribological performance of the same oil-based and water-based drilling fluids, namely OBM, WBM and KCl brine.

**Preparation of graphene-loaded muds**

Figure 14 shows photographs of OBM and WBM loaded with 2.5 wt. % and 5.0 wt. % of graphene after fully mixing, respectively. Figure 15 shows photographs of KCl brine and distilled water loaded with 2.5 wt. % and 5.0 wt. % of graphene after fully mixing, respectively.

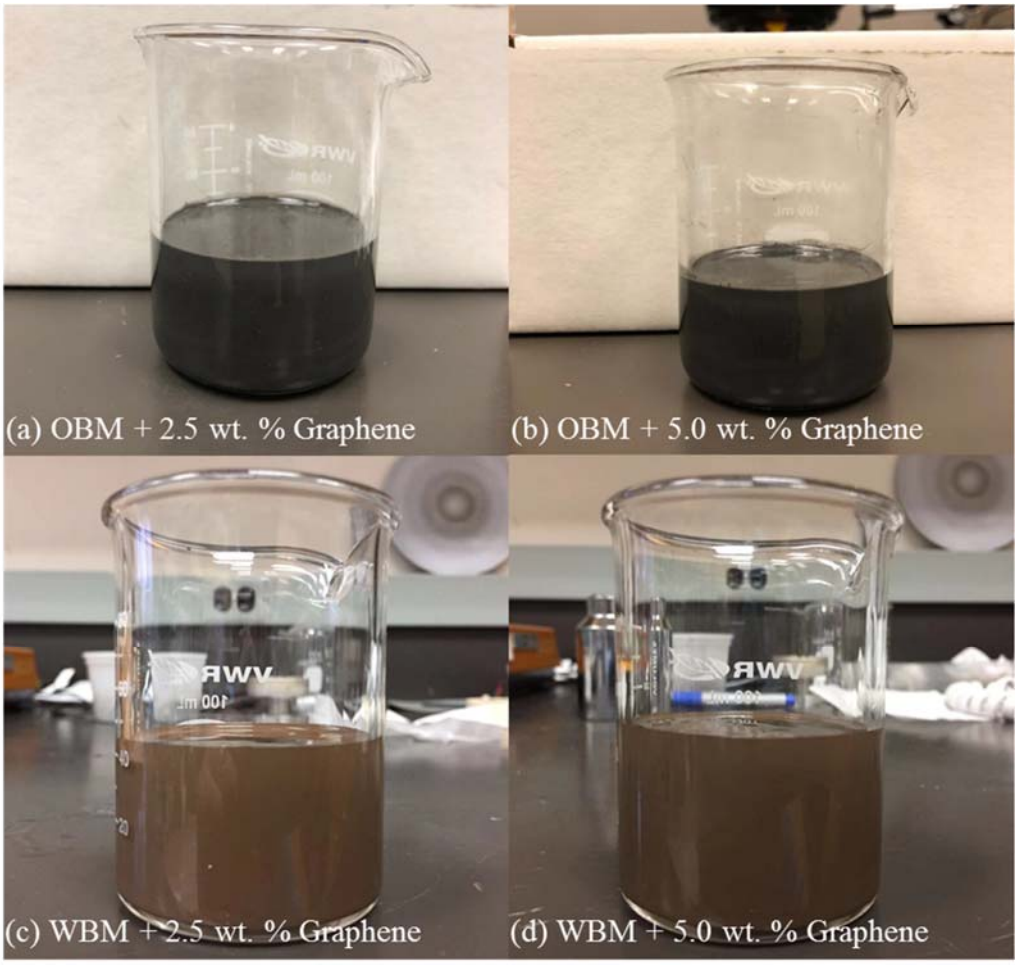


Figure 14. Graphene loaded drilling fluid samples: (a) OBM + 2.5 wt. % graphene; (b) OBM + 5.0 wt. % graphene; (c) WBM + 2.5 wt. % graphene; (d) WBM + 5.0 wt. % graphene.

**Table 6. Composition of graphene added in drilling fluids.**

| **Element Characterizations** | | | | **$C_1S$** | | **$O_1S$** | | **Ratio of $Sp^2/Sp^3$** |
|---|---|---|---|---|---|---|---|---|
| C (%) | O (%) | C (%) with $H_2O$ | C (%) without $H_2O$ | C-O (%) | C=C (%) | C-O (%) | $H_2O$ (%) | $I_{D/G}$ |
| 92.84 | 7.16 | 98.98 | 1.02 | 2.25 | 97.75 | 14.29 | 85.71 | < 0.15 |

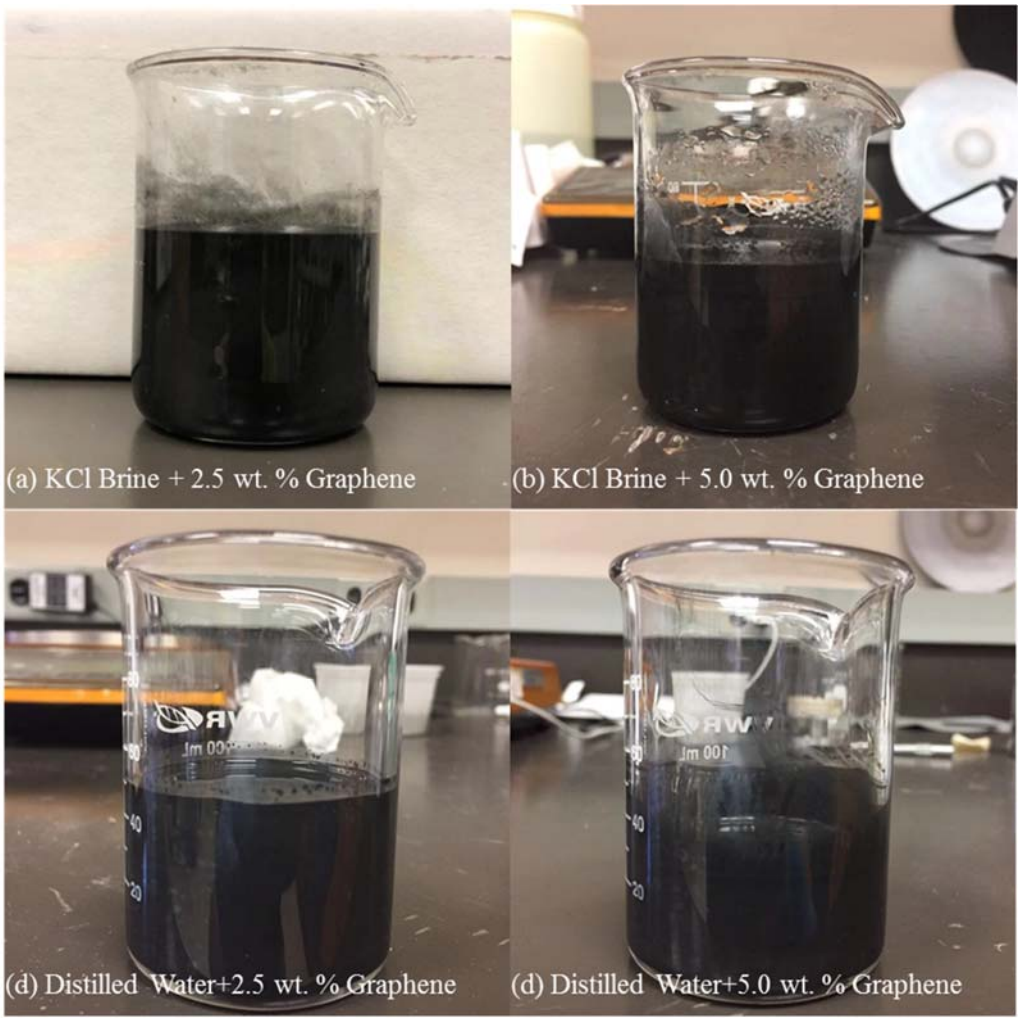

Figure 15. Graphene loaded drilling fluid samples: (a) KCl brine + 2.5 wt. % graphene; (b) KCl brine + 5.0 wt. % graphene; (c) water + 2.5 wt. % graphene; (d) water + 5.0 wt. % graphene.

**Table 7. Thermophysical and morphological attributes of graphene.**

| Thickness | Purity | In-plane dimensions | Electrical conductivity | Physical appearance | Melting point |
|---|---|---|---|---|---|
| < 3 nm | > 99% | 1 – 40 µm | $0.6\times10^{6}$ S/m | Black fine or granulated powder | > 3600 °C |

### 3.2.2 Materials for Tests with UHPT

The wear tests with Falex 4-Ball tester proved that the feasibility of using WBM and KCl brine as competitive replacements of OBM, with the aid of friction-modifying additives. To better simulate the downhole HPHT drilling environment and explore the performance of other water-based drilling fluids, a series of wear tests involving 3 new aqueous (water-based) mud systems were investigated for their tribological performance using UHPT.

Fresh water spud mud, polymer mud, and KCl polymer mud as three novel water-base or aqueous drilling fluid systems are employed in this study. A proprietary Amphiphile S developed by a leading oil & gas company is loaded into the aforesaid water-based drilling fluids for reducing friction and wear rate. As mentioned in the earlier work, comprehensive study investigating and comparing the tribological performance of water-based against oil-based drilling fluids has been few. Further performance screening and evaluation of these three novel aqueous/ water-based drilling fluids and their additive-loaded versions is not available in published literatures. The Amphiphile S used is an amphiphile-featured chemical in the appearance of dark amber liquid. Amphiphile is a chemical that demonstrates both hydrophilic and lipophilic properties, such as soap, detergent, etc. Due to proprietary protection, composition and chemical structures of the Amphiphile S applied in this study is not available. Test samples involved composes two different tribopairs, i.e., O1 stainless steel pin vs. O1 stainless steel disk shown in Figure 16 (a), and hardbanded (hb) pin vs. O1 stainless steel (ss) disk shown in Figure 16 (b).

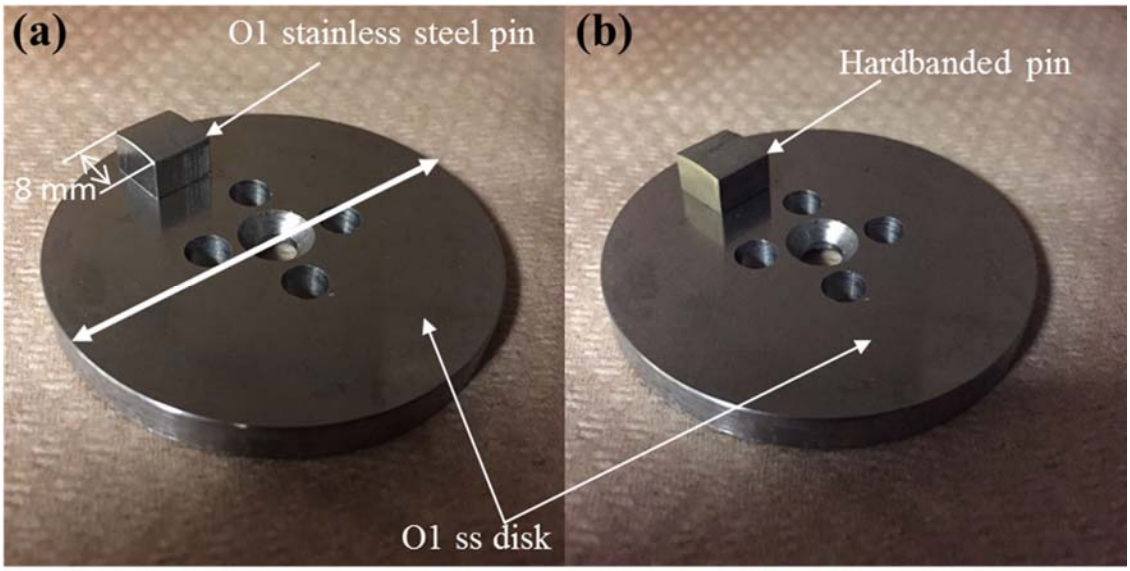


Figure 16. Photograph of tribopairs applied in this study: (a) O1 ss pin vs. O1 ss disk; (b) hardbanded pin vs. O1 ss disk.

**Preparation of Amphiphile S-loaded muds**

The desired amount of the Amphiphile S, 3.12 grams per 100 ml of base fluid, was added to the base aqueous drilling fluid in a beaker, which corresponds to a volume fraction of ~3%. Each sample was then stirred at a constant speed of 600 rpm for 60 minutes to produce homogenous suspension/solution, using a magnetic pill driven by a magnetic heating plate. The temperature of the beaker was heated up to 40 °C and then maintained at the same temperature during loading procedure of Amphiphile S. Figure 1 shows a photo of pure aqueous muds, solubility of the applied additive loaded in these three muds before and after fully mixing. Figure 17 (a-d) show photographs of the pure aqueous muds, Figure 17 (e-h) show the appearance of aqueous muds after loading Amphiphile S but before fully mixing, while Figure 17 (i-l) show the solubility of Amphiphile S in the aqueous muds after fully mixing.

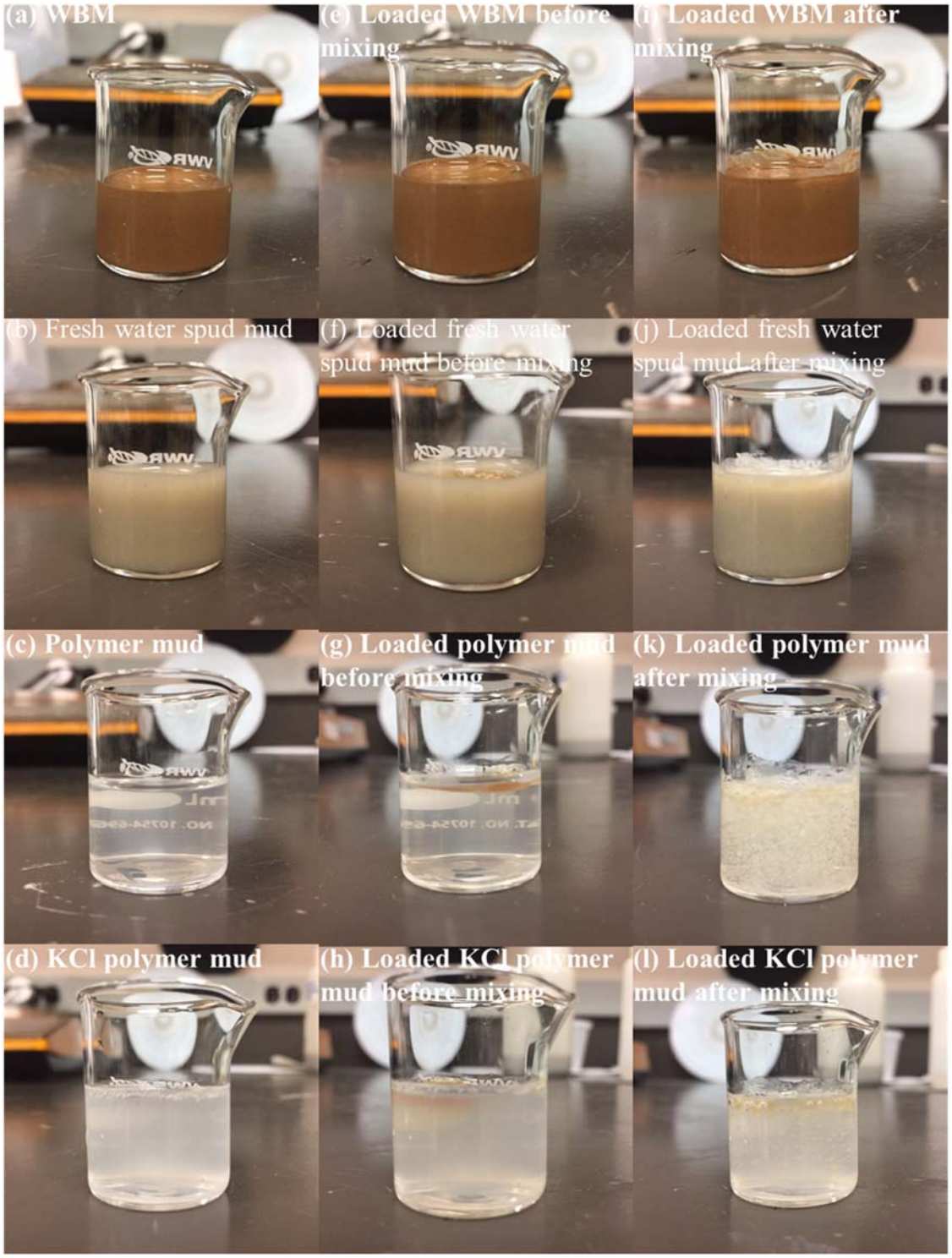


Figure 17. Aqueous muds and solubility of Amphiphile S in them: (a-d) pure aqueous muds; (e-h) loaded aqueous muds before mixing; (i-l) loaded aqueous muds after fully mixing. The based fluid is fresh water spud mud, polymer mud and KCl polymer mud, from top to bottom.

Upon completion of experiments, samples tested were cleaned, further examined and analyzed in terms of wear scar microscopy, 2D/3D wear track profiling, and tribochemical analysis with SEM-EDS (ultra-high emission resolution field emission scanning electron microscope JEOL JSM-7500F are performed.

### 3.2.3 Materials for Tests with Controlled Atmospheric Furnace

The materials used for the self-welding behavior investigation with the Controlled Atmosphere Furnace are nickel alloys Inconel® 617 and 800 HT. Inconel® 617 is a solid-solution, strengthened, nickel-chromium-cobaltmolybdenum alloy with an exceptional combination of high-temperature strength and oxidation resistance. It has excellent resistance to a wide range of corrosive environments, and it is readily formed and welded by conventional techniques. The high nickel and chromium contents make the alloy resistant to a variety of both reducing and oxidizing media. Because of its resistance to high-temperature corrosion, Inconel 617® also offers attractive properties for components of power-generating plants, both fossil fueled and nuclear [74]. Table 8 lists the chemical Composition of Inconel 617®.

800 HT is well known for meeting requirements for a heat- and corrosion-resistant alloy with a relatively low nickel content. For decades it has been widely used for its strength at high temperatures and its ability to resist oxidation, carburization, and other types of high-temperature corrosion [75]. Table 9 lists the chemical Composition of 800 HT®.

**Table 8. Chemical Composition of Inconel 617®. Adapted from** [74]**.**

| **Inconel 617® Composition** | **Weight %** |
|---|---|
| Nickel | 44.5 |
| Chromium | 20.0-24.0 |
| Molybdenum | 10.0- 15.0 |
| Cobalt | 8-10.0 |
| Aluminum | 0.8-1.5 |
| Carbon | 0.05-0.15 |
| Iron | 3.0 Max. |
| Manganese | 1.0 Max. |
| Silicon | 1.0 Max. |
| Sulfur | 0.015 Max. |
| Titanium | 0.6 Max. |
| Copper | 0.5 Max. |
| Boron | 0.006 Max. |

**Table 9. Chemical Composition of 800 HT®. Adapted from** [75]**.**

| **800 HT® Composition** | **Weight %** |
|---|---|
| Nickel | 30.0-35.0 |
| Chromium | 19.0-23.0 |
| Iron | 39.5 Min. |
| Carbon | 0.06-0.10 |
| Aluminum | 0.25-0.60 |
| Titanium | 0.25-0.60 |
| Aluminum + Titanium | 0.85-1.2 |
| ASTM grain size | 5 or coarser |
| Titanium | 0.6 Max. |

Figure 18 shows the dimensions of the nickel alloy samples used for the self-welding experiments. The overall dimension of a single sample is 25 mm in length, 5 mm in height and 10 mm in width. A step with height of 2 mm on the side of the contacting surface and another one with a height of 1 mm on the other side, together demarcate the contacting area from the other surfaces that will be exposed to the atmosphere during the experiment. The maximum available apparent contact area is 10 mm in width, and 15 mm in length.

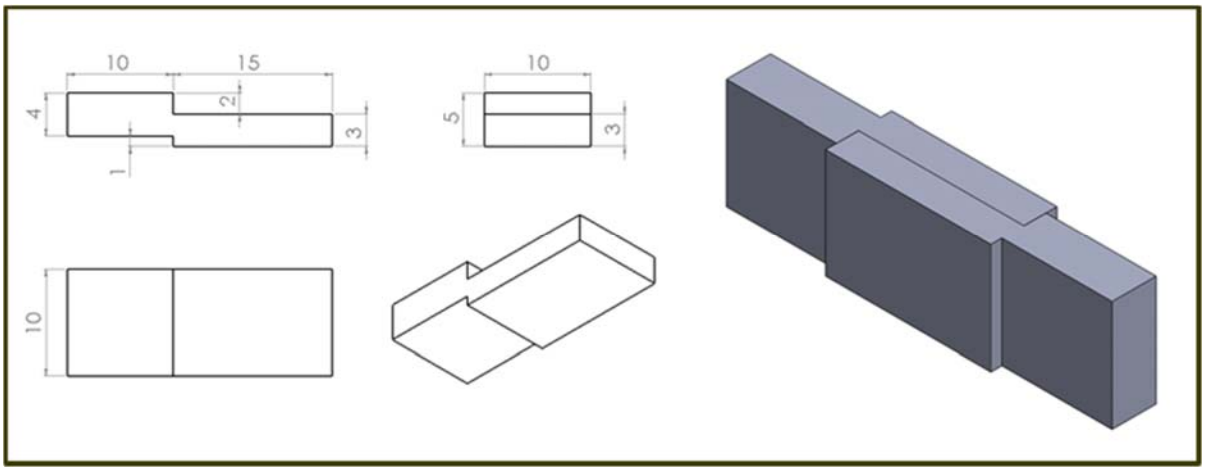

Figure 18. Dimensions of nickel alloys for self-welding experiment.

Figure 19 shows the procedure in which the nickel sample pairs are set up with specified contact pressure through control of the apparent contact area under static load. The material used as static load is Inconel alloy 625, which is resistant to corrosion as well.

Figure 19. Experimental setup for self-welding behavior investigation of Inconel 617® and 800 HT®.

# CHAPTER 4

# INFLUENCE OF ADDITIVES ON THE TRIBOLOGICAL PERFORMANCE OF WATER-BASED AND OIL-BASED MUDS UNDER AMBIENT PRESSURE

Continuous oil & gas exploration has reduced the availability of conventional fossil fuels onshore to a level of scarcity, pushing oil & gas industry to extend their exploration activities from onshore to offshore sites, as well as to unconventional techniques such as shale oil & gas. Accordingly, applied drilling techniques have turned from simpler conventional vertical drilling to extended-reach drilling (ERD), which not only impose new challenges on drilling progress under high pressure and high temperature (HPHT) conditions, but also significantly escalate the importance of considering potential threat to the environment, when selecting drilling fluids to improve the drilling efficiency, and protect the drill bit, and pipelines from potential failures due to excessive heat and material wear during the drilling process.

For ERD drilling under HPHT conditions, both oil-based muds (OBM) and water-based muds (WBM) have been used. OBMs have been a more popular option [76,77] due to their excellent lubricity, shale inhibition, high drilling penetration rates, thermal stability, corrosion-resistance and stable viscosity [15,77,78]. However, OBM also have several concern-raising drawbacks, including high cost, high toxicity, low bio-degradability, environmental contamination, and disposal restrictions, less sensitive to kick due to relatively high gas solubility in OBM [15,77,78]. Further, OBM interferes with the geochemical analysis of cuttings and cores, and for determination of API (American Petroleum Institute) gravity, as OBM masks the oil returned from the formation. Using OBMs also requires extra precautions against allergic reactions due to direct contact with skin and irritating caused by inhalation of the highly volatile fumes from OBM [77]. OBMs can

also damage the rubber parts of the circulating system, making it infeasible to use special oil-resistant rubber components. They are potentially hazardous at high operating temperatures due to low flash point of vapors obtained from volatile ingredients of the oil.

Considerations on the economic and environmental drawbacks of OBMs have attracted attention to WBMs as a promising alternative for OBMs. This has become increasingly urgent as more areas/ regions impose stringent regulations against OBMs, and their cuttings' disposal [15,77]. WBMs automatically resolve most of the disadvantages/concerns of OBMs, by being more cost-effective and eco-friendly [15]. In addition, the immiscibility of formation gas or oil in WBMs not only makes WBMs more reliable in avoiding and detecting formation kick, but also allows a more accurate geochemical analysis of the detected oil. Potential hazardous risks related to inhalation, skin contact, and fire are also eliminated due to WBMs' low toxicity, low volatility, and inflammability. WBMs allow using special oil resistant rubber that is typically needed to protect the drilling equipment from formation of oil and chemicals, without the need for extra drilling equipment modification. The only problem with the WBM is their poor tribological properties. So, different chemicals have been added to WBMs to meet tribological standards, which have been presented by its counterparts, OBMs [78,79].

Potassium, normally in the form of chloride salt, ammonium, and amine-based chemicals are common additives that have been widely added to drilling fluids for shale inhibition [78]. However, WBMs, even after additive treatment, are typically less effective in terms of lubricity and wear resistance than OBMs, rendering it necessary for post-development interference to reduce the friction coefficient (COF) and wear rate of WBMs. To this end, introducing an anti-friction and anti-wear additive is a straight forward and cost-effective approach. Note that the mechanisms through which additives help improve the tribological performance of base fluids are

diverse, including mechanical separation, formation of chemical tribofilms, application of metal soap [2,32,80], and mechanical/chemical polishing. That is, different additives behave differently in various base fluids to optimize the tribological parameters. For instance, long-chain polar compounds (i.e., long-chain alcohols, esters, and fatty acids) act primarily by inducing the "wedging effect" while not by providing direct protection to the metal surface [7,32].

Some wear preventing agents are effective through chemical polishing, by which the load-bearing area increases between the contacting surfaces and hence achieving lower local pressure and temperature [8]. Additives containing phosphorus (P), nitrogen (N), sulfur (S), and chlorine (Cl), which are considered "active elements" for ferrous-based contact surfaces, have been widely used for friction reduction and wear resistance [41]. These additives typically involve the formation of functional groups, phosphate, and sulfide [37,41,81,82] and halide films [83,84] on the surface that attaches to the metal substrate, lowering its melting point and thus maintaining a polish [8]. Introducing 1.5% triphenyl phosphine or triphenyl arsine in white oil leads to a wear prevention factor of 7.2 and 12.2, respectively. Adding 1% long-chain polar compounds result in a wear prevention factor as high as 17.6, showing that the use of long-chain polar compounds in conjunction with chemical polishing agents can be highly effective [8].

Besides COF and wear rate, introducing additives to base fluid can also be beneficial to address seizure between sliding surfaces under extreme pressure (EP) conditions. Remarkable tribological enhancement is obtained after adding chlorinated hydrocarbons (methylene chloride, chloroform, carbon tetrachloride) as additives [42,85–87]. The improvements were attributed to the formation of halide films such as ferrous chloride ($FeCl_2$) on the substrate surface. Oil-based lubricants with nanolamellar disulfide (e.g., $WS_2$, $MoS_2$) additives display better anti-friction and anti-wear performance, than their counterparts of the same disulfide [88].

Other additives that have been proven in their anti-wear effect for water-based fluids include long-chain polyoxyethylene glycol phosphate and zinc salt [39,44]. Recently, nanomaterials have opened a new gateway. Boron nitride (BN) and $Fe_2O_3$ nanoparticles with an insignificant concentration of 0.0095 wt. are able to reduce COF of water-based drilling fluid by 37% and 43%, respectively [45]. Adding nanostructured α-zirconium phosphate into mineral oil and water decreases the COF by 65% and 91%, respectively [89]. Surface-capped Cu nanoparticles improve the tribological performance of distilled water through tribochemical reaction in the sliding between steel surfaces, forming boundary lubrication films consisting of Cu, FeS and $FeSO_4$ on the rubbing surfaces [90]. While there are ample investigations on additives in operating fluids, the literature is absent as far as direct comparison of the effect of additives on both WBMs and OBMs.

Herein, four commercially available friction-modifying additives (Vikinol® 18, 6010®, EvoLube® G, and Ultra Lube® II) and three base fluids (WBM, OBM and KCl brine) were used to investigate their tribological performance. This study provide a direct and systematic comparison of the tribological performance among OBM, WBM and KCl brine and quantitatively evaluates the potential of water-based working fluids as an environmentally-friendly alternative for OBMs in oil & gas production activities. It also provides engineering guidelines for the selection between WBMs and OBMs, as well as promising additives for improved tribological performance improvement of WBMs, OBMS and KCl brine.

### 4.1 Wear Tests

Under similar conditions as in the practical application, wear tests enable direct evaluation of the tribological performance of the drilling fluid from a perspective of how the simulated wear process is influenced, favorably or adversely, and to what extent. Figure 20 shows the results obtained from wear tests with OBM before and after the additives.

Figure 20 (a) shows the COF development profile as a function of time for OBM and additives in OBM solutions/dispersions. At the early period ($0 < t < 20$ minutes), for all working fluids, the difference in the COF was negligible, which could be considered as a running-in stage between the top rotating and bottom stationary balls. As each experiment proceeded ($t > 20$ minutes), deviations became significant, as the system's dependence on the fluid's lubricating performance became more predominant. To better quantify the COF and evaluate the influence of the additives, the average COF is calculated based on the data collected during the last 30 minutes of each test, as shown in Figure 20 (b). Pure OBM showed an average COF of 0.264. Adding Vikinol® 18 and Ultra Lube® II additives reduced the average COF to 0.228 and 0.242, representing 13.6% and 8.3% reductions, respectively. On the other hand, 2.3% and 23.5 % enhancements in the average COF were obtained with EvoLube® G and 6010®, respectively.

Figure 20 (c) shows the average line wear scans of the stationary balls for the OBM and the OBM plus 4 additives. These scans are verified through wear scar size measurement using microscopy images, as shown in Figure 21. Specifically, the results show that the wear scar diameter of pure OBM is 810 µm. With Vikinol® 18, the scar reduced to 735 µm, which is the lowest value among the additives. Unexpectedly, the wear scar diameter of the stationary ball increased to 899 µm for 6010®, to 870 µm for Ultra Lube® II, and to 960 µm for EvoLube®, as better illustrated through wear rate difference shown in Figure 20 (d).

Figure 20 (d) shows a summary of the tribological performance of the tested OBM by plotting the COF vs. wear rate. Vikinol® 18 demonstrated lower values in both COF (by 13.6%) and wear rate (by 9.3%) than that of the pure OBM. Ultra Lube® II showed lower COF (by 8.3%), but higher wear rate (by 7.4%). Additives 6010® and EvoLube® G exhibited deteriorated tribological performance.

Clearly, the OBM itself is very effective in reducing the COF and wear, as compared to its counterparts, WBMs. The base stock of the OBM as the main working fluid Escaid 110, which contains iso- and cycloalkanes [91]. It has a chemical structure of hydrophobic hydrocarbon tails with double polar head groups. The polar head end adsorbs on metal surfaces and the hydrophobic tail assists in the formation of a lubricant layer. A simple comparison shows that Vikinol® 18 resulted in a proper reduction in both COF and wear rate of OBM. The main component of Vikinol® 18 is Dihydroxyl Alkane ($C_{18}H_{38}O_2$), which can easily bond with the OBMs. It contains a large amount of $H^+$ releasing positive charge because of the hydrogen nucleus. This positive charge attracts the hydrogen atoms to electrons on the steel surface. Though the individual bonding is weak, the total bonding caused by a large number of hydrogen atoms in the long chain Dihydroxy Alkane is considerably greater than in a short carbon chain. A shorter carbon chain could therefore be removed more easily by the force acting upon the surfaces. The forces that attract the molecules to the surface must be greater than the forces that attract the molecule to other molecules. So, the possibility of adhering lubricant to the surface increases and friction is reduced by having lubricant molecules rubbing against one another, rather than metal surfaces rubbing together.

Additive 6010® shows no improvement in the tribological properties of OBM. In fact, 6010® additive involves particles of nanoscale size, very close or much smaller than the size of surface asperities and valleys. Therefore, these nanoparticles fail to separate the two sliding surfaces or to

sustain the normal load, resulting in direct metal-to-metal contact. The amide contained in Ultra Lube® II could easily react with the cycloalkanes in the base stock oil and form carboxamide. The good affinity with metal surfaces allows the formation of a protection layer separating the two sliding surfaces, resulting in a COF reduction. However, as the interface temperature increases, amide hydrolyzes and yields the carboxylate ion and ammonia. This may partially corrode the metal surface, removing the protecting layer and exposing the underlying ferrous substrate. EvoLube® G, a fatty acid, becomes thermally unstable when is subjected to heat as the experiment proceeds. Further, fatty acids tend to corrode metal parts and form sludge, causing higher wear than OBM. Table 10 lists the summary of test results for pure OBM and its mixtures with different additives.

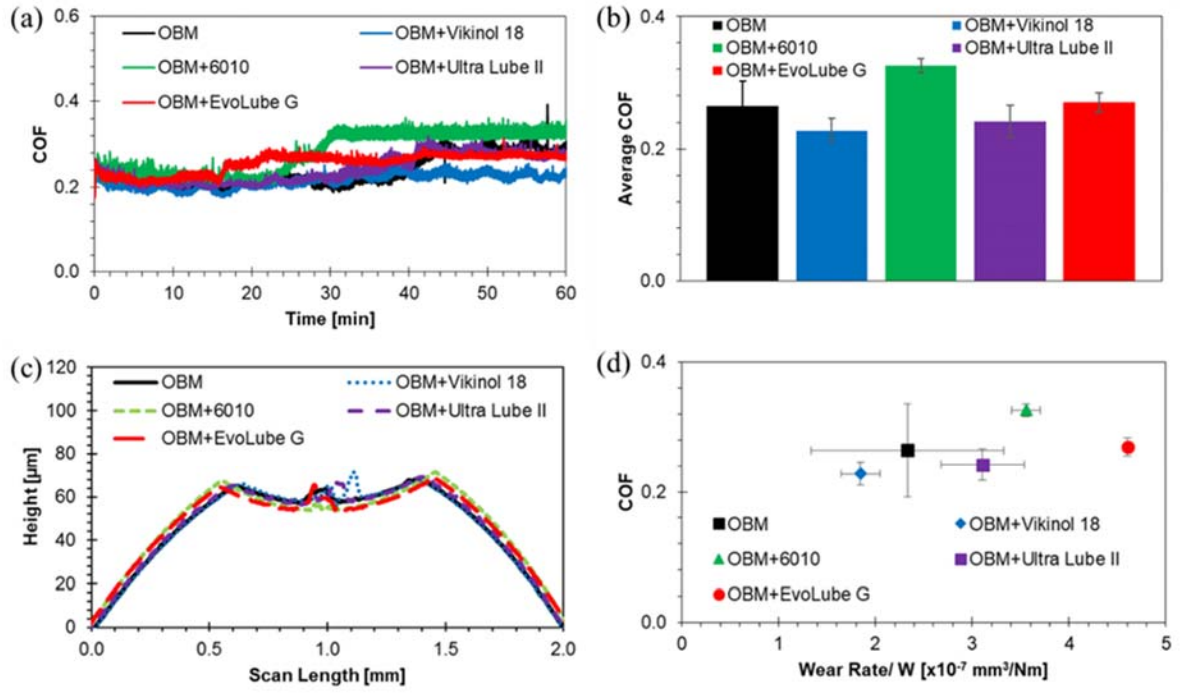


Figure 20. Wear experiment results of OBM before and after loading additives: (a) Development of COF during test procedure; (b) Average COF; (c) COF vs. wear rate; (d) Profilometry of wear scar on stationary ball sample.

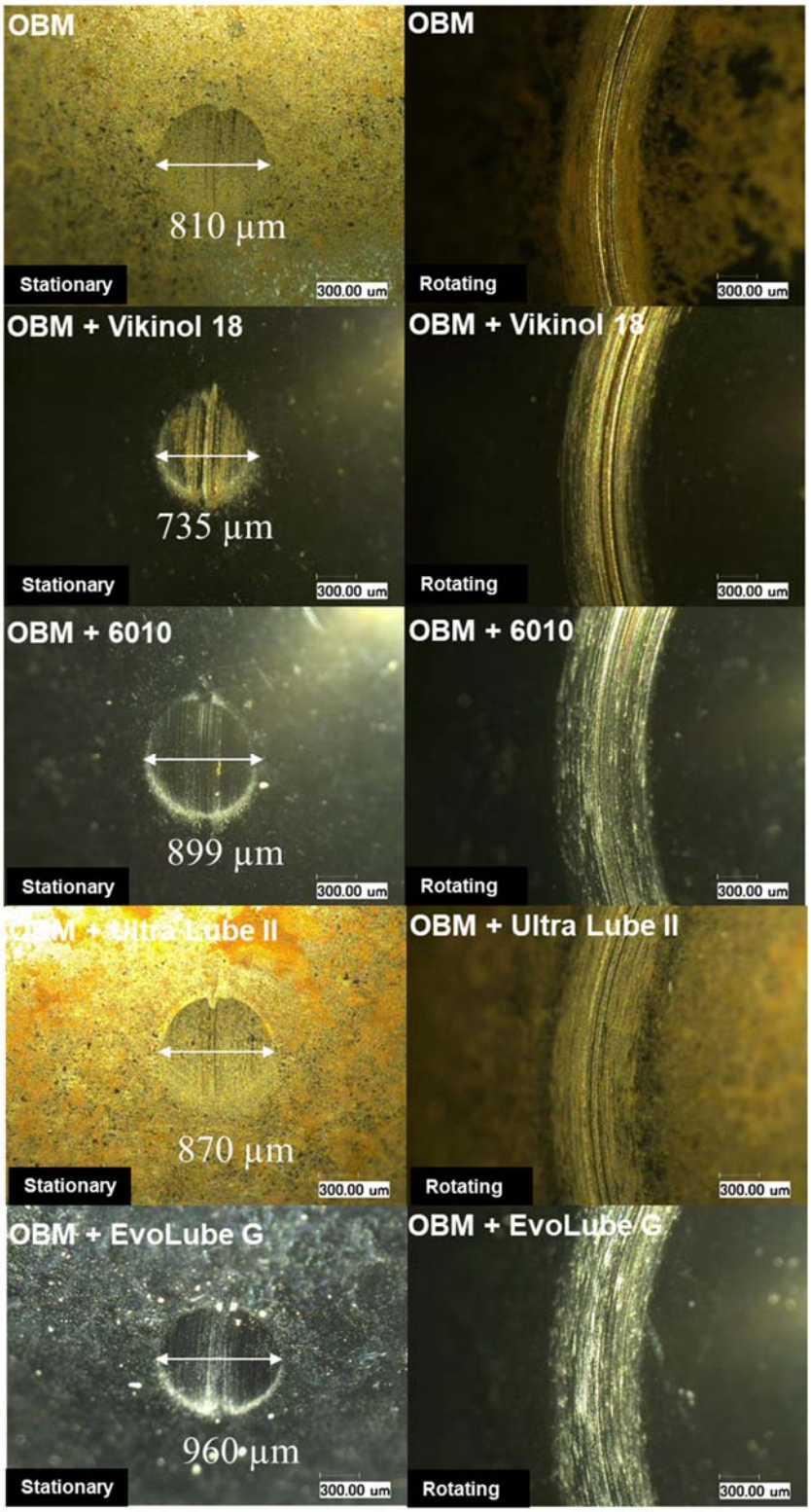


Figure 21. Micro images of stationary and rotating test sample, tested in oil-based mud and without additives using OBM as base mud.

**Table 10. Summary of wear test results for OBM with and without additives.**

| Mixture | COF reduction [%] | Wear diameter [µm] | Wear diameter reduction [%] | Contact pressure [GPa] |
|---|---|---|---|---|
| OBM | N/A | 810 ± 2.05 | N/A | 0.095 |
| OBM+Vikinol® 18 | 13.6% | 735 ± 4.03 | 9.1% | 0.107 |
| OBM+6010® | -23.5% | 899 ± 8.60 | -11.1% | 0.077 |
| OBM+Ultra Lube® II | 8.3% | 870 ± 12.26 | -7.4% | 0.068 |
| OBM+EvoLube® G | -2.3% | 960 ± 3.74 | -18.5% | 0.082 |

Figure 22 shows COF and wear results for pure and with additives WBM. As shown in Figure 22(a), a significant reduction in the COF of WBM was achieved with the addition of EvoLube® G and Vikinol® 18, while COF changes for 6010® and Ultra Lube® II were fairly small. Carboxyl functional groups in EvoLube® G make it partially soluble in aqueous media. So, it may act as a viscosity modifier and improves the lubricity of the WBM with altering viscosity. It is effective when used in systems formulated with low clay content or in clay-free formulations. Carboxyl functional groups are not sufficiently active to chemically bond on the surface and form a protective tribofilm.

Similar to the case with OBM as base fluid, the superior performance of Vikinol® 18 is attributed to the formation of a lubricant layer. Vikinol® 18 is composed of large molecules with hydrophobic hydrocarbon tail and polar head groups. The polar head groups adsorb on metal surfaces and the hydrophobic tail assists in the formation of a lubricant layer. Although chemical ingredients like cycloalkanes contained in OBM is absent in WBM, its relatively higher concentration of solid particles (see SI, i.e., Barium sulfate, Bentonite, Limestone, Kaolin and Quartz) greatly weakens the affinity between its amides and the metal surface, namely less area is covered by the protective layer on the surface due to amides' affinity. Instead, solid particles behaving as third body agents

between the sliding surfaces play a dominant role in this case. While physically increasing the actual load bearing area and reducing the contact pressure, extra frictional forces between these solid particles and the sliding surfaces is inevitable, accompanied by material loss due to abrasion. As mentioned, 6010® particles are of sizes similar to or smaller than the asperities of the sample surfaces. Therefore, even as third body abrasive agents, direct metal-to-metal contact is unavoidable, resulting in insignificant improvement in the system's tribological performance.

The trends of the COF for EvoLube® G and Vikinol® 18 WBM mixtures were similar. A comparison of the average COF in Figure 22 (b) shows that EvoLube® G performs slightly better in lowering the COF, reducing it by 47%, as compared to 44% reduction obtained by Vikinol® 18. Both 6010® and Ultra Lube® II showed less effectiveness, ending up with 8% and 18% reduction in COF, respectively. Despite possessing COF values lower than that of Vikinol® 18, EvoLube® G performed best in reducing wear loss and eventually wear rate, as shown in Figure 22(c) and Figure 22 (d).

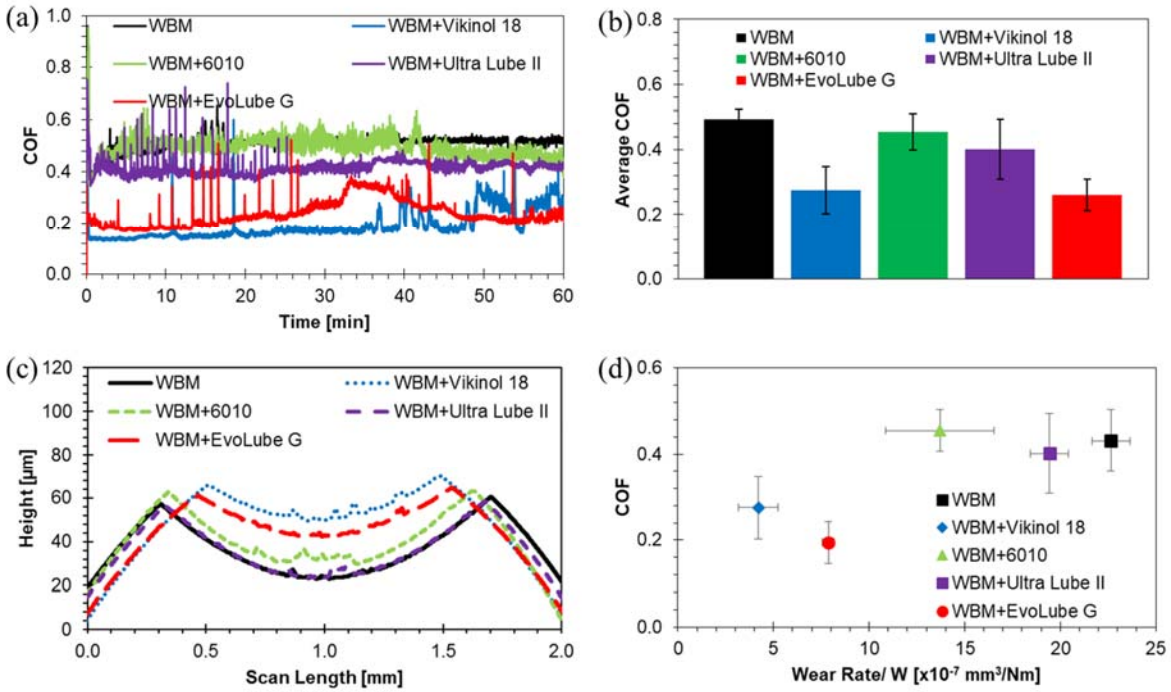


Figure 22. Wear experiment results of WBM before and after loading additives: (a) Development of COF during test procedure; (b) Average COF; (c) Profilometry of wear scar on stationary balls sample; (d) COF vs. wear rate.

With no additives introduced, the average wear scar radius for the stationary balls was 714 μm. Presence of Vikinol® 18 in the WBM decreased the wear scar radius by 35.7% to 459 μm, while EvoLube® G led to a reduction of 23.2% (548 μm). Microscopy images in Figure 23 provide a better visualization in the difference of wear scar size among the stationary balls tested, showing the varying wear-reducing of the four additives on WBM. For samples tested in pure WBM, Vikinol® 18, 6010® and Ultra Lube® II, the rotating balls showed abrasive wear scars on the wear track. On the other hand, the abrasion on the wear track is mild in the presence of EvoLube® G. Also, changes in the width of the wear tracks on the rotating ball samples clearly shows good agreement with the relative superiority in terms of COF values. Table 11 summarizes the wear test results for WBM and its mixtures after adding additives. Compared to OBM, the effect of additives in WBM is more significant as far as improving friction and wear.

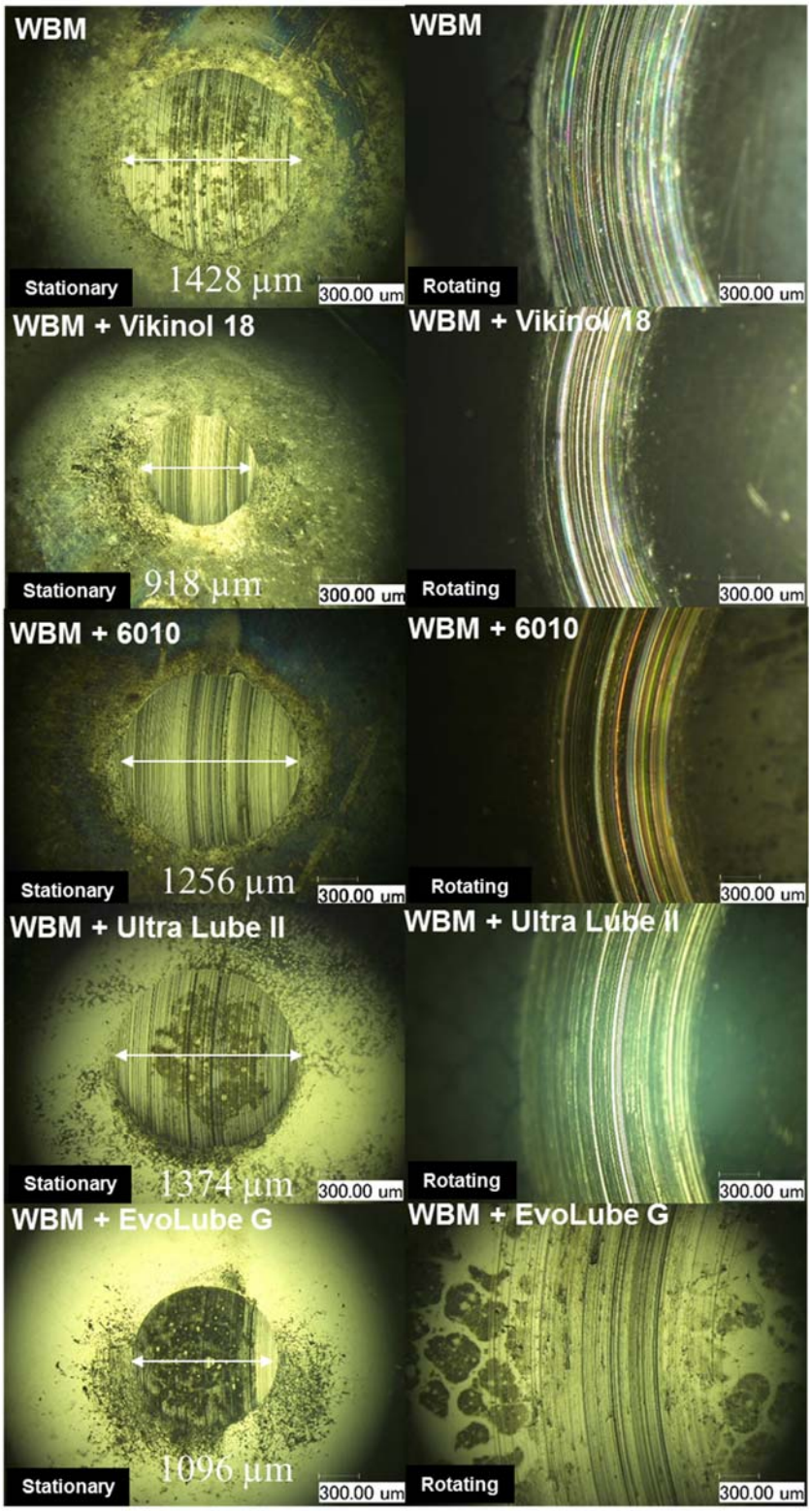


Figure 23. Micro images of stationary and rotating test sample, tested in WBM with and without additives.

**Table 11. Summary of wear test results for WBM with and without additives.**

| Mixture | COF reduction [%] | Wear radius [µm] | Wear radius reduction [%] | Contact pressure [GPa] |
|---|---|---|---|---|
| WBM | N/A | 714 ± 7.03 | N/A | 0.031 |
| WBM + Vikinol® 18 | 44.1% | 459 ± 22.05 | 35.7% | 0.078 |
| WBM + 6010® | 7.7% | 628 ± 37.40 | 12.0% | 0.040 |
| WBM + Ultra Lube® II | 18.5% | 687 ± 8.57 | 3.7% | 0.033 |
| WBM + EvoLube® G | 46.9% | 548 ± 5.36 | 23.2% | 0.052 |

The abundance of problem-causing shales encountered during the drilling process could lead to wellbore instability issues, specifically when WBMs are used as the drilling fluid. So, we repeat the same experiments under the same conditions, e.g., type of additives, temperatures, concentration of additives, and experimental parameters, in the presence of KCl brine as the base fluid. We used KCl since it has been widely introduced in the design of WBM systems as a routine shale inhibitor [92,93]. Figure 24 (a) shows the results for wear tests of KCl brine and its altered versions with additives. As shown in the in-situ COF, the COF of pure KCl brine, Vikinol® 18, and 6010® mixtures show the same trend, ramping up from ~0.20 to ~0.70 within the first 20 minutes, then decreased to a stabilized value of ~ 0.60. On the other hand, Ultra Lube® II and EvoLube® G exhibited stable COF profiles and remained nearly constant at ~0.20, representing drastic reductions in the COF, as compared to the base fluid and the other additives. Figure 24 (b) shows that the average COF of KCl brine was 0.617 ± 0.067, which dropped to 0.608, 0.560, 0.209, and 0.190 after adding Vikinol® 18, 6010®, EvoLube® G and Ultra Lube® II, respectively.

Figure 24 (c) shows the wear tracks on the stationary ball for KCl brine with and without additives. Compared with KCl brine, the addition of Vikinol® 18, 6010® and Ultra Lube® II to the KCl brine significantly reduced the material loss caused by wear. Though the addition of EvoLube® G reduced the COF, the wear scar radius (wear volume) increased. In contrast, the wear scar of the stationary sample tested in Ultra Lube® II showed negligible material loss. Figure 24(d)shows that adding Ultra Lube® II into KCl brine resulted in the lowest values of both COF (69.2% reduction) and wear scar radius (49.4% reduction), rendering it as the best choice for KCl brine among the additives tested. EvoLube® G is the second best additive herein, reducing the COF and wear rate of KCl brine by 66.1% and 25.9%, respectively.

Unlike cycloalkanes as the main components of the OBM, Ultra Lube® II has amide terminal groups, which can easily hydrolyze in KCl brine to form chemical structures, including amine groups. Amine terminal groups can uniformly attach on the steel surface as a protective layer against sliding. In the presence of KCl, the carboxyl terminal groups of EvoLube® G can react with $K^+$ and negatively charged Cl is released. This ion forms a protective halide film (ferrous chloride), which is proven as an efficient tribofilm. EvoLube® G is particularly effective when used in systems formulated with low clay content or in clay-free formulations, like KCl brine.

Vikinol® 18 contains active OH groups. This terminal group can easily react with KCl to form KOH. This balance equation reduced the positive charge, resulting in lack of formation of a tribofilm on the metal surfaces. In addition, KCl brine is essentially a form of simplified artificial sea water, waxy and polymer-featured Vikinol® 18 does not dissolve in KCl brine. So, the emulsion obtained after sonication imposed minor influence on the relative sliding and friction, as well as provided limited buffering effect.

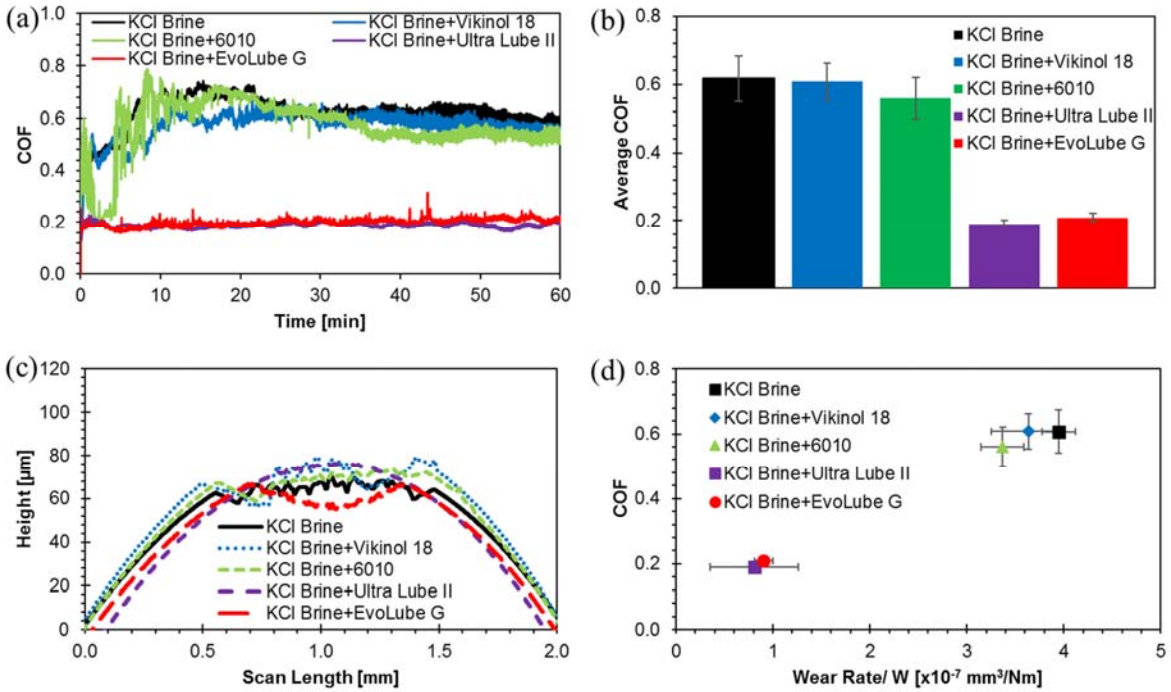


Figure 24. Wear experiment results of KCl brine before and after loading additives: (a) Development of COF during test procedure; (b) Average COF; (c) Profilometry of wear scar on stationary ball sample; (d) COF vs. wear rate.

Figure 25 shows microscopy images for both the rotating and stationary balls. For both KCl brine and its altered versions with Vikinol® 18 and 6010® nanoparticles, the surface finish of the tested samples are very similar to each other (stationary and rotating samples), with no tribofilms developed on the sample surfaces but only signs (blackish areas) of oxidation. However, for KCl brine with Ultra Lube® II and EvoLube® G, layers with certain patterns are noticed for both cases, especially for the samples tested under in EvoLube® G, where a clear snake-skin pattern is observed. The tribolayer might play a key role in the system's superior tribological performance, such as stable and low COF, and reduced wear. Table 12 summarizes the wear test results for KCl brine and its altered versions with additives.

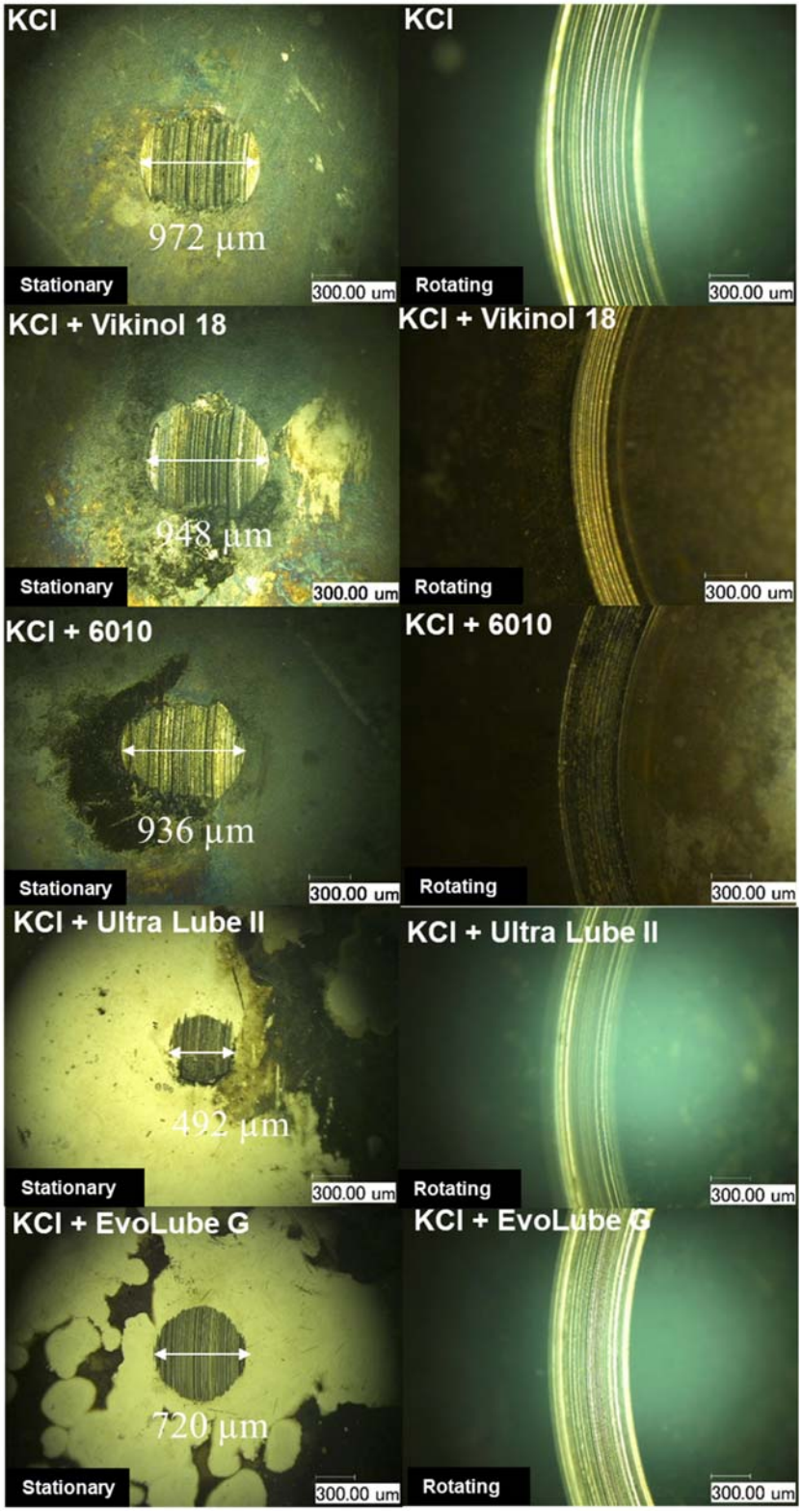


Figure 25. Micro images of stationary and rotating test sample, tested in KCl brine with and without additives.

Figure 26 shows the overall tribological performance comparison among OBM, WBM and KCl brine in pure forms and with the 4 additives. Compared with pure OBM (COF: 0.233; wear rate: $2.82\times10^{-7}$ $mm^3/Nm$), Vikinol® 18 was able to reduce the COF of WBM to a fairly low value of 0.275, though the wear rate was still significantly higher than that of OBM by 49%. Using EvoLube® G and Ultra Lube® II, KCl brine outperformed OBM with 10-18% reduction in COF and 67-71% reduction in wear rate. Based on the above results, the tribological performance of KCl brine can be improved by adding EvoLube® G or Ultra Lube® II, to be competitive against and even supersede conventional OBMs.

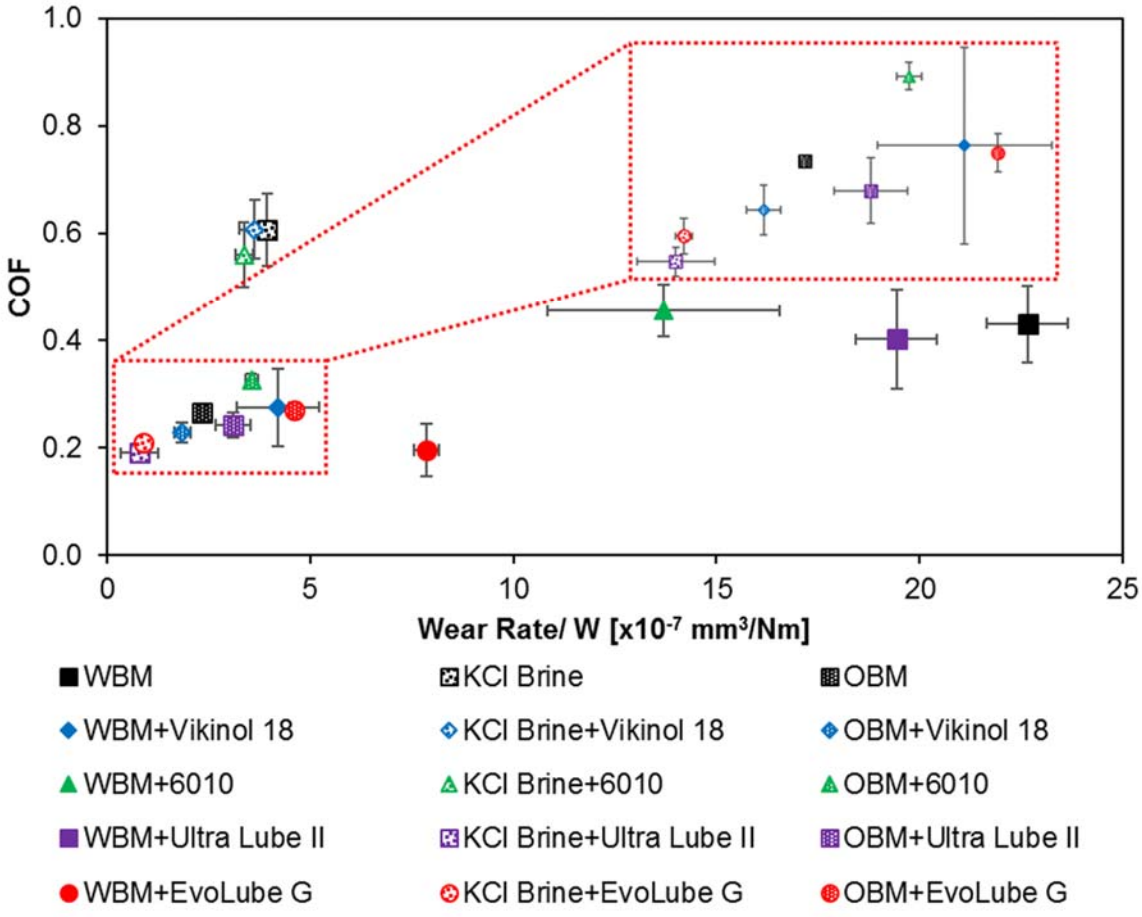


Figure 26. Comprehensive comparison among OBM, WBM and KCl: COF vs. wear rate.

**Table 12. Summary of wear test results for KCl with and without additives.**

| Mixture | COF reduction [%] | Wear radius [µm] | Wear radius reduction | Contact pressure [GPa] |
|---|---|---|---|---|
| KCl | N/A | 486 ± 5.09 | N/A | 0.073 |
| KCl + Vikinol® 18 | 1.5% | 474 ± 12.74 | 2.5% | 0.077 |
| KCl + 6010® | 9.2% | 468 ± 7.21 | 3.7% | 0.079 |
| KCl + Ultra Lube® II | 69.2% | 246 ± 40.61 | 49.4% | 0.179 |
| KCl + EvoLube® G | 66.1% | 360 ± 8.71 | 25.9% | 0.153 |

### 4.2 Stribeck Curve Analysis

The Stribeck curve is a fundamental concept and shows the friction in fluid-lubricated contacts as a function of the contact load, the lubricant viscosity and the lubricant entrainment speed in Figure 27 (a) shows a schematic of the Stribeck curve, showing three regimes of lubrication: (I) boundary, (II) mixed or starved, and (III) hydrodynamic lubrication regimes [94]. At the beginning of the Stribeck curve, there is the highest COF, which could be taken as the static COF. For most material interfaces, static friction is the largest resistive force before the two contacting surfaces start relative movement. In the boundary lubrication regime, there is a layer of lubricant with minute thickness, through which the two counter-acting surfaces experience considerable asperity contact with each other. With the hydrodynamic regime, lubricant film separates the two surfaces and the internal fluid friction alone determines the COF. Mixed lubrication is a regime where boundary and hydrodynamic lubrication coexist with each other, with the fluid film thickness being similar to the surface roughness [94]. In this case, the lubricant film supports more contact load than the boundary lubrication regime. For the Stribeck-type experiments, the most effective additive for different base fluids, EvoLube® G, was selected and tested with OBM, WBM and KCl brine.

Figure 27 (b) shows the COF-speed relationship for the three base fluids and their mixtures with EvoLube® G. As expected, comparing the three base fluids without the additive, the COF of OBM

was significantly lower than WBM and KCl brine. As the sliding speed increased, both OBM and WBM demonstrated a continuous decreasing trend for the COF, while the COF of KCl brine increased as the sliding speed ramped up from 10 to 1200 rpm. It can be concluded that the lubrication regime/s associated with OBM and WBM were both mixed, caused by the presence of the abrasive particles in these two base fluids. On the other hand, pure KCl brine contains no particles and the only ingredient that provides limited lubrication is the dissolved potassium chloride.

The addition of EvoLube® G in both WBM and KCl brine caused a reduction in the COF for the entire speed range. In contrast, negligible drop in the COF was obtained for OBM with EvoLube® G. Specifically, the increasing trend of the COF vs. speed for KCl brine was eliminated after adding EvoLube® G; this is likely because EvoLube® G eliminated the effect brought by increasing the gap between the contacting surfaces through increasing speed, thus avoided the transitioning in lubrication regime from mixed to hydrodynamic. In a nutshell, besides reducing the COF, EvoLube® G extended the speed range for the mixed lubrication with KCl brine.

With OBM or WBM as base fluids, except for COF reduction, similar influence on lubrication regime by EvoLube® G was not observed, as it was dominated by the abrasive particles. It is worth noting that introducing EvoLube® G resulted in COF values even lower than that of OBM for the full speed range, covered in the presence of both WBM and KCl brine. Therefore, as already shown through the wear test results, Stribeck curve analysis further proves that WBM and KCl could be promising and competitive alternatives for OBM with a proper additive.

Table 13 summarizes the test results of the Stribeck curve tests with base fluids and additive EvoLube® G. For OBM as base fluid, introducing EvoLube® G resulted in reduction of COF ranging 3%-17%, with the benefit in reducing COF attenuating along with the increase in the

sliding speed. While for WBM and KCl brine as base fluids, EvoLube® G brought in relatively consistent reduction rate in COF values, 48% - 63% and 60% - 71%, respectively.

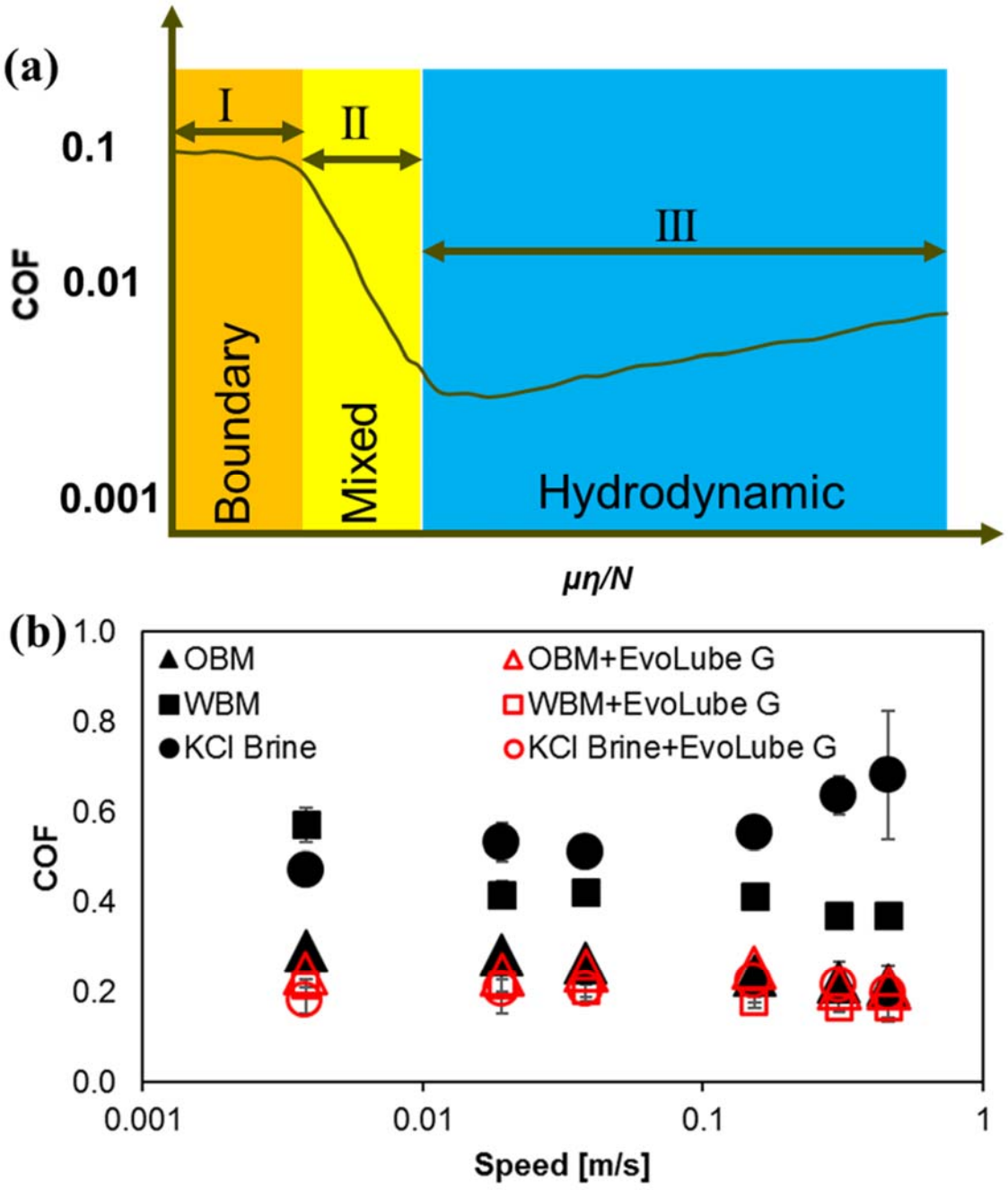


Figure 27. Schematic of the Stribeck curve, (I) boundary, (II) mixed, and (III) hydrodynamic lubrication regimes.

**Table 13. Summary of Stribeck curve tests for base fluid and base fluid + EvoLube® G.**

| Speed [rpm] | Speed [m/s] | OBM | | OBM + EvoLube® G | |
|---|---|---|---|---|---|
| | | COF | ΔCOF | COF | ΔCOF |
| 1200 | 0.459 | 0.216 | 0.017 | 0.210 | 0.016 |
| 800 | 0.306 | 0.222 | 0.014 | 0.210 | 0.029 |
| 400 | 0.153 | 0.237 | 0.015 | 0.254 | 0.015 |
| 100 | 0.038 | 0.265 | 0.014 | 0.249 | 0.018 |
| 50 | 0.019 | 0.283 | 0.012 | 0.240 | 0.008 |
| 10 | 0.004 | 0.292 | 0.012 | 0.242 | 0.007 |
| | | | | | |
| **Speed [rpm]** | **Speed [m/s]** | **WBM** | | **WBM + EvoLube® G** | |
| | | **COF** | **ΔCOF** | **COF** | **ΔCOF** |
| 1200 | 0.459 | 0.384 | 0.102 | 0.171 | 0.034 |
| 800 | 0.306 | 0.373 | 0.055 | 0.167 | 0.013 |
| 400 | 0.153 | 0.410 | 0.046 | 0.178 | 0.012 |
| 100 | 0.038 | 0.423 | 0.028 | 0.201 | 0.015 |
| 50 | 0.019 | 0.417 | 0.052 | 0.215 | 0.013 |
| 10 | 0.004 | 0.571 | 0.030 | 0.214 | 0.015 |
| | | | | | |
| **Speed [rpm]** | **Speed [m/s]** | **KCl Brine** | | **KCl Brine + EvoLube® G** | |
| | | **COF** | **ΔCOF** | **COF** | **ΔCOF** |
| 1200 | 0.459 | 0.677 | 0.138 | 0.199 | 0.030 |
| 800 | 0.306 | 0.640 | 0.057 | 0.214 | 0.018 |
| 400 | 0.153 | 0.559 | 0.031 | 0.223 | 0.020 |
| 100 | 0.038 | 0.513 | 0.029 | 0.207 | 0.026 |
| 50 | 0.019 | 0.531 | 0.042 | 0.206 | 0.031 |
| 10 | 0.004 | 0.472 | 0.030 | 0.183 | 0.039 |

### 4.3 XPS Analysis of Ball Samples Tested with 4-Ball Tester

XPS was employed to study the chemical structure of the wear track and formed tribofilms. To this end, all the treated samples were firstly washed with IPA (isopropyl alcohol) to avoid interferer of untreated elements and then the data were executed. As verified in the previous sections, the tribological performance of OBM and WBM enhanced most in the presence of Vikinol® 18. Also, KCl brine showed remarkable tribological enhancement with the addition of either Ultra Lube® II

or EvoLube® G. Therefore, the possibility of formation a tribofilms in the presence of the most effective additives is investigated via XPS. Note that we found no special element outside of the wear track in all of the samples after washing with IPA. To avoid separation of the tribofilm, we didn't use sonicator and rinsed samples perfectly a couple of times with API. Chemical analysis outside the wear track for the treated samples and non-treated samples done by XPS (Figure 71) were almost the same, verifying the existence of two elements of carbon and oxygen with mean atomic percentages of 90.7 and 9.3, respectively. It can be concluded that there is a passive film on the balls, which is mainly composed of C and O with thickness greater than 10 nm.

Figure 28 presents the XPS survey spectra of the inside wear track for the balls tested in the presence of pure WBM and WBM/Vikinol® 18. As shown in Figure 28 (a), the inside wear track of the WBM treated balls (similar to nontreated sample) contain 16.3% oxygen, ~6.6% greater than the non-treated sample. After the tribo-tests in the presence of WBM/Vikinol® 18, the oxygen atomic percentage jumped to 29.9%. Comparing O1s peaks in the survey spectra presented in Figure 28 (a) and 27 (b) clearly show the higher degree of oxidation with Vikinol® 18. The hydroxyl terminal groups of Vikinol® 18 may bond with the bare iron elements on the surface of the balls and accelerate the oxidation process.

Figure 28 (c) and 27 (d) show the high-resolution Fe 2p spectra of the inside wear track for the balls tested with WBM and WBM/Vikinol® 18. Unlike the non-treated ball with very weak Fe 2p peaks (Figure S2), the tribo-tested balls showed the sharp electron binding energy for Fe $2p_{3/2}$ at ~ 712 eV and Fe $2p_{1/2}$ at ~ 724eV in agreement with reported data [95,96]. After adding Vikinol® 18, three main differences are obtained: (i) an increase in water oxygen content, (ii) a dramatic increase in the energy peak at 710.1 eV, which is attributed to the $Fe^{2+}$ ions, and (iii) the appearance of $Fe^{0}$ species at a binding energy of 707.1 eV [96]. Therefore, the XPS results show

the formation of a thin $Fe_3O_4$ oxide film. Recent studies showed that formation of $Fe_3O_4$ film on the surface can be beneficial in decreasing COF and wear [97]. The presence of $Fe^0$ in the XPS spectrum of WBM/Vikinol® 18 sample was another reason for formation of a thin layer of ferromagnetism [98]. The high-resolution O 1s spectra (Figure 28 (e) and 27(f) were deconvoluted into three components: bonded oxides, hydroxide groups and surface absorbed water. Comparing the O 1s spectra reveals that the percentage of oxygen inside the wear tracks on the balls increased after adding Vikinol® 18.

The same experiments were repeated for the OBM and OBM/Vikinol® 18-treated samples. As shown in Figure 72, no practical difference is obvious after adding Vikinol® 18. The tribological performance results including wear and COF showed small changes after adding Vikinol® 18 into OBM. Therefore, the tribological results and chemical analysis are in a good agreement. However, the insignificant alternation in both COF and wear results may be associated with the change in the viscosity and improved lubricity level of OBM in the presence of Vikinol® 18.

On the other hand, we observed considerable improvements in the COF and wear results after addition of Ultra Lube® II and EvoLube® G into the KCl brine samples. Noteworthy, pure KCl brine showed appropriate tribological performance and better than WBM. Figure 12 shows the survey, Fe 2p and Cl 2p spectra for different samples (balls tested in KCl brine, KCl brine/Ultra Lube® II and KCL brine/EvoLube® G). The main differences between the three sets of samples in the survey results are intensification of the Cl 2p peak and appearance of N 1s peaks after adding both additives. The survey results (Figure 29 (a)-(c)) also show that both oxidation and chlorination occurred after tribotests in the presence of KCl brine.

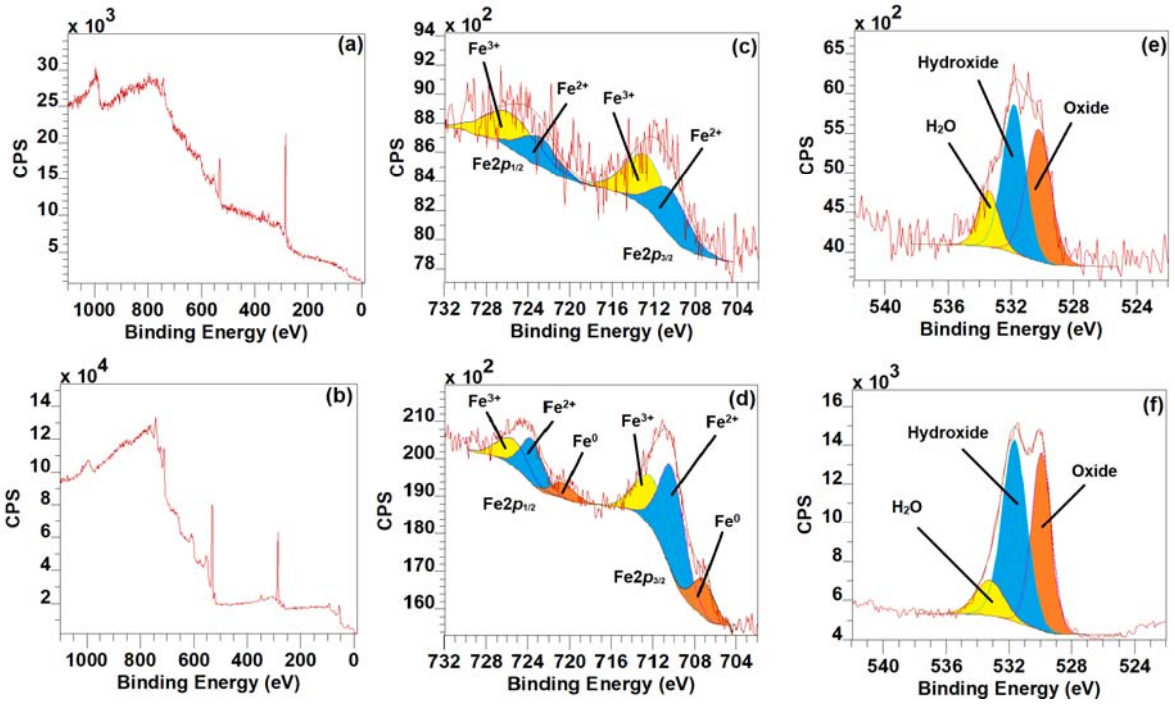


Figure 28. XPS survey spectra on the inside wear track for balls tested in the presence of (a) pure WBM and (b) WBM/ Vikinol® 18. High resolution Fe 2p spectra of balls tested in the presence of (c) pure WBM and (d) WBM/ Vikinol® 18. High resolution O 1s spectra of balls tested in the presence of (e) pure WBM and (f) WBM/ Vikinol® 18.

To find the highlighted elements, Fe 2p and Cl 2p peaks were deconvoluted, confirming published results [99]. Figure 29 (d), 12(e) and 28(f) show the high-resolution Fe 2p spectra of the inside wear track for balls tested in KCl brine, KCl brine/Ultra Lube® II and KCl brine/EvoLube® G, respectively. All the tested balls showed the Fe $2p_{3/2}$ and Fe $2p_{1/2}$ peaks. Although the fitted components are the same for balls treated with KCl brine and KCl brine/EvoLube® G, the relative intensities of the Fe $2p_{3/2}$ and Fe $2p_{1/2}$ peaks enhanced with addition of EvoLube® G into KCl, implying higher percentages of chlorine- or oxygen-containing groups inside the wear tracks [100]. In addition to the above-mentioned peaks, a pre-peak was also initiated in both Fe $2p_{3/2}$ and Fe $2p_{1/2}$ envelopes after adding Ultra Lube® II into KCl brine, which can be assigned to intercalation of Cl in the carbon-based passive layer on balls, or formation of a thin layer of $FeCl_3$.

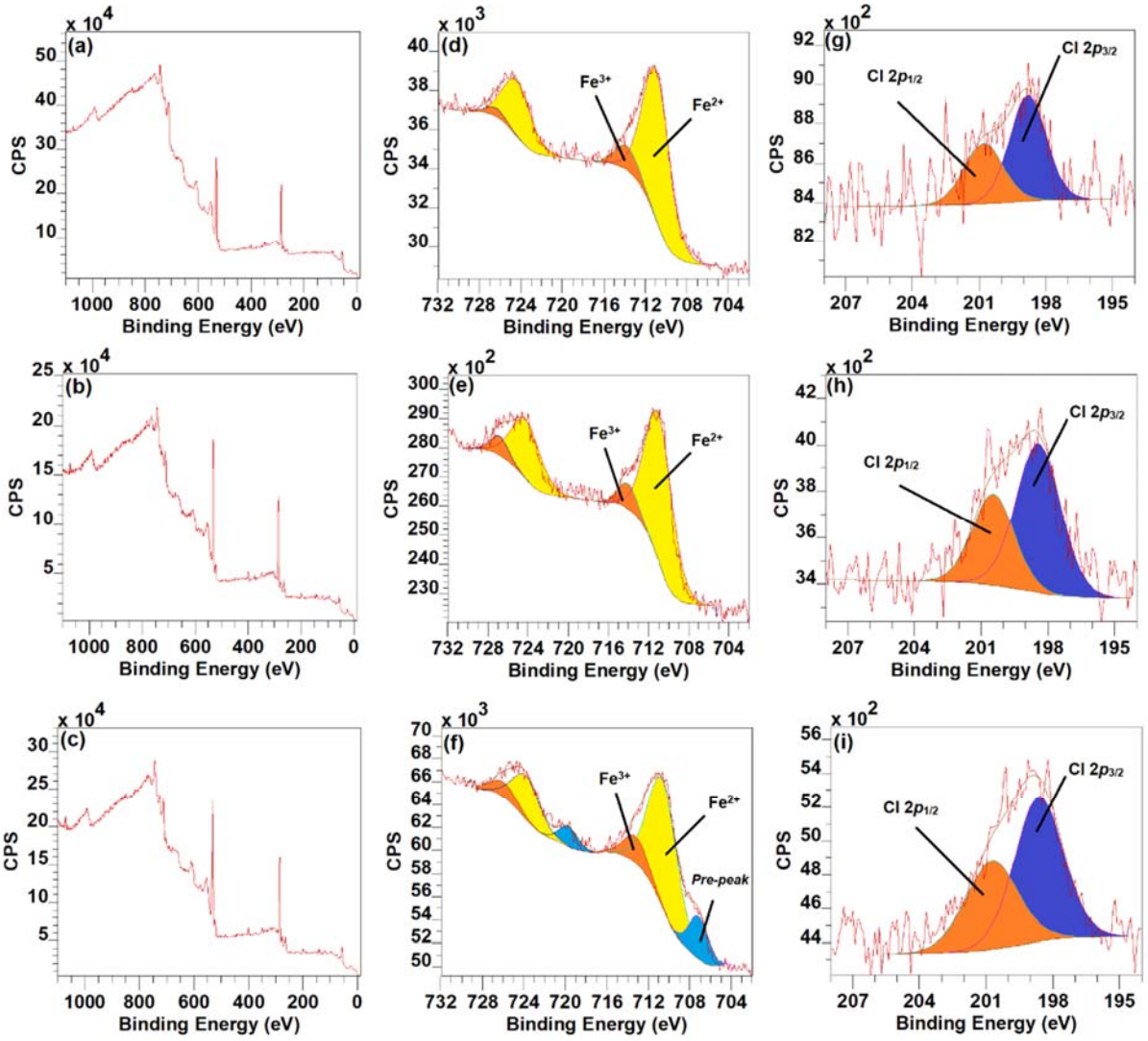


Figure 29. XPS survey spectra of the inside wear tracks for balls tested in the presence of (a) pure KCl brine, (b) KCl brine/ EvoLube® G and (c) KCl brine/ Ultra Lube® II. High resolution Fe 2p spectra of balls tested in the presence of (d) pure KCl brine, (e) KCl brine/ EvoLube® G and (f) KCl brine/ Ultra Lube® II. High resolution Cl 2p spectra of the balls tested in the presence of (g) pure KCl brine, (h) KCl brine/ EvoLube® G and (i) KCl brine/ Ultra Lube® II.

Note that both Fe $2p_{3/2}$ and Fe $2p_{1/2}$ spectra were fitted with two components of $Fe^{2+}$ and $Fe^{3+}$. Presentation of $Fe^{2+}$ and $Fe^{3+}$ make the formation of a thin layer of $FeCl_2$, $Fe_2O_3$, and $Fe_3O_4$ possible. To future verify the presence of $FeCl_2$ thin layer, high-resolution Cl 2p is presented in

Figure 29. The occurrence of Cl $2p_{3/2}$ and Cl $2p_{1/2}$ XPS signals at 198.5 and 200.7 eV can be attributed to the chlorine in $FeCl_2$ and again verifying the formation of a tribofilm inside the wear track [101]. Recent studies showed that formation of $FeCl_2$ layer on the surface can be beneficial in decreasing COF and wear [102,103]. In this case, we have a combination of $FeCl_2$ and $Fe_3O_4$, which is shown to be an effective tribofilm in reducing both wear and COF. Note that employing KCl-based mixtures, the surface color of the balls changed from shiny to dark gray, due to oxidation and chlorination.

### 4.4 Summary

Part of the efforts to explore promising environmentally friendly alternatives for conventional OBM in drilling applications for oil & gas production activities, the current study comprehensively investigated the tribological performance (COF and wear) of WBM and KCl brine, and compared with OBM in the presence of additives. A four-ball experimental configuration was used to evaluate the performance-improving effect of the selected additives. All the experiments were performed at the same operational conditions, i.e., temperature of 75 °C under a normal load of 15 kgf for a duration of 60 minutes, to provide standard conditions for comparison. Adding Vikinol® 18 into OBM reduced the COF by 13.6%, however the other three additives all resulted in increase in the COF. Without interference of additives, the COF of pure WBM (0.493) and KCl (0.617) were significantly higher than that of pure OBM (0.264), by 86.7% and 133.7%, respectively. With additives introduced, the tribological performance of both WBM and KCl was dramatically improved to a level where they were fully competitive against, or even superior, to OBM and its mixtures. Particularly, adding Vikinol® 18 and EvoLube® G to WBM demonstrated an average COF of 0.275 and 0.261, respectively, which were similar to that of pure OBM. Interestingly, the addition of Ultra Lube® II and EvoLube® G in KCl brine reduced the COF of the base fluid from

0.617 to 0.190 and to 0.209, respectively, representing values lower than OBM by 28.0% and 20.1%. Chemical analysis showed the formation of a thin tribolayer of $Fe_3O_4$ in the presence of WBM/Vikinol® 18 and a layer composed of $FeCl_2/Fe_3O_4$ in KCl/Ultra Lube® II. The $FeCl_2/Fe_3O_4$ layer is an effective tribofilm and reduces both COF and wear. Taking into account both wear and COF results, it was found that with the aid of selected friction modifying additives, the tribological performance of environmentally friendly alternatives such as artificial sea water (KCl brine) could be promoted to a level where they are completely qualified replacement for conventional OBM for oil & gas industry.

# CHAPTER 5

# INFLUENCE OF GRAPHENE ON THE TRIBOLOGICAL PERFORMANCE OF WATER-BASED AND OIL-BASED MUDS UNDER AMBIENT PRESSURE

Under exactly the same conditions as applied in Chapter 4, where we investigated the influence of commercial additives on the tribological performance of base drilling fluids, in this chapter the potential anti-friction and anti-wear effects of graphene were evaluated with the same base fluids, considering the fact that graphene is an allotrope of carbon in the form of a single layer of atoms in a two-dimensional hexagonal lattice [104], and the thickness of a single layer of carbon atoms is in the scale of ~0.1 nanometers. Figure 30 shows the scanning electron microscopic image showing the crystalline structure of the graphene tested in this chapter.

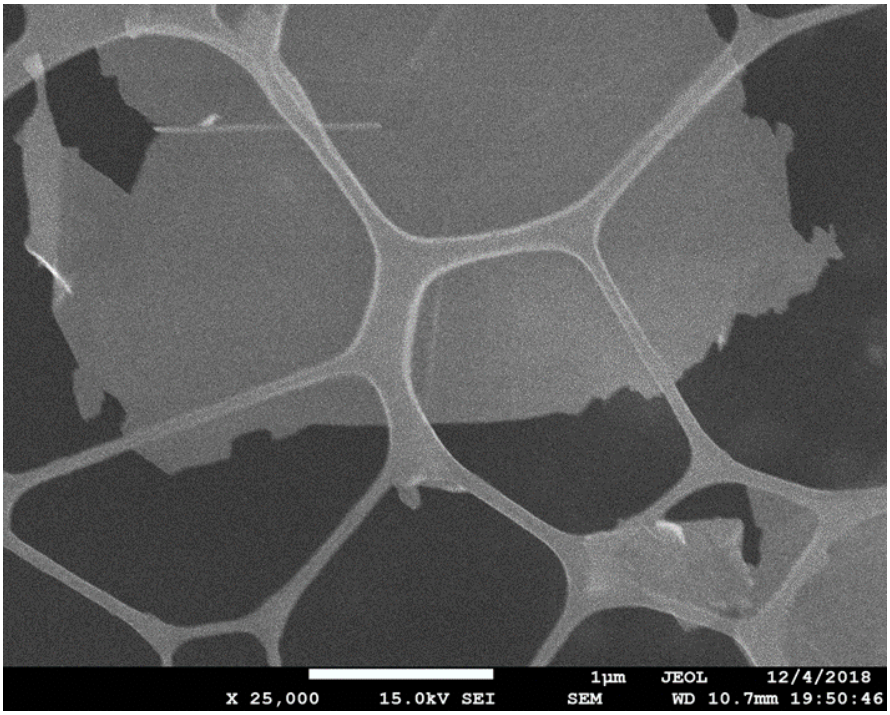


Figure 30. Scanning electron microscopic image of graphene crystalline structure.

### 5.1 Wear Tests

Figure 31 shows the results obtained from wear tests with OBM before and after adding the graphene, with a concentration of 2.5 wt. % and 5.0 wt. %, respectively.

Figure 31 (a) shows the in-situ COF as a function of time for OBM and graphene-added OBM solutions/dispersions. At the early period ($0 < t < 20$ minutes), the difference among all three lubricants in the COF was negligible due to running-in between the top rotating and bottom stationary balls. As each experiment proceeded ($t > 20$ minutes), the deviations between the pure OBM and the graphene-added OBM became more distinguishable, as the system's dependence on the fluid's lubricating performance became more dominant. To better quantify the COF and evaluate the influence of the added graphene, the average COF is calculated based on the data collected during the last 30 minutes of each test, as shown in Figure 31 (b). Pure OBM showed an average COF of 0.264. Adding 2.5 wt. % wt. and 5.0 wt. % graphene reduced the average COF to 0.239 and 0.236, representing a reduction of 9.5% and 10.6%, respectively.

Figure 31 (c) shows the average line wear scans of the stationary balls for the OBM and the OBM plus graphene of 2 different concentrations. These scans are verified through wear scar size measurement using microscopy images, as shown in Figure 32. Specifically, the results show that the wear scar diameter of pure OBM is 810 μm. With 2.5 wt. % graphene, the wear scar was slightly reduced to 784 μm, representing a reduction of 3%. As the concentration increased from 2.5 to 5.0 wt. %, the wear scar diameter was further reduced to 375 μm, representing a significant reduction of 54%, which is the lowest value among the 3 lubricants.

Figure 31 (d) shows a summary of the tribological performance of the tested OBM with and without graphene by plotting the COF vs. wear rate. Adding graphene with two different concentrations resulted in lower COF and lower wear rate. Specifically, adding 2.5 wt. % and 5.0

wt. % graphene demonstrated lower values in COF and wear rate than those of pure OBM. Further increasing the concentration delivered negligible further reduction in COF, but drastic reduction in wear rate. Compared with pure OBM, adding 2.5 wt. % and 5.0 wt. % graphene reduced the wear rate by 12.3% and 95.4%, respectively.

Recall that the OBM has a chemical structure of hydrophobic hydrocarbon tails with double polar head groups. The polar head end adsorbs on metal surfaces and the hydrophobic tail bonds with the graphene lattice forming a physical protection layer between the tribopair sliding against each other. Increase in the concentration of graphene resulted in formation of protection layers of higher density and bonding strength, hence allowing continuous reduction in COF and wear rate, when compared with pure OBM. However, considering the fact that the lubricant viscosity would also increase as graphene of higher concentration is added, it is likely that an optimum concentration may exist for OBM, beyond which the lubricating performance of the added mixture will degrade due to deterioration of lubricity. Table 14 lists the summary of the test results for pure OBM and its mixtures with different concentrations of graphene.

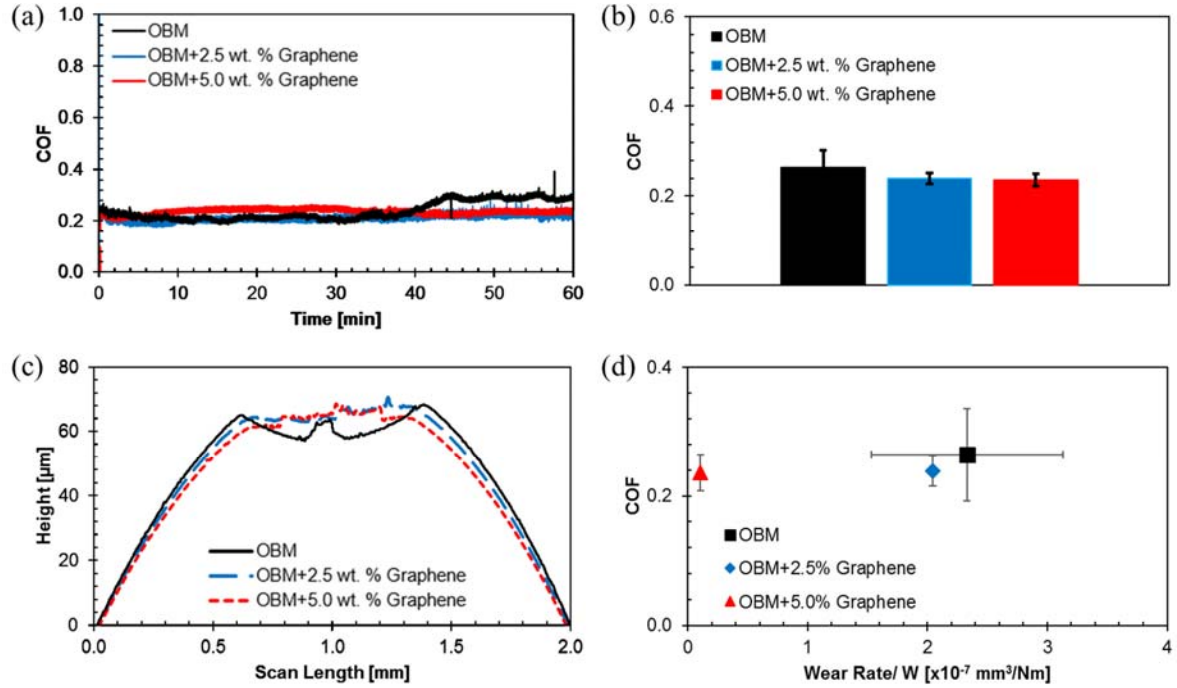


Figure 31. Wear-type experimental results for OBM before and after adding graphene: (a) In-situ COF; (b) Average COF; (c) Profilometric scans of wear scars on stationary balls; (d) COF vs. wear rate. Error bars designate ± 1 standard deviation.

**Table 14. Effect of graphene on the tribological performance of OBM.**

| Mixture | COF reduction | Wear diameter [µm] | Wear rate reduction | Contact pressure [GPa] |
|---|---|---|---|---|
| OBM | N/A | 810 ± 2.05 | N/A | 0.095 |
| OBM+2.5 wt. % Graphene | 9.5% | 784 ± 8.21 | 12.3% | 0.102 |
| OBM+5.0 wt. % Graphene | 10.6% | 375 ± 4.55 | 95.4% | 0.444 |

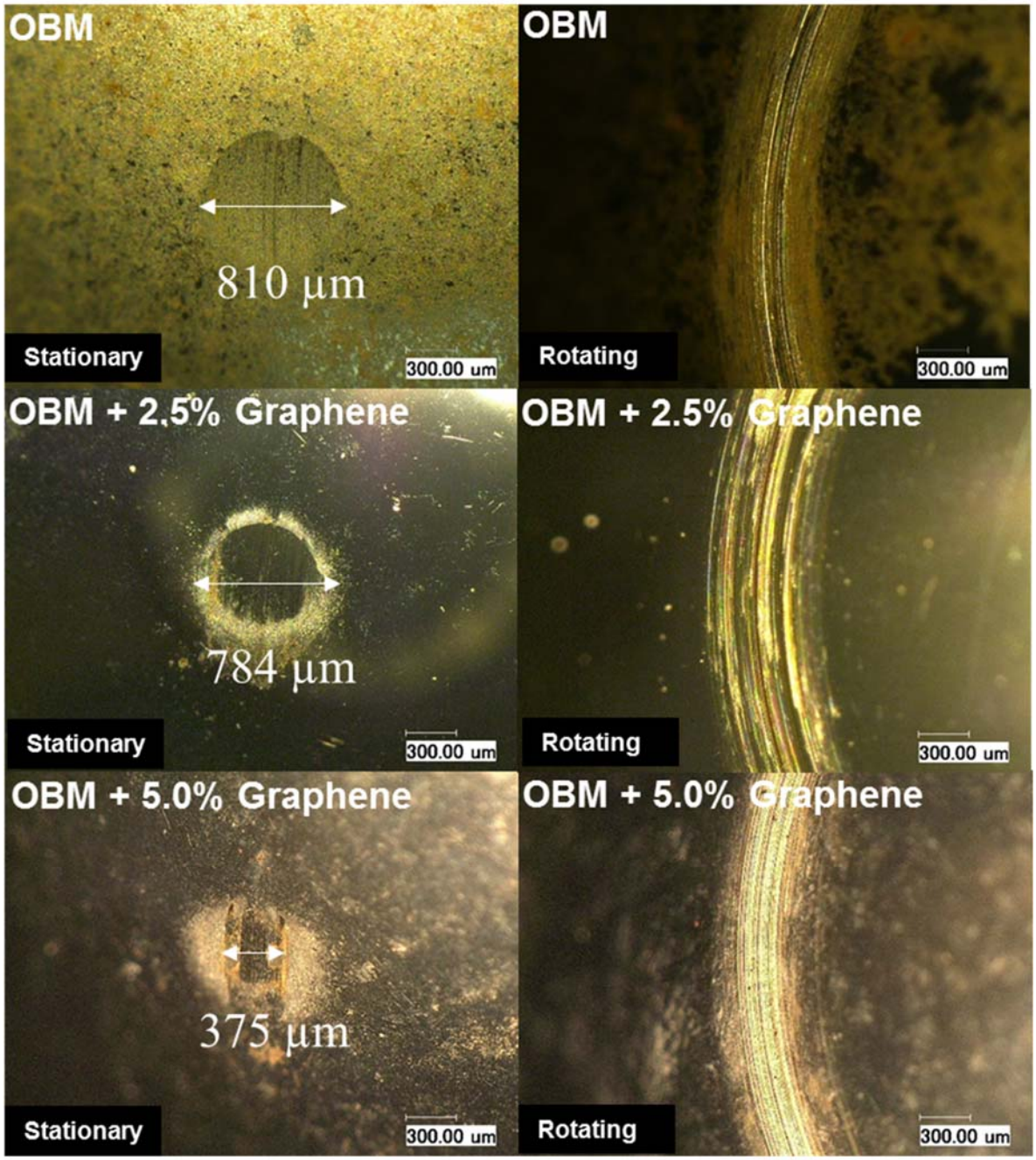

Figure 32. Microscopy images of stationary and rotating test samples, tested in pure and graphene-added OBM.

Figure 33 shows COF and wear results for pure and graphene-added WBM. As shown in Figure 33 (a), the overall development of the COF is fairly stable for all tested lubricants with WBM as the base fluid. This overall stable trend as the COF develops along with time was also observed for tests with OBM and its graphene-added versions, as shown in Figure 31 (a). A significant reduction in the COF of WBM was achieved with the addition of graphene with both concentrations. However, it is noteworthy to realize that as the graphene concentration increased to 5.0 wt. %, increase instead of reduction of COF was observed, as also evidenced by the average COF obtained, based on data recorded during the last 30 minutes of the experiments, shown in Figure 33 (b). Specifically, adding graphene to WBM with a concentration of 2.5 wt. % and 5.0 wt. % resulted in reduction in COF by 16.0% and 13.2%, respectively, as evidenced by a comparison of the average COF in Figure 33 (b), suggesting the existence of an optimum concentration of graphene for best anti-friction performance with WBM as base fluid.

As illustrated in Chapter 4, the relatively higher concentration of solid particles in WBM compared with OBM behaving as third body rolling bearings between the sliding surfaces and play a dominant role in the lubricating performance of the WBM system. These tiny rolling bearings physically increase the actual load bearing area and reduce the contact pressure, inevitably accompanied with extra frictional forces between these solid particles and the sliding surfaces, eventually leading to material loss due to abrasion. Figure 33 (c) shows the linear scan of the wear scar of stationary ball samples tested in pure WBM and its graphene-added versions. With no graphene, the average wear scar radius for the stationary balls was 714 μm. adding 2.5 wt. % graphene decreased the wear scar radius by 19.9% to 572 μm, while 5.0 wt. % graphene led to a reduction by 13.2% with a wear scar radius of 589 μm.

Microscopy images in Figure 34 provide a better visualization in the difference of wear scar size among the stationary balls tested, showing the varying wear-reducing effect depending on the graphene concentration.

Graphene is an allotrope of carbon in the form of a single layer of atoms in a two-dimensional hexagonal lattice [104], and the thickness of a single layer of carbon atoms is in the scale of ~0.1 nanometers. When the concentration is relatively low, considerable amount of sub-nanoscale graphene particles quickly fill-up the gap among asperities, reducing the originally unavoidable metal-on-metal contact, leaving the rolling bearing effect from the solid particles contained in WBM. Further, part of the metal surface area on which the solid particles originally were rolling is now covered by a layer of graphene. Therefore, the lubricity was improved without sacrificing extra material loss due to abrasion caused by direct contact between metal surfaces and abrasive wear, due to solid particles against the raw metal surface. However, despite its strength, graphene is extremely light and has a significant high theoretical specific surface area (SSA) of 2630 $m^2/g$ [105]. Doubling the concentration of added graphene resulted in dramatic increase in the volume of graphene within the same amount of the base WBM, which further filled up the space/ gap among solid particles rolling on the sliding surface as tiny bearings. As the available space for the solid particles to move around between of the sliding surfaces was further reduced, the 'ball bearing' effect benefiting the lubricity was weakened, thus leading to a slight increase in COF and wear rate, as shown in Figure 33 (d). Table 15 summarizes the wear test results for WBM and its mixtures after adding graphene. Compared to OBM, the effect of additives in WBM is more significant as far as improving friction.

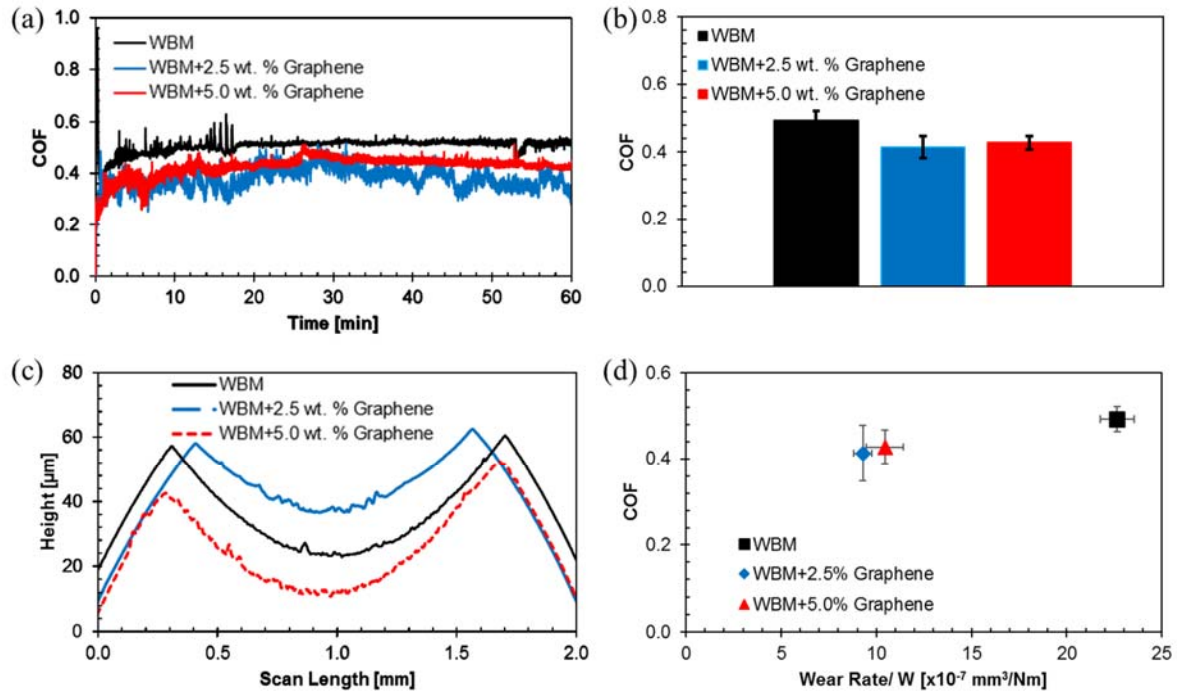


Figure 33. Wear-type experimental results for WBM before and after adding graphene: (a) In-situ COF; (b) Average COF; (c) Profilometric scans of wear scars on stationary balls; (d) COF vs. wear rate. Error bars designate ± 1 standard deviation.

**Table 15. Effect of graphene on the tribological performance of WBM.**

| Mixture | COF reduction [-] | Wear diameter [µm] | Wear rate reduction [-] | Contact pressure [GPa] |
|---|---|---|---|---|
| WBM | N/A | 1428 ± 7.03 | N/A | 0.031 |
| WBM+2.5 wt. % Graphene | 16.0% | 1144 ± 12.93 | 59.0% | 0.048 |
| WBM+5.0 wt. % Graphene | 13.2% | 1178 ± 15.54 | 53.9% | 0.045 |

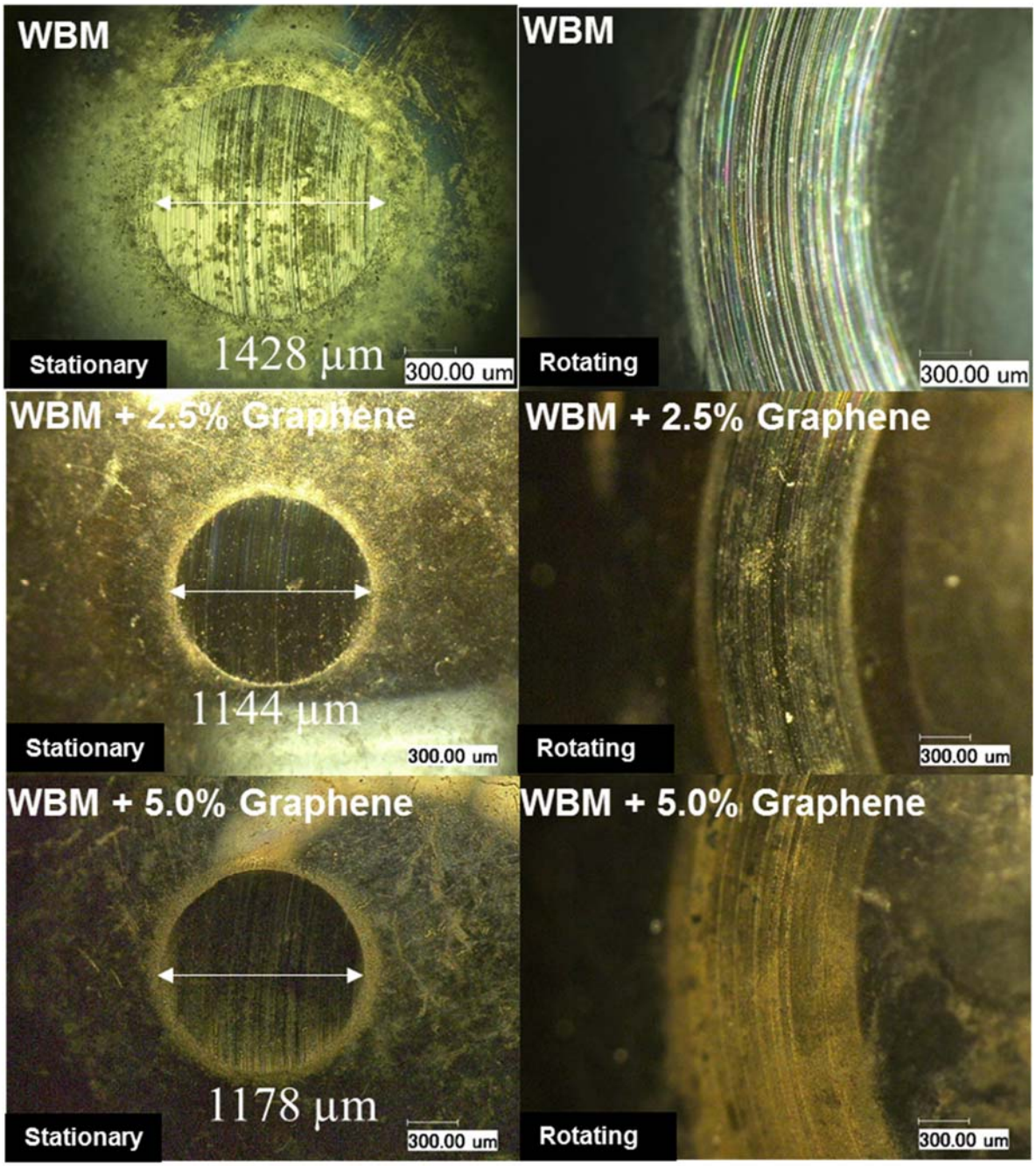

Figure 34. Microscopy images of stationary and rotating test samples, tested in pure and graphene-added WBM.

The potential influence of graphene on the tribological performance of KCl brine was also investigated, as a continuation of the evaluation of commercial friction-modifying additives. Figure 35 (a) shows the results for wear tests of KCl brine and its altered versions with graphene. As shown in the in-situ COF, the COF of pure KCl brine, and introducing graphene into the lubricant resulted in remarkable reduction in COF, with the mixture with 2.5 wt. % graphene being slightly superior to that with 5.0 wt. % graphene. The two graphene mixtures remained nearly constant for the whole test protocol. Figure 35 (b) shows that the average COF dropped from 0.617 with pure KCl brine to 0.246 and 0.266 after loading 2.5 wt. % and 5.0 wt. % graphene, respectively.

Figure 35 (c) shows the wear tracks on the stationary ball for KCl brine with and without graphene. Compared with pure KCl brine, both concentrations of graphene significantly reduced the material loss caused by wear. The wear scar diameter from the two mixtures are very close to each other, with the higher concentration of graphene causing slightly more material loss. Figure 35 (d) shows that adding 2.5 wt. % graphene into KCl brine resulted in the lowest values of both COF (60.1% reduction) and wear scar radius (16.7% reduction), rendering it as the better choice of concentration for KCl brine. Graphene with a concentration of 5.0 wt. % resulted in reduction in COF and wear scar radius of KCl brine by 56.9% and 6.3%, respectively.

Figure 36 shows microscopy images for both the rotating and stationary balls. For KCl brine added with both concentrations of graphene, the surface finish of the tested samples are similar to each other (stationary and rotating samples). Off the wear scars/ tracks, sample surfaces are covered by a black layer, which is likely a result of the sub-nanoscale graphene particles being rubbed into the substrate surfaces, and also possibly signs of oxidation.

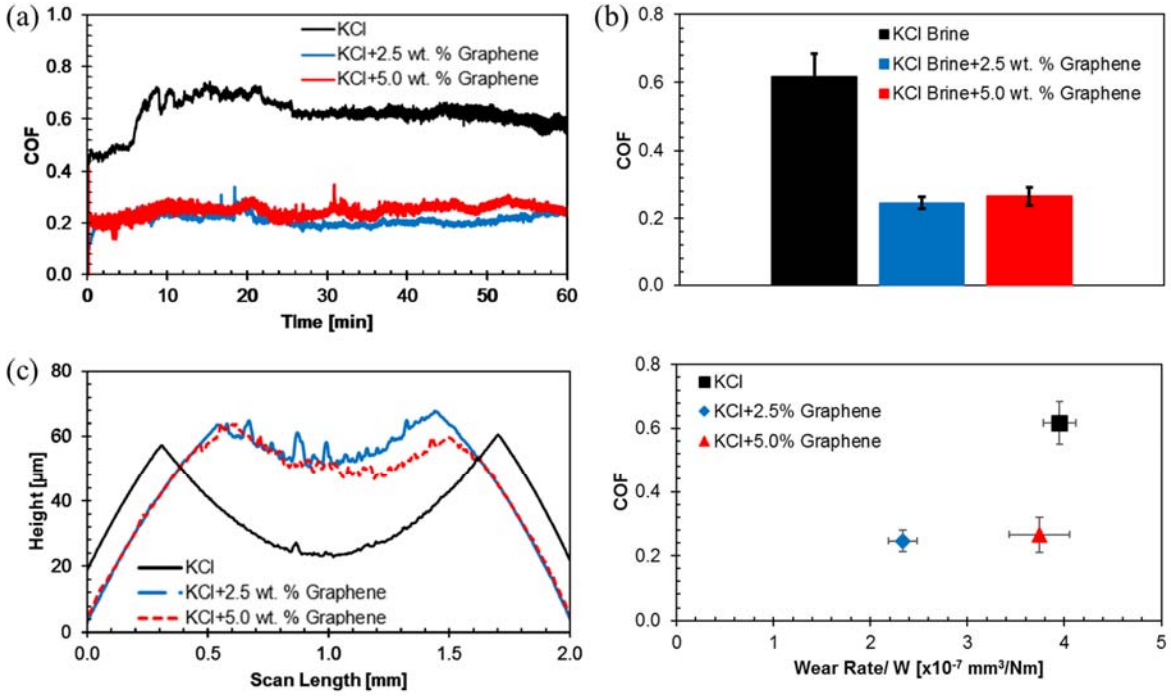


Figure 35. Wear-type experimental results for KCl brine before and after adding graphene: (a) In-situ COF; (b) Average COF; (c) Profilometric scans of wear scars on stationary balls; (d) COF vs. wear rate. Error bars designate ± 1 standard deviation.

This tribolayer might have played an important role in improving the system's tribological performance, delivering a stable and lower COF, and reduced wear. Table 16 summarizes the wear test results for KCl brine and its altered versions with graphene.

**Table 16. Effect of graphene on the tribological performance of KCl brine.**

| Mixture | COF reduction [%] | Wear diameter [µm] | Wear rate reduction [-] | Contact pressure [GPa] |
|---|---|---|---|---|
| KCl Brine | N/A | 972 ± 5.09 | N/A | 0.073 |
| KCl Brine+2.5 wt. % Graphene | 60.1% | 810 ± 9.42 | 40.9% | 0.095 |
| KCl Brine+5.0 wt. % Graphene | 56.9% | 911 ± 1.94 | 5.3% | 0.075 |

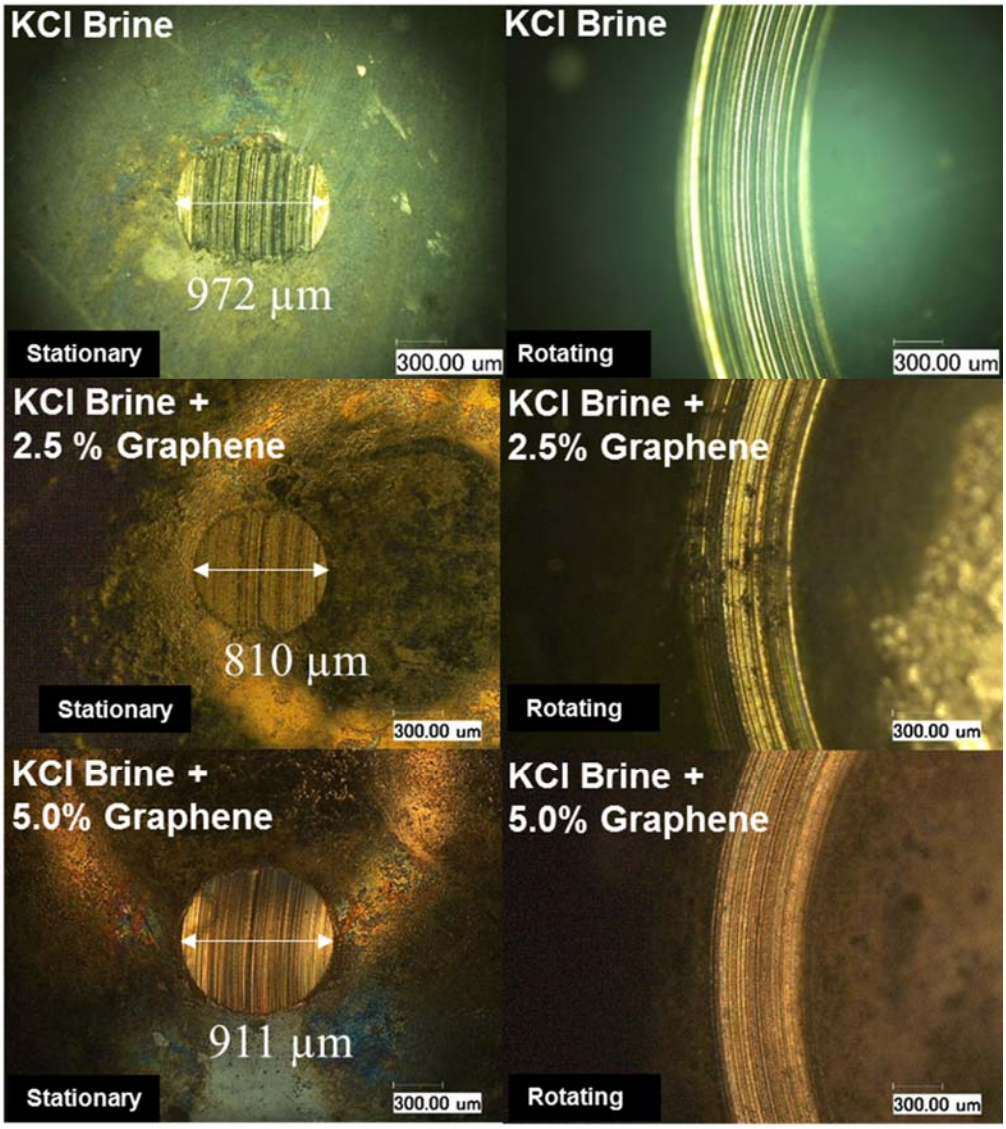


Figure 36. Microscopy images of stationary and rotating test samples, tested in pure and graphene-added KCl brine.

Water in general is well known for its deficiency in lubricity and anti-wear properties. Without tailoring its tribological performance with the help of target chemicals or functional groups, it is never any close to be considered as a potential drilling fluid. However, considering the fact that graphene/ graphene-based additives function through their layered/ cubic crystalline structures,

which is a physical lubricating mechanism rather than chemical, the tribological performance of graphene-added distilled water was investigated in this study.

For the purpose of comparison, wear tests with pure distilled water under the same test protocol were first performed, however, the test was aborted due to excessive friction. Figure 37 shows COF and wear results for distilled water added with two concentrations of graphene. As shown in Figure 37 (a), presence of graphene resulted in superior anti-friction performance, the COF development was rather low and stable for the whole test process.

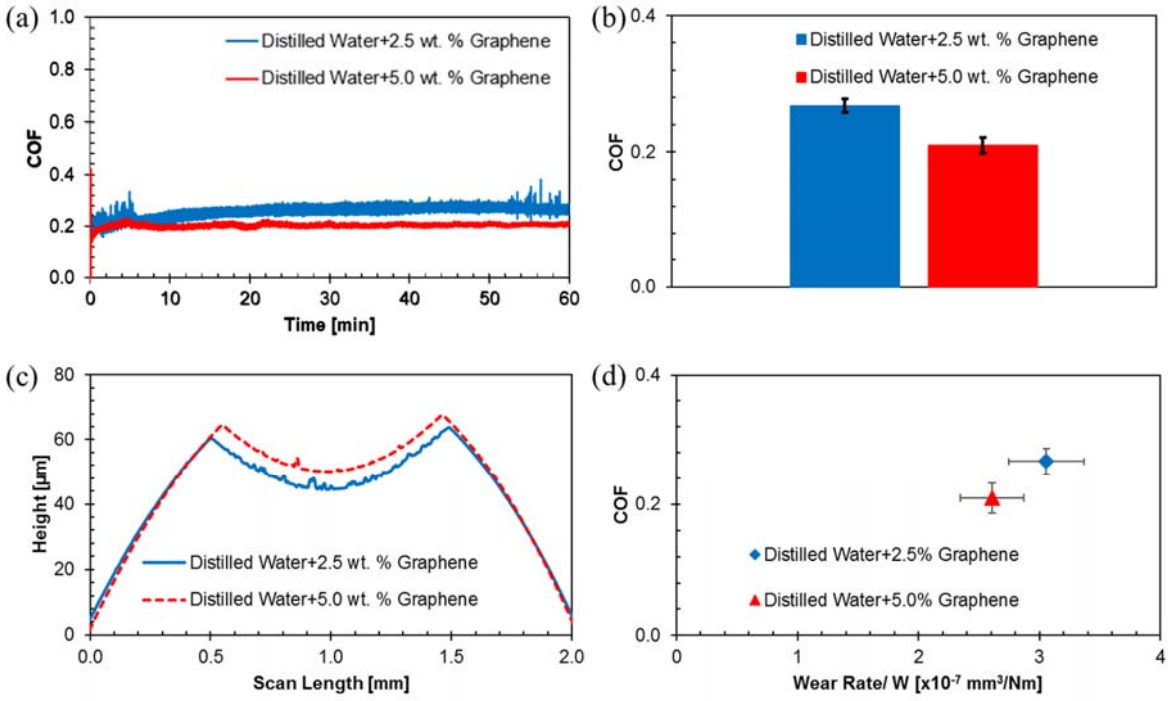


Figure 37. Wear-type experimental results for distilled water after adding graphene: (a) In-situ COF; (b) Average COF; (c) Profilometric scans of wear scars on stationary balls; (d) COF vs. wear rate. Error bars designate ± 1 standard deviation.

At the beginning and the end of the test, the lower concentration of graphene demonstrated limited fluctuation in COF, while the higher 5.0 wt. % graphene delivered a nearly constant COF at ~0.20.

Figure 37 (b) shows the average COF obtained as 0.267 and 0.210, for 2.5 wt. % and 5.0 wt. % graphene mixed with distilled water, respectively. Figure 37 (c) shows that a higher concentration of graphene further reduced the wear scar, as better illustrated in Figure 37 (d) showing the COF versus wear rate. Figure 38 shows the microscopic images of stationary and rotating test samples tested in graphene added distilled water. The samples surfaces do not show any obvious tribofilms, confirming that the layered crystalline structure of the added graphene has been the main contributing factor towards the survival and superior lubricating performance of the mixture.

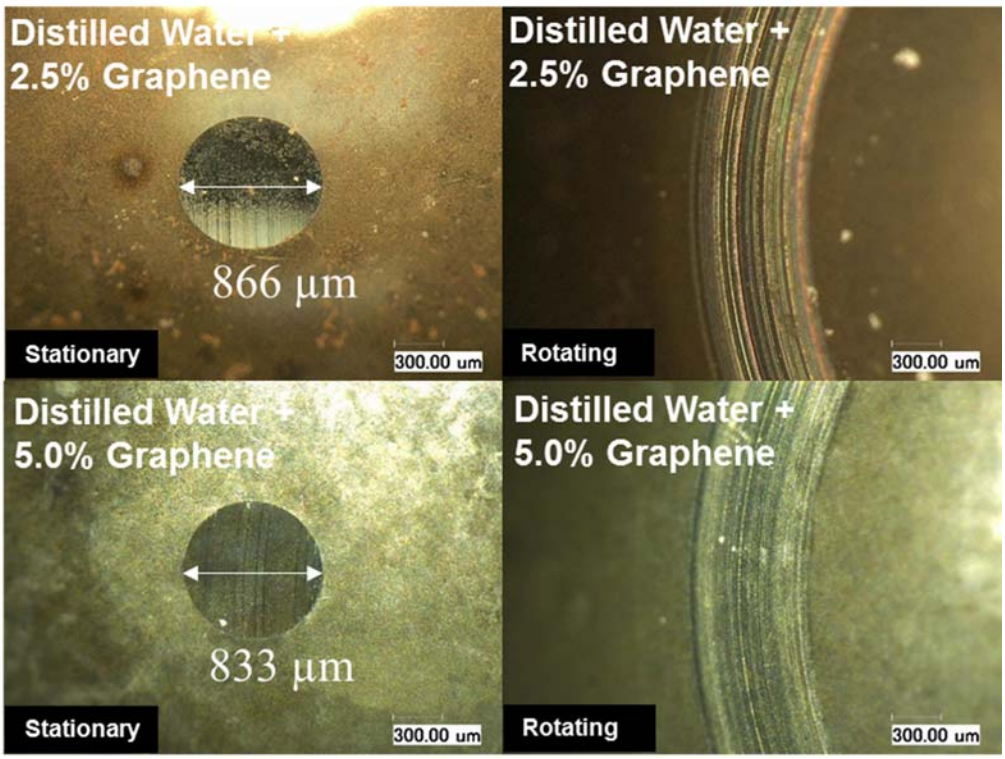

Figure 38. Microscopy images of stationary and rotating test samples, tested in distilled water added with graphene.

As illustrated above, adding graphene with either concentrations improved the tirbological performance of all the three base fluids, as well as distilled water, Figure 39 shows the overall tribological performance comparison among OBM, WBM and KCl brine, each added with 2.5 wt. % and 5.0 wt. % graphene, respectively. Except for WBM/ graphene mixtures, both KCl brine and distilled water demonstrated COFs very close to and even lower than those obtained from OBM/ graphene mixtures, with slightly higher wear rates. Table 17 summarizes the wear test results for distilled water added with graphene.

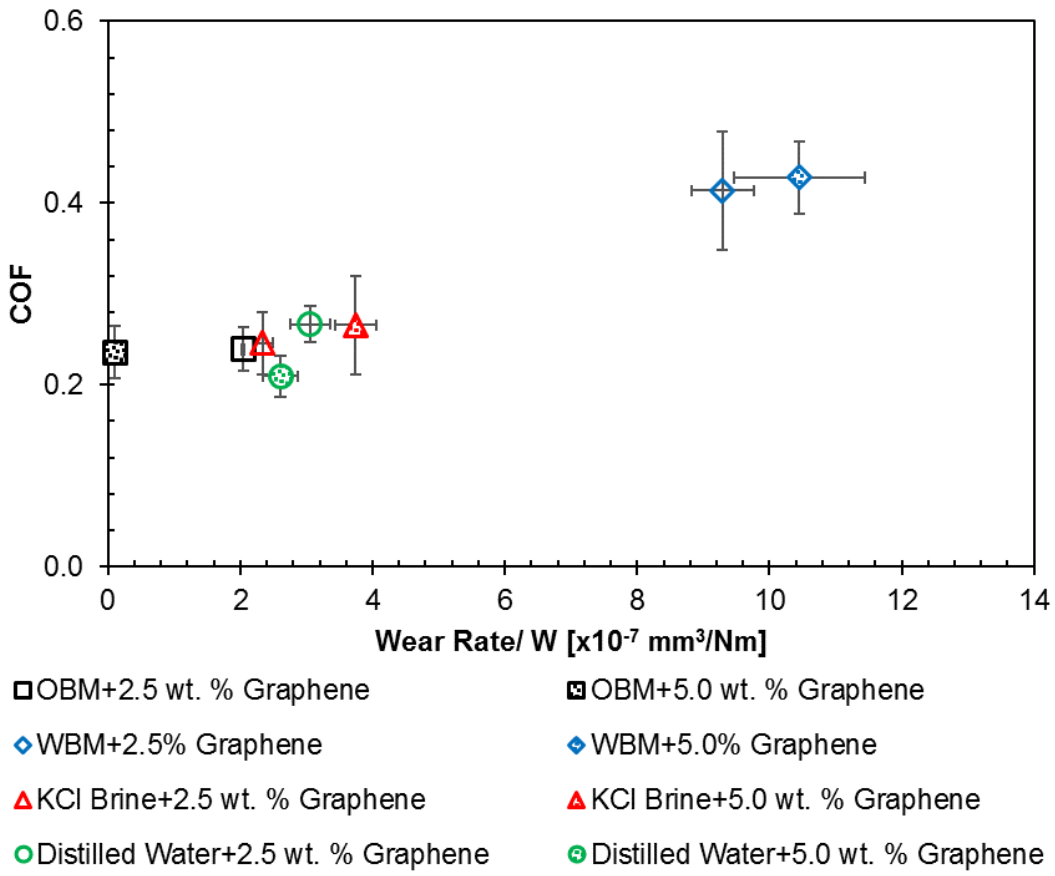


Figure 39. Comprehensive comparison among graphene-added OBM, WBM, KCl brine and distilled water: COF vs. wear rate.

**Table 17. Effect of graphene on the tribological performance of distilled water.**

| Mixture | COF | Wear diameter [μm] | Contact pressure [GPa] |
|---|---|---|---|
| Distilled Water+2.5 wt. % Graphene | 0.267 ± 0.01 | 866 ± 3.01 | 0.083 |
| Distilled Water+5.0 wt. % Graphene | 0.210 ± 0.01 | 833 ± 8.99 | 0.090 |

## 5.2 Summary

In this chapter, the potential influence of graphene on the tribological performance (COF and wear) of OBM, WBM and KCl brine, as well as distilled water was investigated. The test results proved that adding graphene is able to improve the lubricant system's anti-friction and anti-wear performance.

The same four-ball experimental configuration was used, with all the experiments performed under the same operational conditions as Chapter 4. Adding 2.5 wt. % graphene into OBM reduced the COF by 9.5%, while adding 5.0 wt. % graphene resulted in further reduction in COF, by 10.6%.

Adding graphene demonstrate rather limited benefits towards the tribological performance of WBM, regardless of the graphene concentration, and the COF and wear of WBM/ graphene mixtures are still inferior to those of OBM and its graphene altered versions. The reason for this is that WBM itself already contains a high concentration (70 wt. %) of solid particles.

The presence of graphene in KCl brine and distilled water demonstrated superior tribological performance. The COF of pure KCl brine (0.617) was drastically reduced to 0.246 (2.5 wt. % graphene) and 0.266 (5.0 wt. % graphene), by 60.1% and 56.9%, respectively. Therefore, with the aid of graphene, the COF of KCl brine could be reduced to a level about the same as or even lower than that of pure OBM (0.264), which is impressive.

Though COF and wear rate of distilled water was not available due to excessive friction during the test, its mixture with graphene demonstrated rather superior performance in both COF and wear. Adding 5.0 wt. % graphene into distilled water resulted in COF as low as 0.210, which represents 20.5% reduction compared with pure OBM, and still lower than that obtained with OBM/ graphene mixtures. Adding 2.5 wt. % graphene also delivered a COF at 0.267, with negligible increase compared with pure OBM at 0.264.

In the presence of graphene, the tribological performance of both KCl and distilled water was remarkably improved to a level where they were fully competitive against, or even superior, to OBM and its graphene loaded mixtures. It was found that graphene is also able to promote the tribological performance of environmentally friendly alternatives such as artificial sea water (KCl brine) and even distilled water, to a level where they are promising replacement for conventional OBM for oil & gas industry as well.

# CHAPTER 6

# TRIBOLOGICAL PERFORMANCE OF WATER-BASED/AQUEOUS MUDS IN HPHT DOWNHOLE ENVIRONMENT

## 6.1 Water-based Muds with No Additives

Simulating the conditions typically encountered in field downhole drilling environment, wear tests allow direct evaluation of the tribological performance of the drilling fluid from a perspective of how the simulated wear process is influenced, favorably or adversely, and to what extent. More importantly, wear tests also shows how the HPHT conditions and normal load.

Figure 40 shows the development of COF within stages 1~3, during wear tests with pure water-based muds using UHPT. The reservoir temperature was maintained at 75 and 125 °C, for stage 1 and stage 2, respectively. For both stage 1 and stage 2, the normal load was constant at 22 N from the beginning of each test till t = 8.4 minute, beyond which, the normal started increasing at a constant rate from 22 to 200 N. For stage 3, the lubricant temperature was maintained at 150 °C, the normal load was maintained at 22 N from the beginning of each experiment till t = 2 minute, after that, the normal load started increasing with a step of 89 N, reaching 111, 200, 289 and 378 N, respectively. The normal load was maintained unchanged for 2 minutes when it reached each of these preset values. Refer Figure 6 for the detailed test conditions within each stage. The tribopairs used was O1 ss pins and O1 ss disks. For clearer understanding of the performance of each drilling fluid under this complex test protocol, an average COF was obtained based on the real-time data collected under each normal load within each stage. For analysis purpose, average COF under normal load was abstracted for tests under normal load of 200 N; while for stage 3, average COF under normal load of 111, 200, 289 and 378 N were obtained, as shown below.

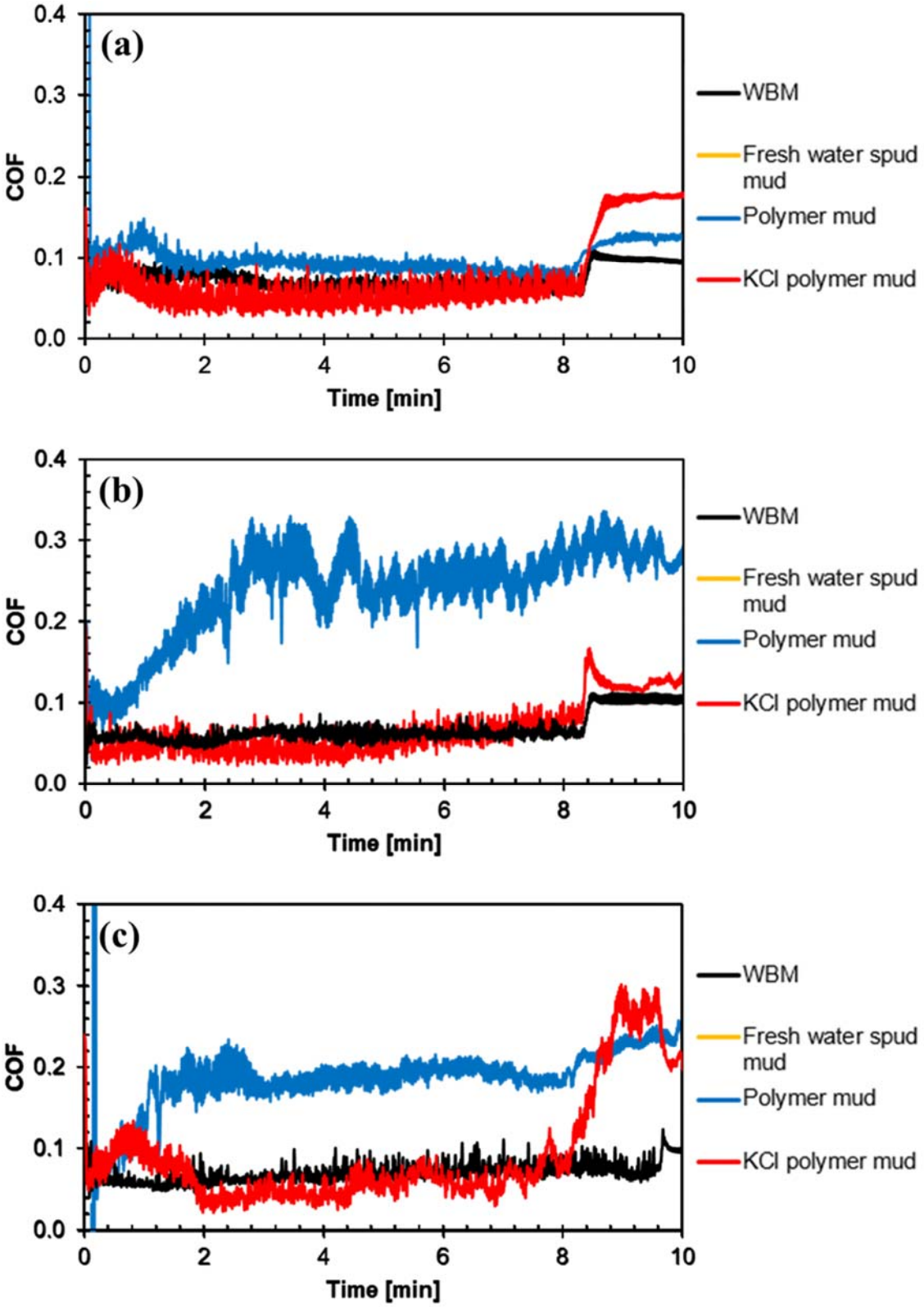


Figure 40. Development of COF during wear tests with pure water-based drilling fluids using UHPT: (a) stage 1; (b) stage 2 and (c) stage 3. Test samples: O1 ss pin vs. O1 ss disk.

Figure 41shows the results obtained from wear tests with aqueous muds before and after loading Amphiphile S. Figure 41 (a) shows the average COF of pure WBM and pure aqueous muds. Without the influence of Amphiphile S, fresh water spud mud failed immediately in stage 1 after the running-in to survive even the very first stage. In both tests with fresh water spud mud at 75 ºC, when the load was increasing from 22 to 200 N, the friction force exceeded the safety limit of the load cell and tests aborted automatically as a result of self-protection mechaism. This indicates poor lubrication of fresh water spud mud with no intereance from additives, even at low temperature and under low normal load. On the other hand, tests in WBM, polymer mud and KCl polymer mud all survived the whole test protocol. In general, the average COF of tribopairs tested in WBM and polymer mud both increased as the test condition transitioned towards more stringent scenarios, i.e., higher temperature and higher normal load, reaching a maximum COF at 0.255 (WBM) and 0.301 (polymer mud) under a normal load of 378 N at 150 ºC. However, the average COF of tests in KCl polymer mud remained nearly constant regardless of the test conditons in terms of temperature or normal load. As the test proceeded from stage 1 to stage 2, the reservoir temperature increased from 75 to 125 ºC, accordingly the COF in KCl polymermud decreased from 0.199 to 0.146. This may be attributed to a tribofilm deposited on the sample surfaces involved in the sliding. As shown in Figure 43, the micro image of the O1 ss pin tested in pure KCl polymer mud clearly demonstrates the existence of a grey-white layer covering a majority of the curved pin surface, including the line-contact area against the disk. On the other hand, existence of similar deposited tribofilms was not observed on pins tested in the pure verion of the other three drilling fluids (WBM, fresh water spud mud, and polymer mud). Note that WBM stands for KCl polymer water-based mud, and the major difference between WBM and KCl polymer mud is that the former contains upto 70 wt.% of solid particles (barium sulfate, bentonite, limestone, kaolin,

sodium hydroxide, quartz and sodium carbonate), which act as abrasives and would remove any deposited tribofilm during the sliding motions.

Figure 41 (b) shows the average COF for WBM and aqueous muds loaded with Amphiphile S following exactly the same test protocol. Introducing Amphiphile S resulted in significant reduction in COF for all mud systems except for KCl polymer mud. For WBM and polymer mud, the average reduction in COF was 65% and 56%, respectively. Instead, the average reduction in COF for KCl polymer mud was only 4%, introducing Amphiphile S actually resulted in increase COF in stage 3, i.e., under all normal load conditions at 150 ºC. Similar to the samples tested in pure drilling muds, the pin tested in KCl polymer mud + Amphiphile S again demonstrated deposition of a grey-white tribofilm on the contact surface, which is missing on pins tested in the other three Amphiphile S-loaded muds, as shown in Figure 44.

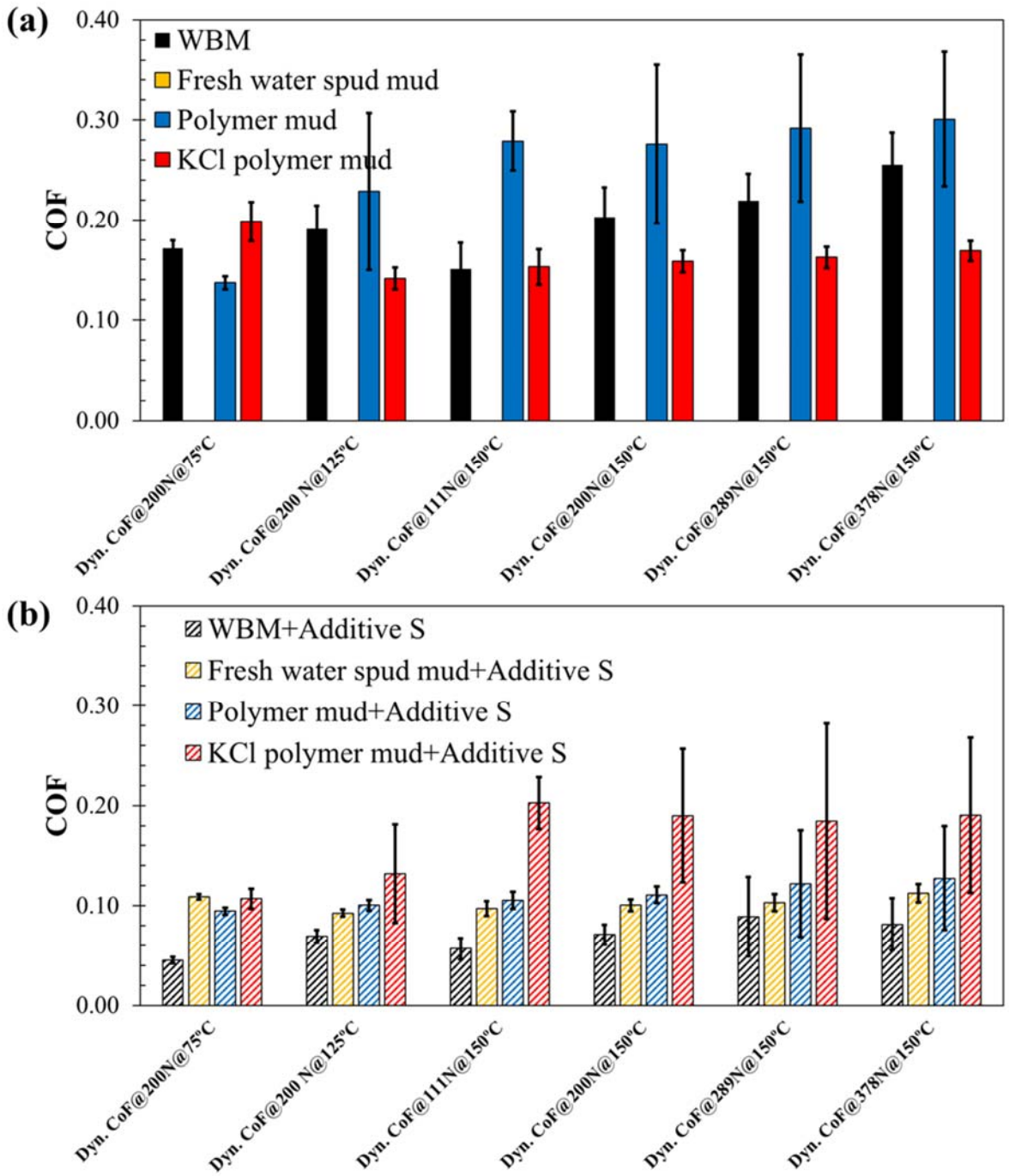


Figure 41. Wear experiment results of aqueous muds with tribopair O1 ss pin vs. O1 disk: (a) Pure aqueous muds; (b) Aqueous muds loaded with Amphiphile S.

Figure 42 shows a comprehensive comparison in COF among the tested WBM and aqueous mud systems with and without Amphiphile S, using O1 ss tribopairs. Overall, WBM + Amphiphile S shows the best performance in COF, with an average value 0.069 for all tested conditions. Closely following is fresh water spud mud + Amphiphile S, with an overall average COF of 0.103 regardess of specific stage or test conditons. It is especially noteworthy that loading Amphiphile S drastically reduced the COF of fresh water spud mud under all tested conditions, transforming the fresh water spud mud from a drilling system not able to survive even stage 1 into one that withstood all the HPHT conditions under ramping normal load, yet demonstrating remarkably low (~0.1) and stable COF through the whole test protocol. Table 18 summarizes the obtained average COF under varying normal load and at different reservior temepratures.

Figure 43 shows the micro images of the wear track on O1 stainless steel pins tested in WBM and aqueous muds, without and with Amphiphile S, respectively. With Amphiphile S absent, the contact surfaces of pins tested in WBM and fresh water spud mud both demonstrate significant abrasive wear, with the latter showing the contact area completely wiped flat and most severe material loss. On the other hand, pins tested in polymer mud and KCl polymer mud both indicate nearly negligible wear. Also, all the tested pins demonstrate a bright polished finish, while only the pin tested in WBM has a relatively darker appearance. This is likely an indicator of penetration of solid particles into the subsurface of the pin, as particles of extremely small sizes could easily enter the lubricating film between the sliding surfaces and act as tiny bearings.

Figure 44 shows the mciro images of the wear track on O1 stainless steel pins tested with Amphiphile S loaded in WBM and the aqueous muds. As indicated, the wear tracks on pins tested in WBM, fresh water spud mud and polymer mud are all much milder than those when Amphiphile S was absent (see Figure 43). In detail, pins tested in fresh water spud mud and KCl polymer mud

are especially noteworthy. The former mud system delivered drastic reduction in wear in the contacting area compared with the pure version shown in Figure 43, the latter mud system instead resulted in more severe abrasive wear on the contacting surface. Note that a similar grey-white layer of tribofilm was still observed on the contacting surface of the pin after testing, but only covering a much smaller portion of the wear track compared to the tribofilm coverage on pin tested in pure KCl polymer mud.

Wear track profilings in Figure 45 are in excellent agreement with the relative superiority suggested by the measured average COF. In detail, when tests were performed in pure mud systems, fresh water spud mud demonsted the most severe material loss due to wear which eventually lead to seizure. The contact surface of pin tested in WBM showed much milder material loss due to abraion wear caused by solid particles. Polymer mud and KCl polymer mud both delivered negligible wear on the pin surface. Specifically, there was even a little bump detected in the wear track profiling for the pin tested in KCl polymer mud, which exactly represents the grey-white tribofilm deposited on the pin surface, as shown in Figure 43.

Comparing the tribologcial performance in both COF and wear loss between pure muds and their altered versions loaded with Amphiphile S, the universal significant reductions in COF for WBM, fresh water spud mud and polymer mud but the opposite trend with KCl polymer mud all strongly suggest that introducing Amphiphile S into the four mud systems my have altered the hardness of the tribopairs. This will be further investigated in following tribological experimental studies where hardbanded pins with elevated surface hardness are used against O1 ss disks.

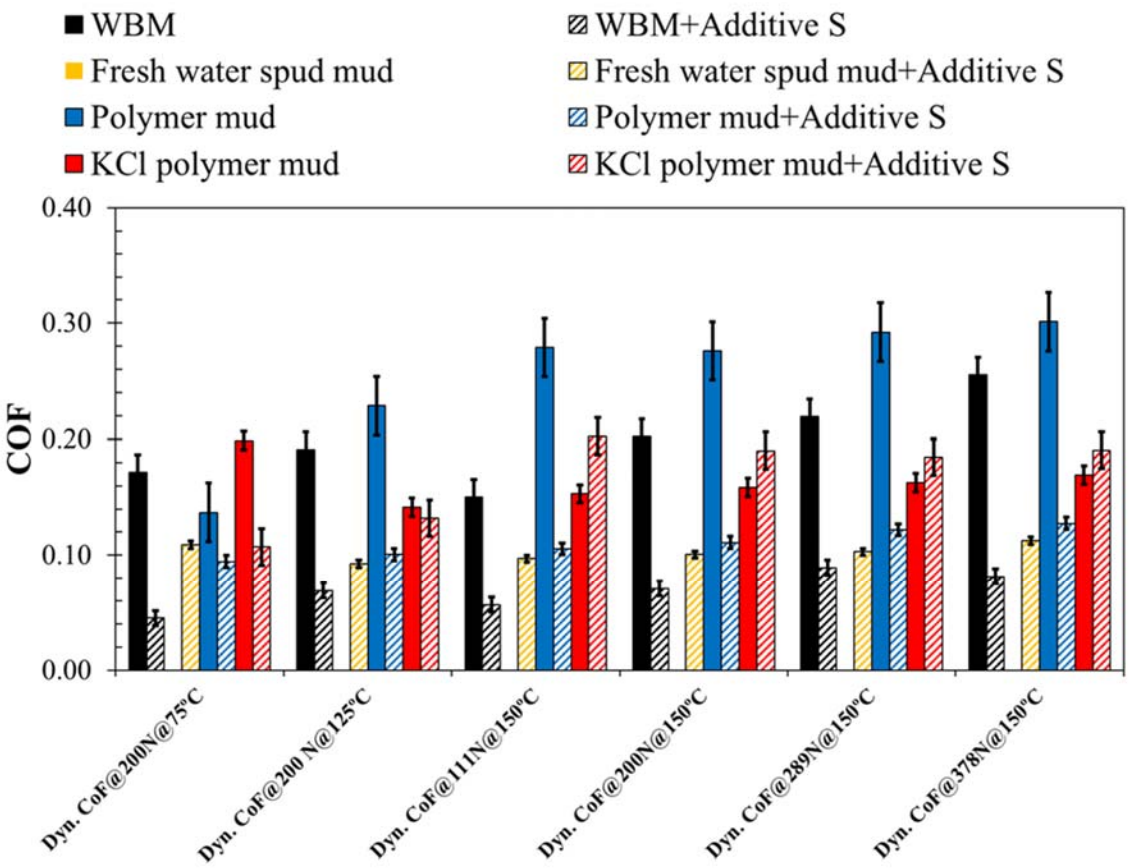


Figure 42. Comparison of wear experiment results of WBM and aqueous muds with and without Amphiphile S. Tribopair: O1 ss pin vs. O1 ss disk.

**Table 18. Average coefficient of friction for WBM and aqueous muds before and after loading Amphiphile S. Tribopair: O1 ss pin vs. O1 ss disk.**

| **Temperature** | **75 ºC** | **125 ºC** | **150 ºC** | | | |
|---|---|---|---|---|---|---|
| **Normal Load** | **200 N** | **200 N** | **111 N** | **200 N** | **289 N** | **378 N** |
| WBM | 0.172 | 0.191 | 0.151 | 0.202 | 0.220 | 0.255 |
| WBM + Amphiphile S | 0.045 | 0.069 | 0.057 | 0.071 | 0.089 | 0.081 |
| Fresh water spud mud | Failed | N/A | N/A | N/A | N/A | N/A |
| Fresh water spud mud + Amphiphile S | 0.109 | 0.093 | 0.097 | 0.101 | 0.103 | 0.113 |
| Polymer mud | 0.137 | 0.229 | 0.279 | 0.276 | 0.292 | 0.301 |
| Polymer mud + Amphiphile S | 0.095 | 0.101 | 0.106 | 0.111 | 0.122 | 0.128 |
| KCl polymer mud | 0.199 | 0.146 | 0.170 | 0.172 | 0.175 | 0.188 |
| KCl polymer mud + Amphiphile S | 0.107 | 0.132 | 0.203 | 0.190 | 0.185 | 0.191 |

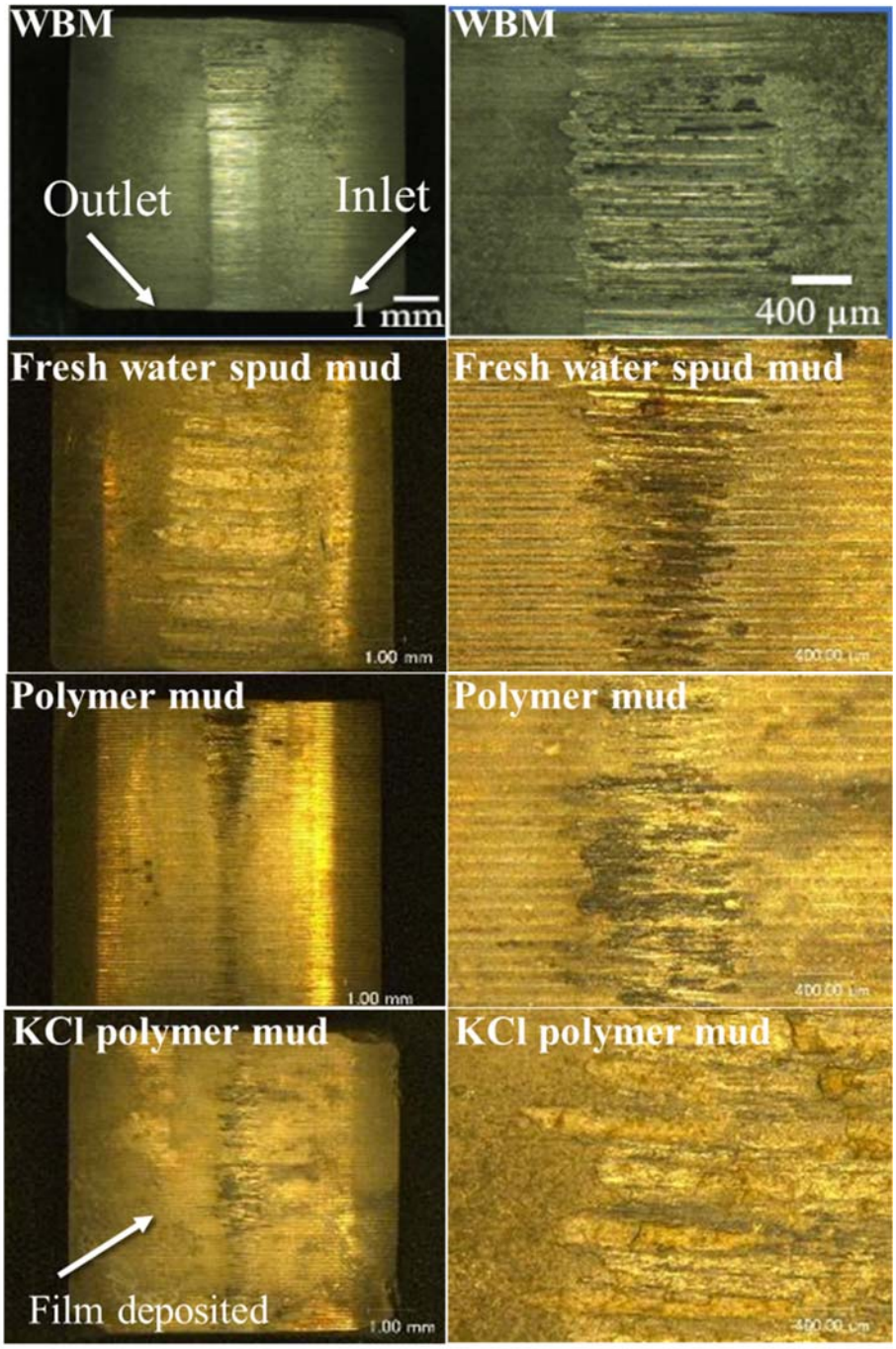


Figure 43. Micro images of O1 ss pins, tested in pure WBM and aqueous muds.

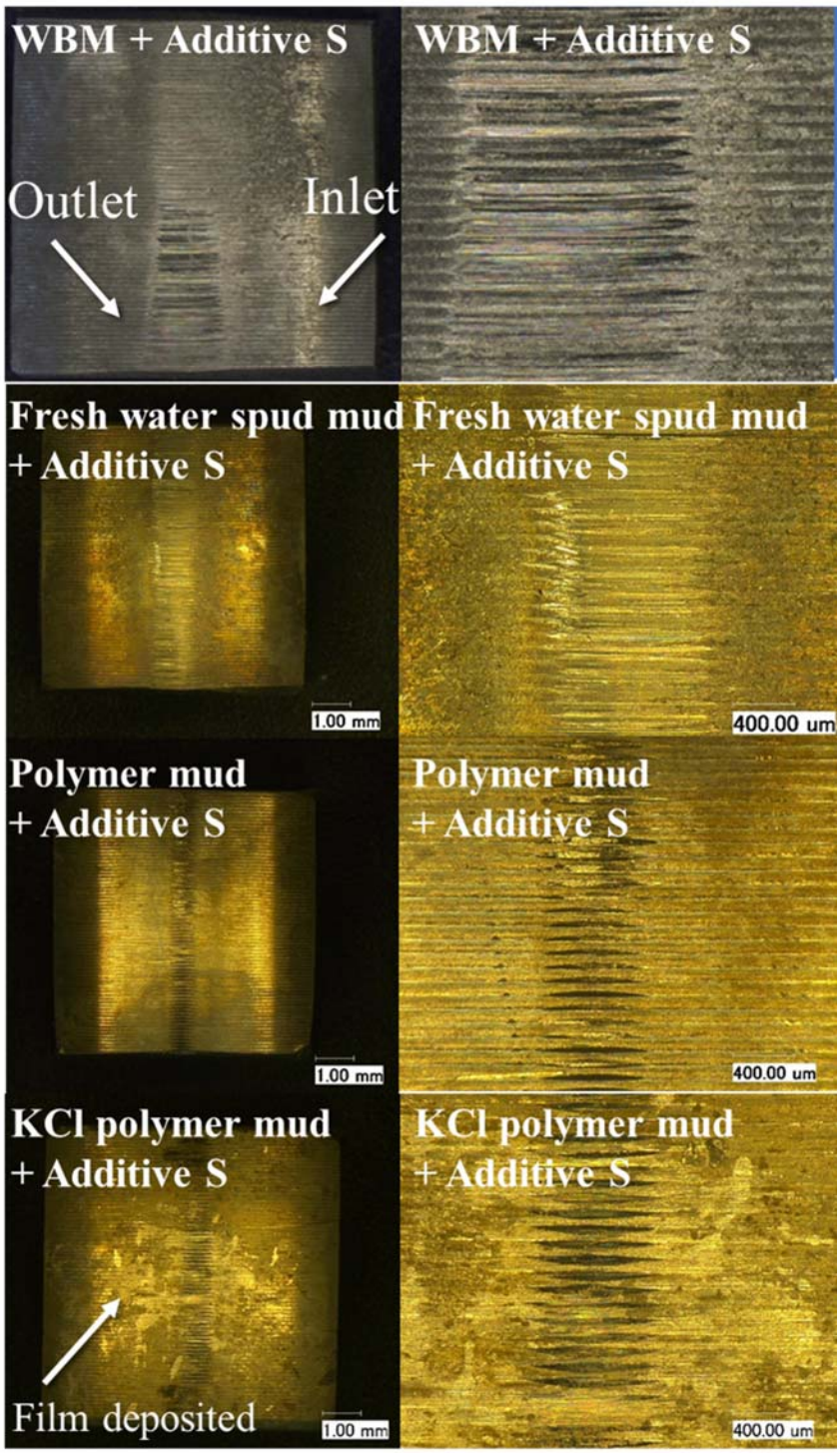


Figure 44. Micro images of O1 ss pins, tested in WBM and aqueous muds loaded with Amphiphile S.

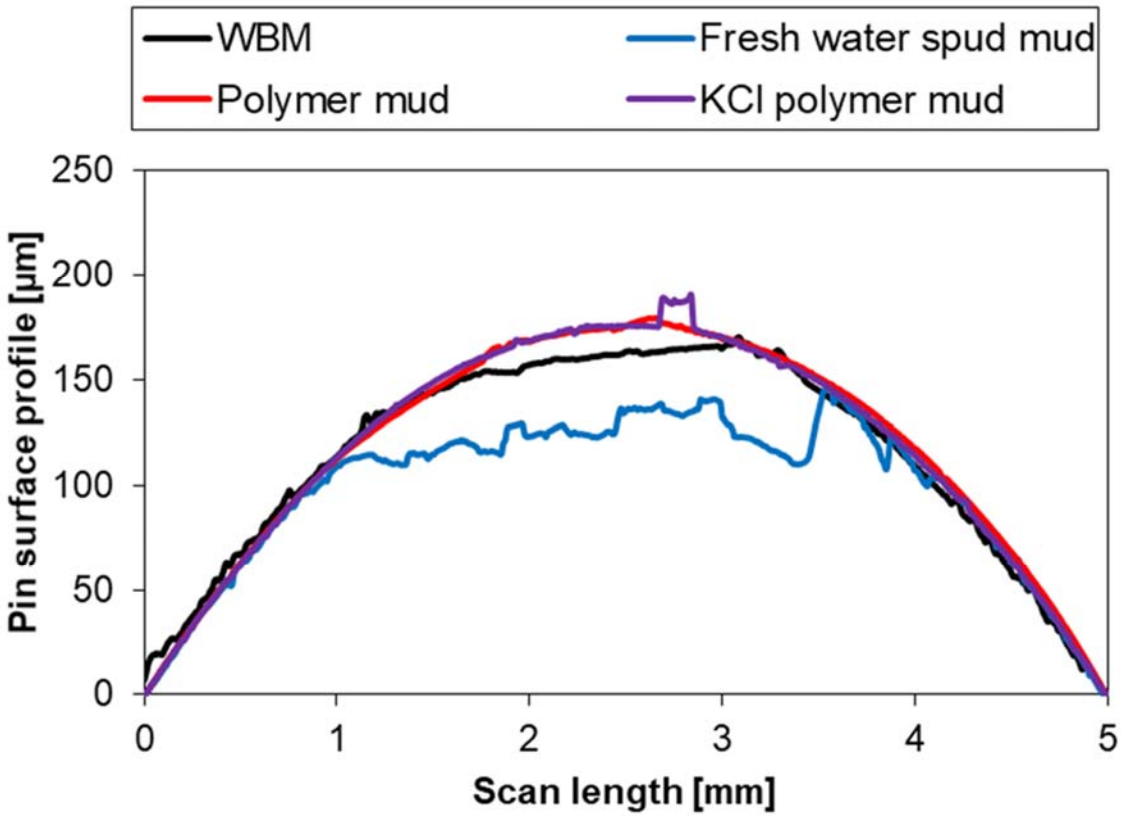


Figure 45. Wear track profiling of O1 ss pin tested in WBM and aqueous muds without Amphiphile S.

### 6.2 Hardbanded pin vs. O1 ss disk

In order to clarify and confirm if introducing Amphiphile S has been responsible, at least to some extent, for the improvement (WBM, fresh water spud mud, and polymer mud) and degradation (KCl polymer mud) in the tribological performance of the four tested mud systems, the above wear tests were performed compliant to exactly the same test protocol, with the only difference lying in that hardbanded pins were used as replacement of O1 ss pins.

Figure 46 shows the average COF obtained with hardbanded pin sliding against O1 ss disks, in pure WBM and aqueous muds, as well as their altered versions with Amphiphile S lodaed and fully mixed. As shown in Figure 46 (a)-(b), with hardbanded pins, the average COF increased

significantly for all the mud systems, with pure KCl polymer mud as the only exception. Figure 47 shows a comprehensive comparison in COF for all the tested mud systems, pure and loaded versions, with hardbanded pins sliding agsint O1 ss disks.

As shown in Figure 46, Figure 47 and Table 19, compared with the previous tests using softer O1 ss pins, the COF increased by 89% and 133% for WBM and WBM + Amphiphile S, resepectively. For polymer mud and its loaded version, temporary reductions in COF was observed at low temperatures (75 and 125 ºC). As the reservoir temperatrue raised to 150 ºC, the tribopair in pure polymer mud experienced seizure as the normal load was ramping up from 111 N towards 200 N. For polymer mud + Amphiphile S, the seizure occurred as the normal was increasing from 200 N to 289 N.

For fresh water spud mud, the deterioration in lubrication effect is further severe. Its pure version delivered early tribopair seizure in stage 1 right after running-in, which is the same as previous tests with O1 ss pins and as expected, considering the pin surface with elevated hardness would impose more strintent metal-on-metal contact. This performance degradation is further amplified when it comes to fresh water spud mud + Amphiphile S. The drastical reversing phenomenon of Amphiphile S, transforming fresh water spud mud from failing as early as in stage 1, to a highly promising system demonstrating a stable COF as low as ~0.10, completely diminished. With the hardbanded pin, the loaded system was only able to survive stage 1 with a COF as high as 0.419 representing a increase by 284% and then failed immediately in stage 2, where the reservoir temperature was raised from 75 to 125 ºC.

For KCl polymer mud and its altered version, the latter system demonstrated an increase in COF by 44% covering the whole test protocol, while the pure version with hardbanded pin showed an average reduction in COF by 30%.

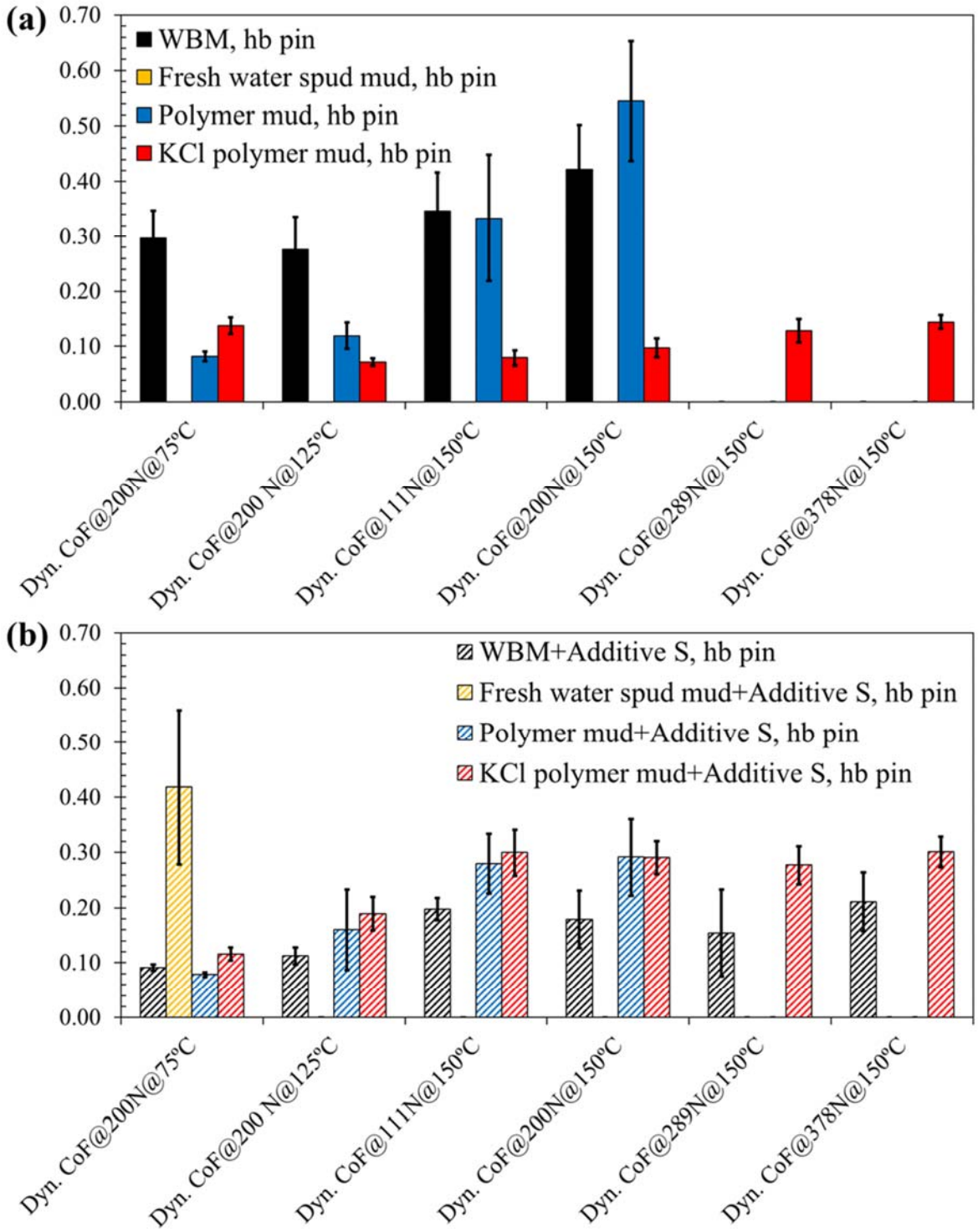


Figure 46. Wear experiment results of aqueous muds with tribopair of hardbanded pin vs. O1 disk: (a) Pure aqueous muds; (b) Aqueous muds loaded with Amphiphile S.

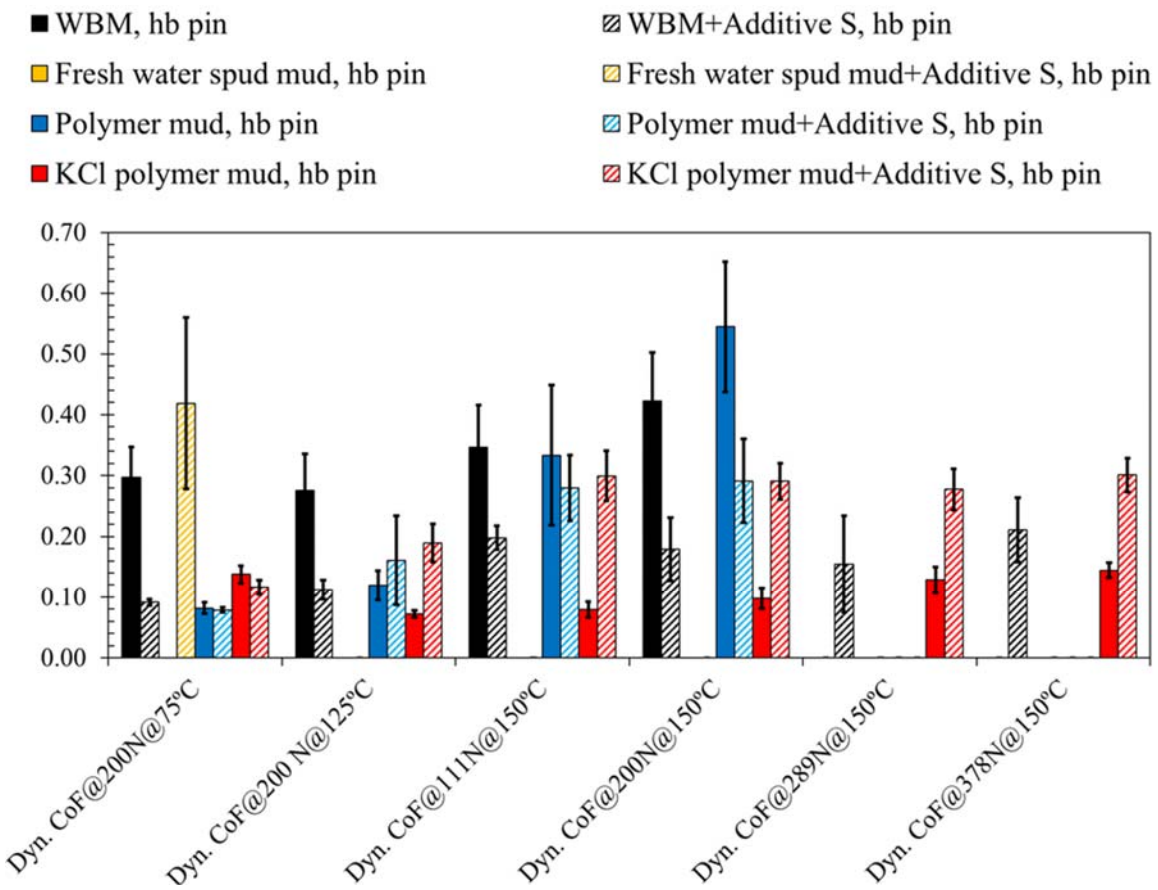

Figure 47. Comparison of wear experiment results of WBM and aqueous muds before and after loaded with additive. Tribopair: Hardbanded pin vs. O1 ss disk.

**Table 19. Average coefficient of friction for WBM and aqueous muds before and after loading Amphiphile S. Tribopair: Hardbanded pin vs. O1 ss disk.**

| **Temperature** | **75 ºC** | **125 ºC** | **150 ºC** | | | |
|---|---|---|---|---|---|---|
| **Normal Load** | **200 N** | **200 N** | **111 N** | **200 N** | **289 N** | **378 N** |
| WBM | 0.297 | 0.276 | 0.346 | 0.422 | Failed | N/A |
| WBM + Amphiphile S | 0.091 | 0.112 | 0.198 | 0.179 | 0.154 | 0.211 |
| Fresh water spud mud | Failed | N/A | N/A | N/A | N/A | N/A |
| Fresh water spud mud + Amphiphile S | 0.419 | Failed | N/A | N/A | N/A | N/A |
| Polymer mud | 0.082 | 0.120 | 0.334 | 0.545 | Failed | N/A |
| Polymer mud + Amphiphile S | 0.079 | 0.160 | 0.280 | 0.292 | 0.413 | Failed |
| KCl polymer mud | 0.130 | 0.093 | 0.127 | 0.127 | 0.120 | 0.142 |
| KCl polymer mud + Amphiphile S | 0.117 | 0.190 | 0.300 | 0.291 | 0.278 | 0.301 |

### 6.3 Effect of Amphiphile S on Tribopair Hardness

Figure 48 (a) depicts the synergic effect between tribopair hardness and Amphiphile S on the COF when fresh water spud mud was used as base fluid. When softer (O1 ss) pins were used, introducing Amphiphile S revered the fresh water spud mud from a system that resulted in seizure in early stage 1 to one that shows nearly constant COF for all load and temperature conditions with a value as low as ~0.10. However, when the softer pins were replaced with hardbanded ones, this significant anti-friction and anti-wear brought in by Amphiphile S was completely eliminated, resulting in a high COF of 0.419 in stage 1 and followed by immediate seizure in early stage 2.

Figure 48 (b) depicts the synergic effect between tribopair hardness and Amphiphile S on the COF when KCl polymer mud was used as base fluid. When softer O1 ss pins were used, KCl polymer mud was the only base fluid that demonstrated degradation in lubricating performance after loading Amphiphile S. When hardbanded pins were used for the same test conditions, the same degrading trend in COF after loading Amphiphile S compared with the pure version was again observed. However, for pure mud scenarios, tribopair with hardbanded pins actually resulted in significant reduction in COF by 25% - 37%.

To further confirm the influence of Amphiphile S over the surface hardness of pins involved in this study and validate potential synergic effect existing between tribopair hardness and Amphiphile S, a series of Vickers hardness measurements were carried out on both fresh untested and tested O1 ss pins. The untested O1 ss pin samples were all cleaned in a sonic cleaner for 15 minutes in acetone to remove any chemical residuals, followed by thorough rinsing with isopropyl alcohol, and then air dried. The tested O1 ss pins samples were obtained from above performed tribological tests followed by the same cleaning process.

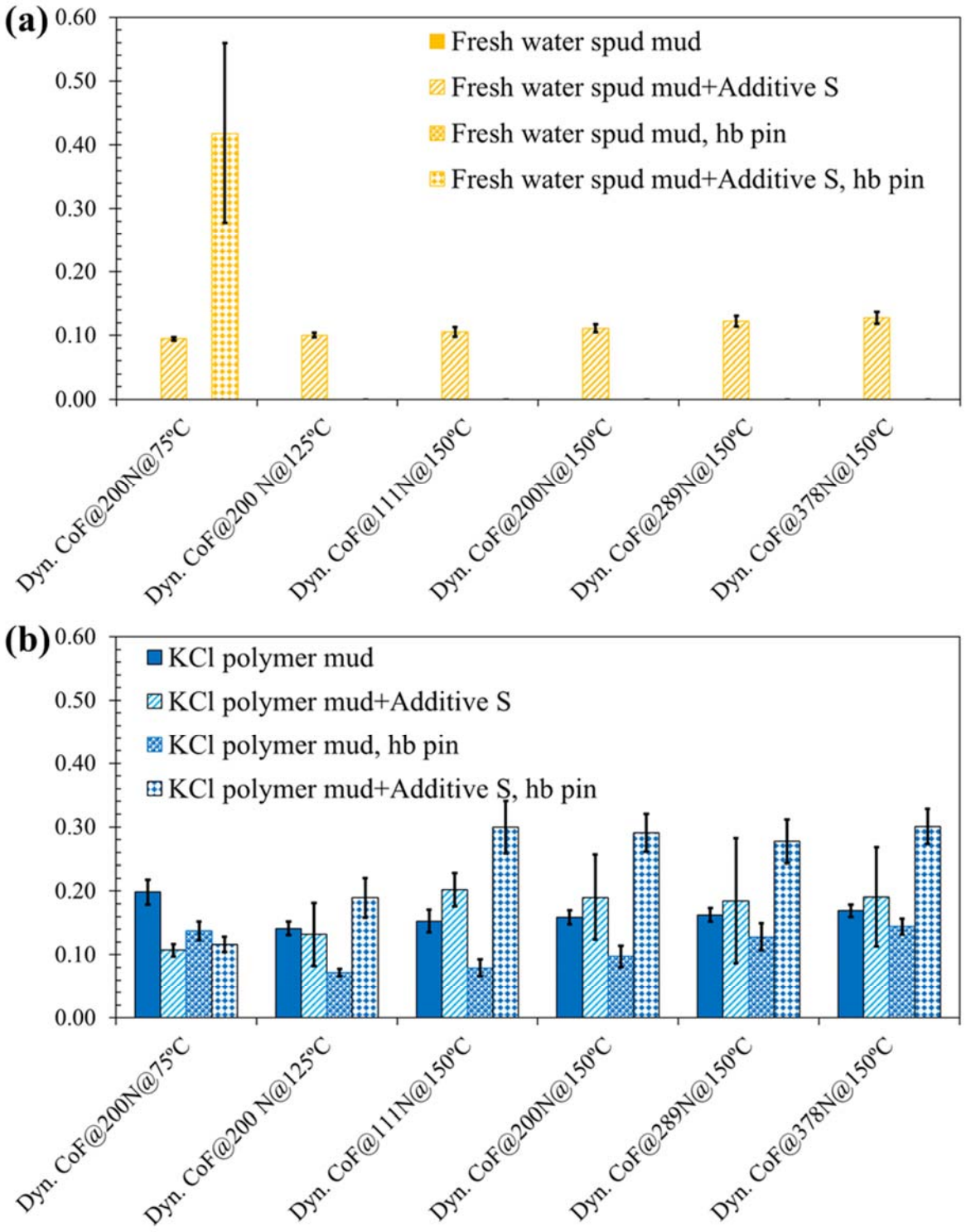


Figure 48. Synergic effect between tribopair hardness and Amphiphile S.

Figure 50 shows a photograph of a Wilson TUKON 1102 Micro-Hardness Tester utilized to measure the Vickers hardness of O1 ss pins by calculating hardness values from measurements of the diagonal lengths of indentations, with an emphasis on the potential influence over tribopair hardness resulting from introduction of the Additive. The Hardness data was obtained in Vickers scale applying ASTM T.1 standard with a load of 1 kgf (9.81 N) and a dwelling period of 10 seconds.

Figure 49 shows the measured Vickers hardness of untested O1 ss pins that were soaked in pure aqueous muds and their additive-loaded versions for 24 hours before measurement, as well as the O1 ss pins tested in above experiments. As indicated, introduction of Amphiphile S resulted in reduction in the surface hardness of O1 ss pins for both fresh water spud mud and polymer mud, fresh and tested pins. For fresh untested pins, the reduction in surface hardness was by 17% and 8% -11% for fresh water spud mud and polymer mud, respectively. For tested pins, the reduction in surface hardness was by 30%– 42% for fresh water spud mud, and 9% - 10% for polymer mud. In contrast, loading Amphiphile S into KCl polymer mud caused increase in the surface hardness, consistently for both untested (by 6-13%) and tested (by 3% - 11%) O1 ss pins.

The above detected varying influence of Amphiphile S over the pin surface hardness among the aqueous muds, together with its varying (favorable/adverse) effect on the COF, confirms the existence and importance of synergic effect between the tribopair hardness and Amphiphile Selected, as well as presence of potential chemical reactions between Amphiphile Selected and the base fluid. Figure 51 shows micro images of the indents on untested O1 ss pin samples after soaking in pure and loaded aqueous muds.

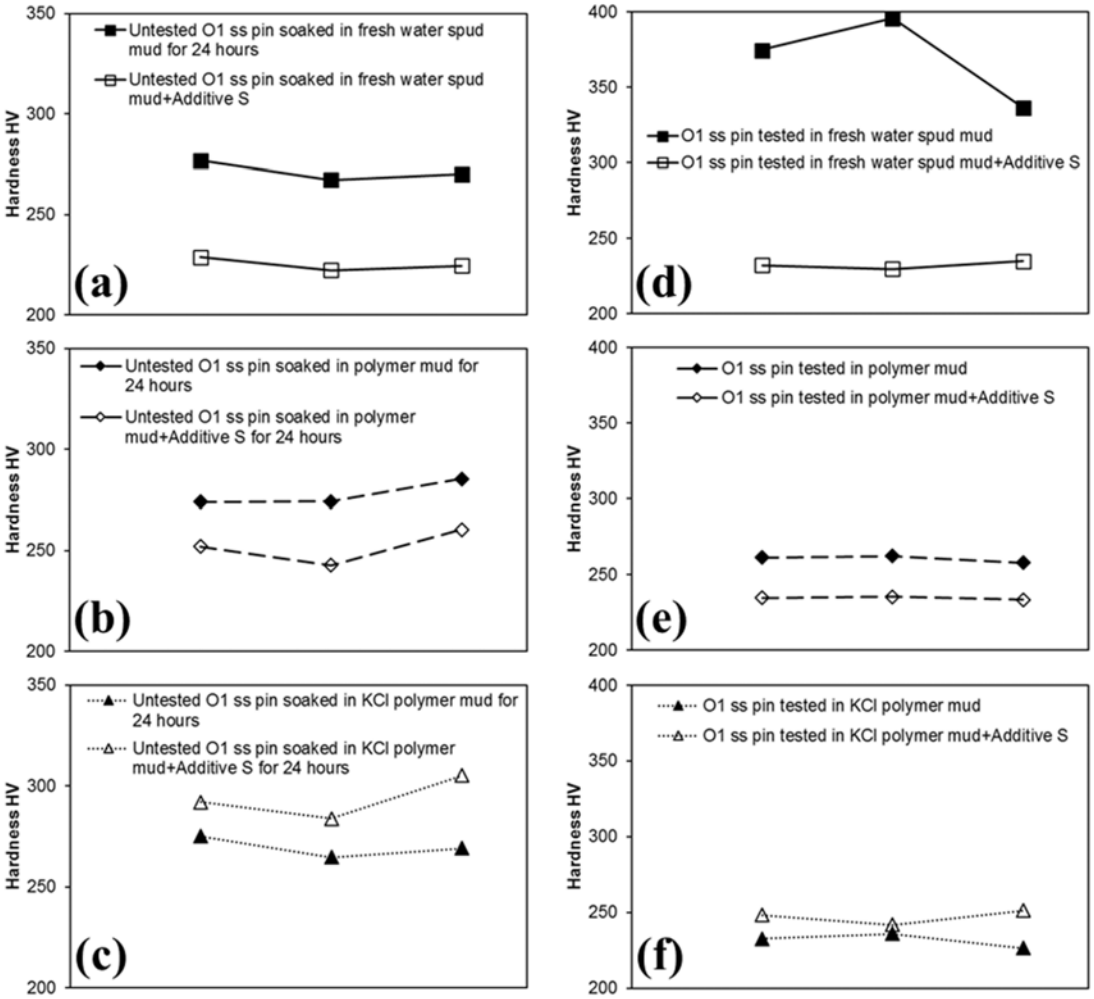


Figure 49. Measured Vickers hardness of O1 ss pins: (a-c) untested pins soaked in fresh aqueous muds and their altered versions for 24 hours; (d-f) pins tested in pure aqueous muds and their altered versions. From top to bottom, the drilling fluid is fresh water spud mud, polymer mud, and KCl polymer mud, respectively.

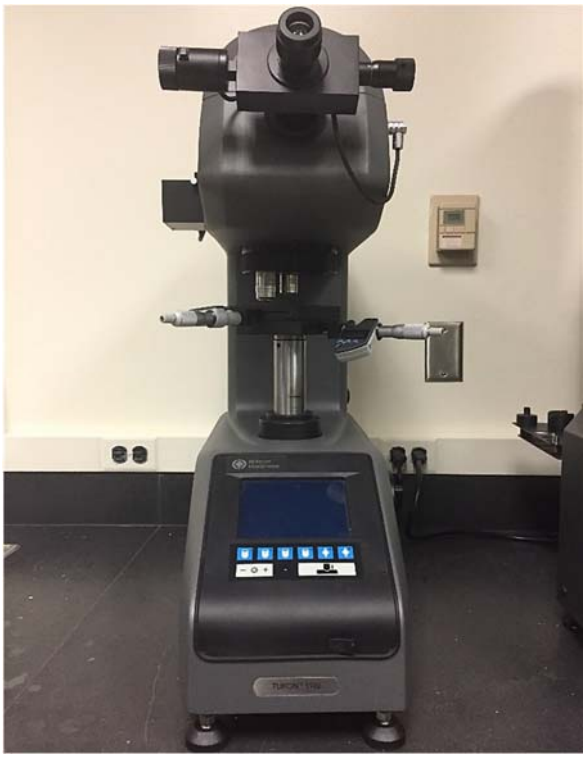

Figure 50. Photograph of Wilson TUKON 1102 Micro-Hardness Tester.

**Table 20. Measured hardness of untested and tested O1 ss pins.**

| Drilling fluid | Pin material | Sample status | Average HV |
|---|---|---|---|
| Fresh water spud mud | O1 ss | Untested | 271.4 ± 4.0 |
| Fresh water spud mud + Amphiphile S | | | 225.2 ± 2.7 |
| Polymer mud | | | 277.9 ± 5.3 |
| Polymer mud + Amphiphile S | | | 251.8 ± 7.2 |
| KCl polymer mud | | | 269.6 ± 4.3 |
| KCl polymer mud + Amphiphile S | | | 293.7 ± 8.8 |
| Fresh water spud mud | O1 ss | Tested | 369.3 ± 24.7 |
| Fresh water spud mud + Amphiphile S | | | 232.2 ± 2.1 |
| Polymer mud | | | 260.5 ± 1.9 |
| Polymer mud + Amphiphile S | | | 234.5 ± 0.8 |
| KCl polymer mud | | | 231.7 ± 3.9 |
| KCl polymer mud + Amphiphile S | | | 247.0 ± 4.0 |

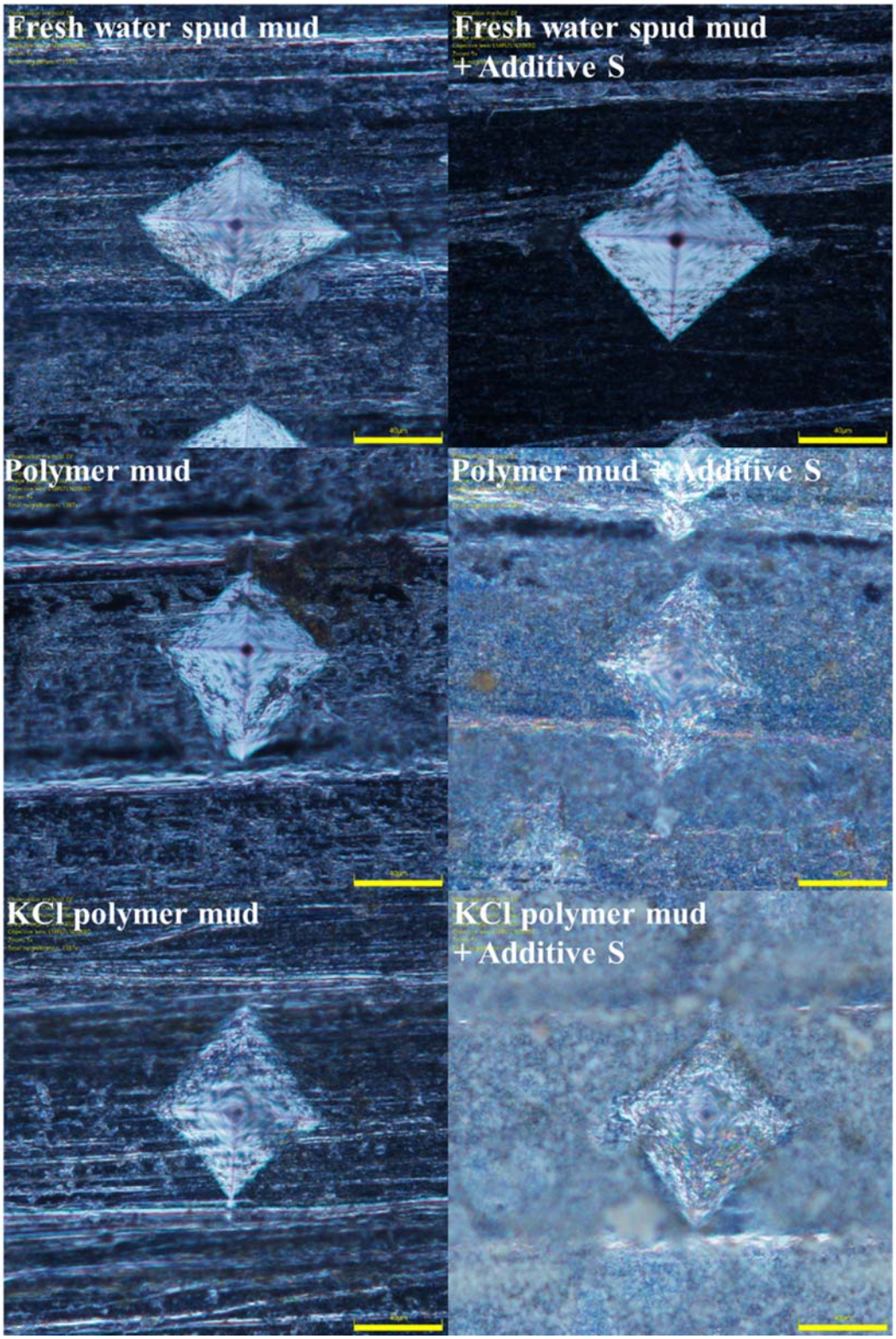


Figure 51. Micro images of indents after Vickers hardness measurement, untested O1 ss pins saturated in pure aqueous muds and additive-loaded aqueous muds for a period of 24 hours.

### 6.4 SEM and EDS analysis on Wear Track of Tested O1 ss Disks

To understand the lubricating mechanisms of pure aqueous muds and the influence of Amphiphile S over the tribological performance of the drilling fluids, SEM-EDS was performed with an emphasis on the wear tracks of tested O1 ss disks. For tests involving fresh water spud mud, either pure or mixture version, tests in 3 out of 4 base/mixture fluids failed with seizure in early stage 1, the only exceptional survival yet with superior stable low COF (~0.10) was tests in fresh water spud mud + Amphiphile S mixture using O1 ss pins. Above analysis on the effect of additive on tribopair hardness in section 3.3 suggests that this was attributable to the softening effect introduced by the Amphiphile S. Hence, the SEM and EDS analysis was mainly focused on the wear tracks of O1 ss disks tested in polymer mud, KCl polymer mud and their additive loaded versions, shown in Figure 53 are the sites of interest under investigation.

A JSM-7500F (JEOL USA, Peabody, MA) SEM was used to perform the SEM-EDS analysis on the tested samples. The main objective for these measurements was to analyze the surface chemistry and explain why Amphiphile S resulted in varying (favorable and adverse) influence on the different mud systems' lubricating performance under the same operating conditions.

Figure 54 and Figure 55 show the element mappings obtained from EDS examination on the wear track of O1 ss disks tested in polymer mud and its additive loaded version, respectively. As Amphiphile S softened the tribopair surface hardness, rendering the surface material more vulnerable to abrasive wear, thus exposing more ferrous (Fe) and tungsten (W) elements underneath. Also, adding Amphiphile S reduced the concentration of sodium (salt), increased the content of silicon, which could have served as third-party particles rolling between the counteracting surfaces as tiny ball bearings.

Figure 52. Tribofilm deposited on the surface of O1 stainless steel disk after testing in KCl polymer mud.

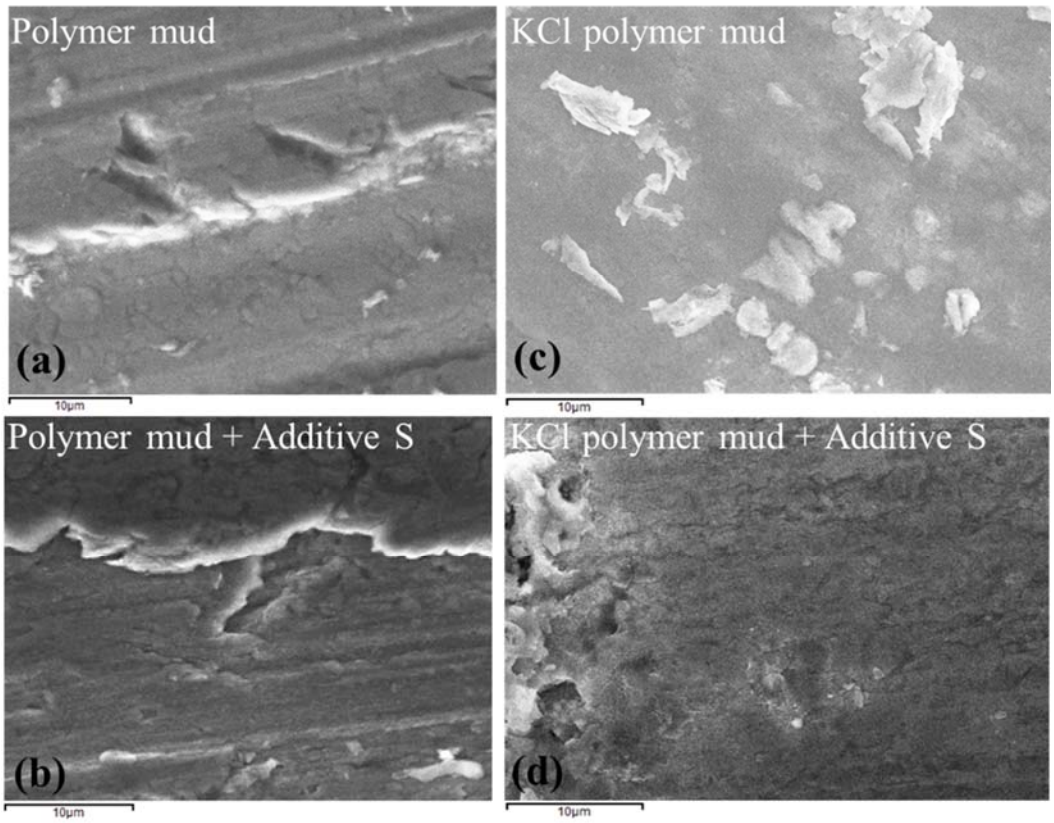


Figure 53. Sites of interest for SEM/EDS analysis of O1 ss pins tested in polymer mud, KCl polymer mud and their altered versions after loading Amphiphile S.

Figure 56 and Figure 57 show the element mappings obtained from EDS examination on the wear track of O1 ss disks tested in KCl polymer mud and its additive loaded version, respectively. Comparison of the element mappings indicates more ferrous (Fe), less chlorine (Cl) and less silicon (Si). The reason for this is that pure KCl polymer mud itself has the tendency to form a protecting film on the surface, as shown in Figure 52 and Figure 53. Combining with the hardening effect of Amphiphile S when added in KCl polymer mud, as shown in Figure 49, it is likely that Amphiphile S interrupted or destroyed the formation of this film through chemical reactions, which exposed the ferrous substrate. Accordingly, the detected element density of element Fe was higher than pure KCl polymer mud, while density of element Cl was lower.

Figure 58, Figure 59, and Figure 60 show the 3-D profilometry of hardbanded pins tested with and without Amphiphile S, with the base drilling fluid being fresh water spud, polymer mud, and KCl polymer mud, respectively. As indicated, the contact area of untested hardbanded pins was nearly the same for all the tests, in pure aqueous muds and aqueous mud/Amphiphile S mixtures. Presence of high spots was not observed through the 3-D profiling. However, distinguishable difference of the finish of the contact area of the hardbanded pins were detected upon completion of tests. Specifically, for tests performed in fresh water spud mud and polymer mud, pure and mixtures with Amphiphile S, the hardbanded pins were all flattened to a certain extent, resulting in a larger contact area bearing the normal load and hence with lower contact pressures. On the other hand, hardbanded pins tested in KCl polymer mud and KCl polymer mud + Amphiphile S both showed no signs of a flattened contact area. Instead, the tested pins indicate higher rougher surfaces with a dense distribution of high spots. More specifically, the hardbanded pin tested in Amphiphile S added KCl polymer mud became rougher than the pin tested in pure KCl polymer mud, which agrees with the increase in COF when Amphiphile S was introduced into KCl polymer mud.

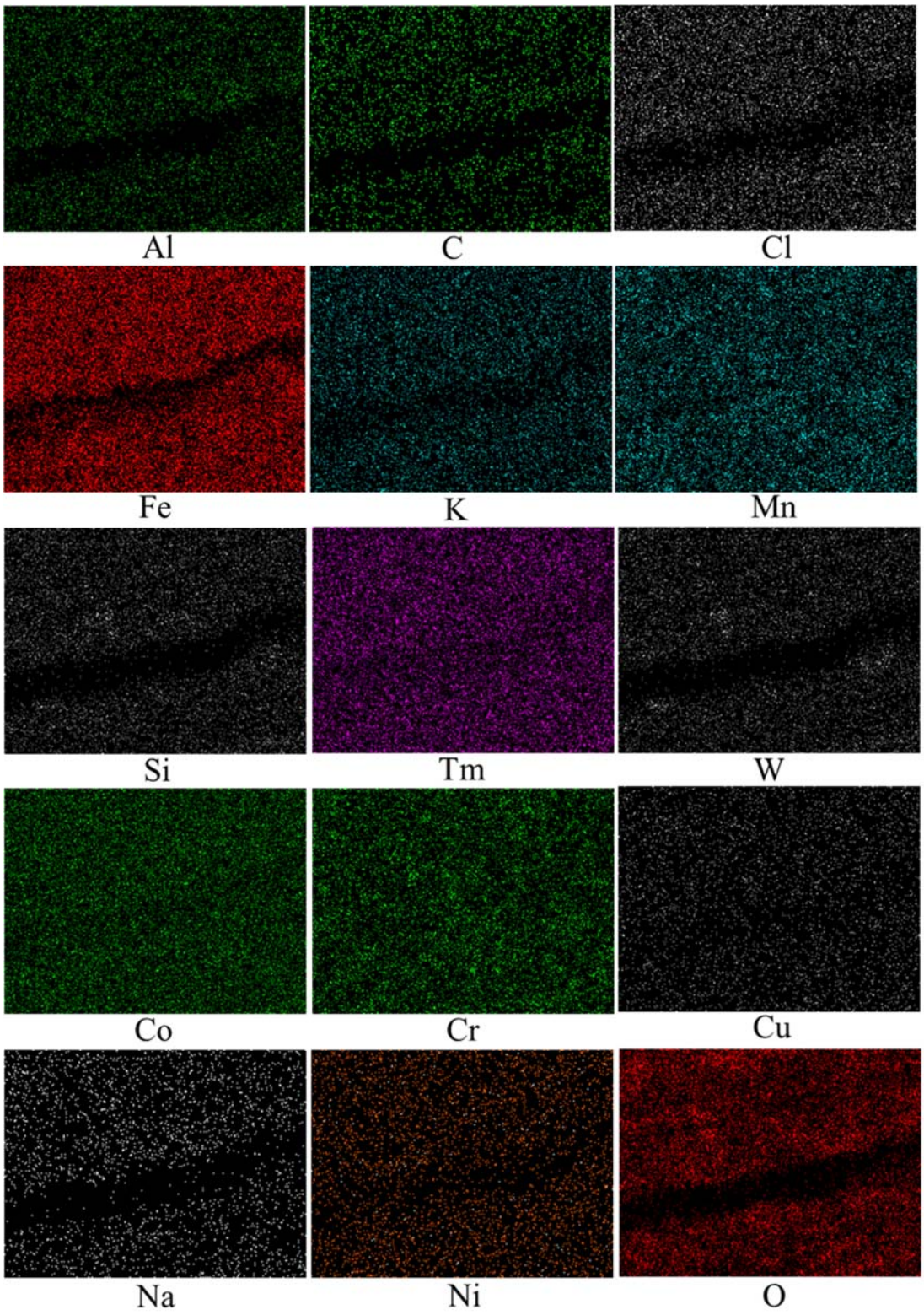


Figure 54. EDS analysis on wear track of O1 ss disks tested in polymer mud.

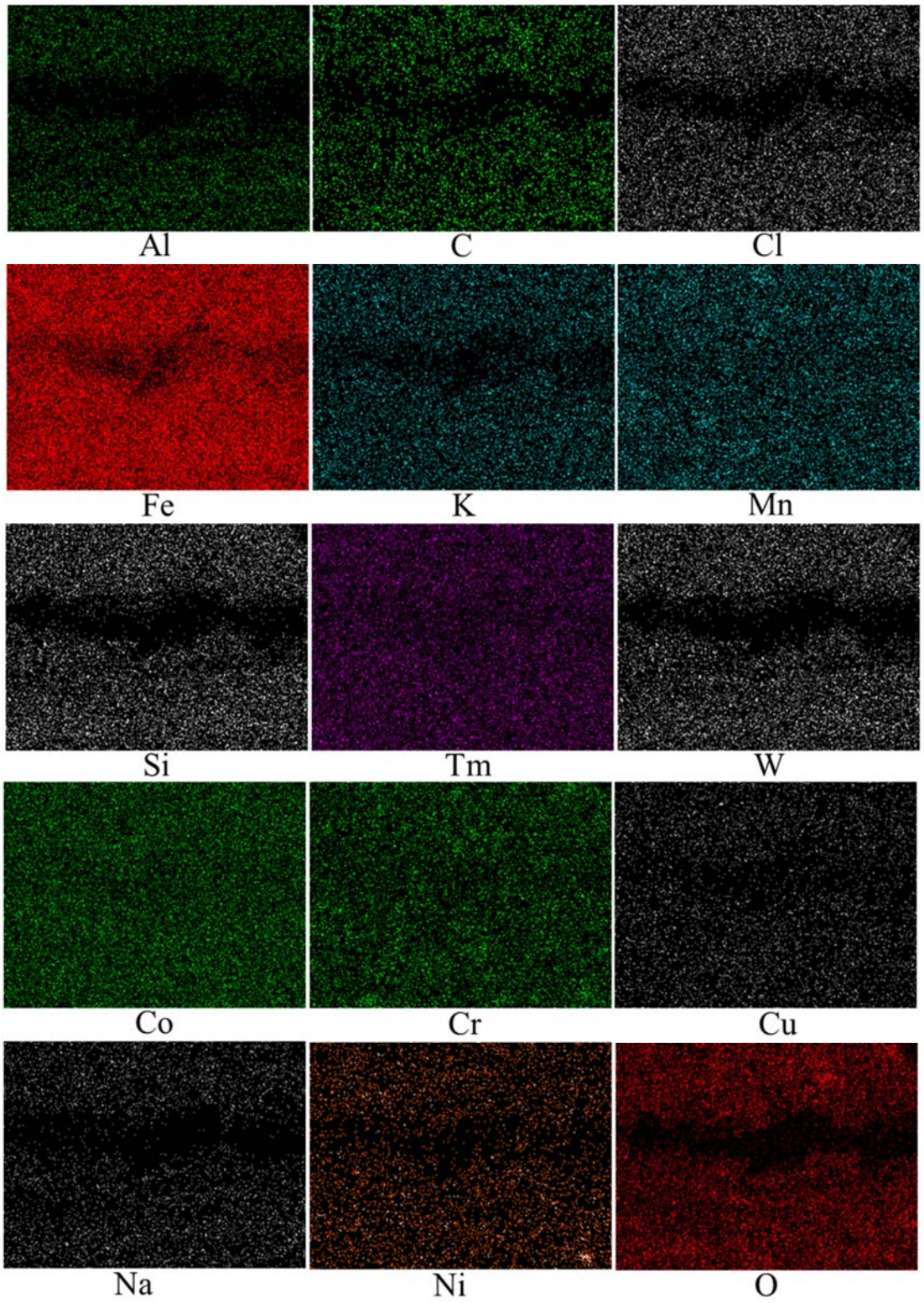


Figure 55. EDS analysis on wear track of O1 ss disks tested in polymer mud + Amphiphile S.

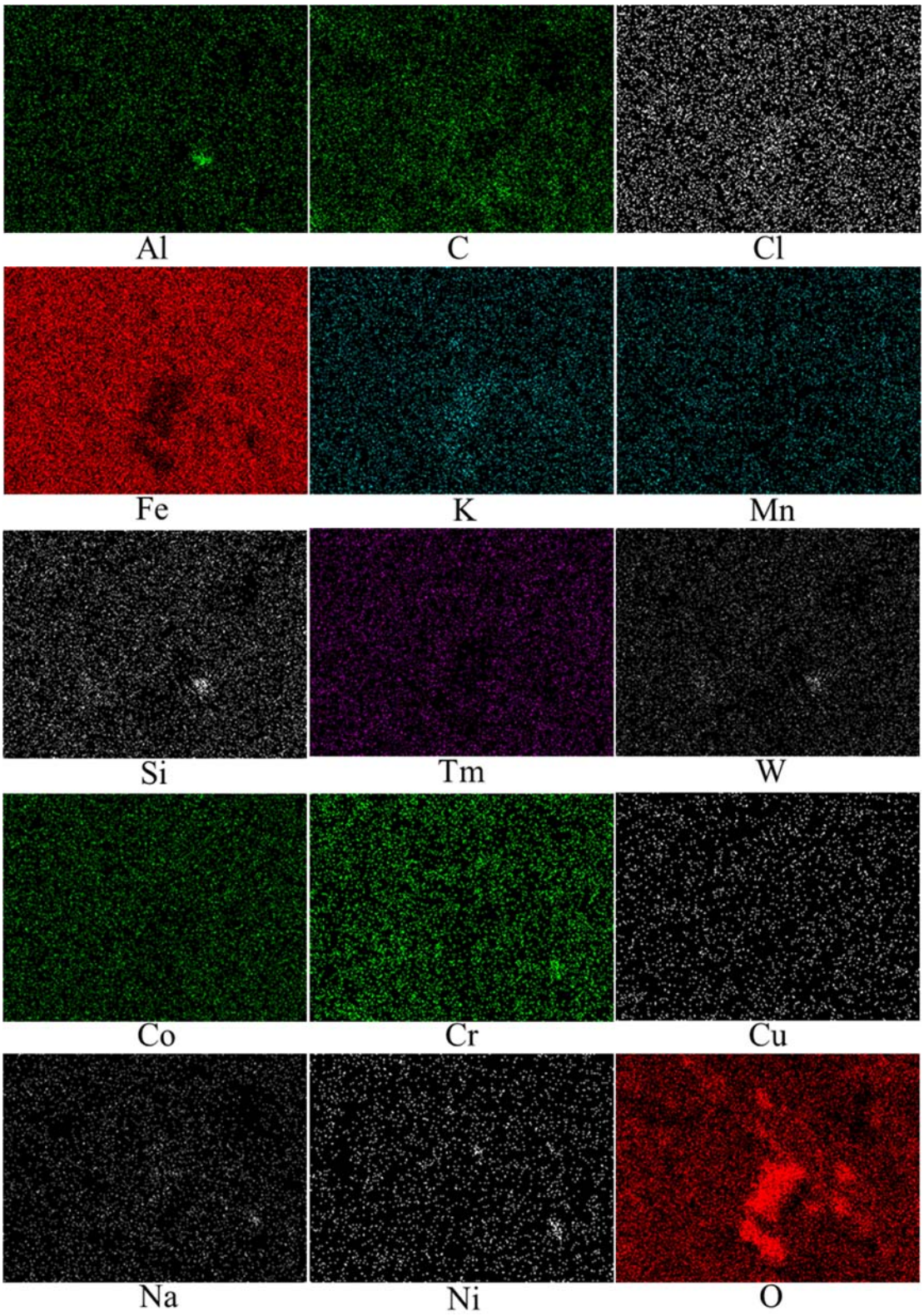


Figure 56. EDS analysis on wear track of O1 ss disks tested in KCl polymer mud.

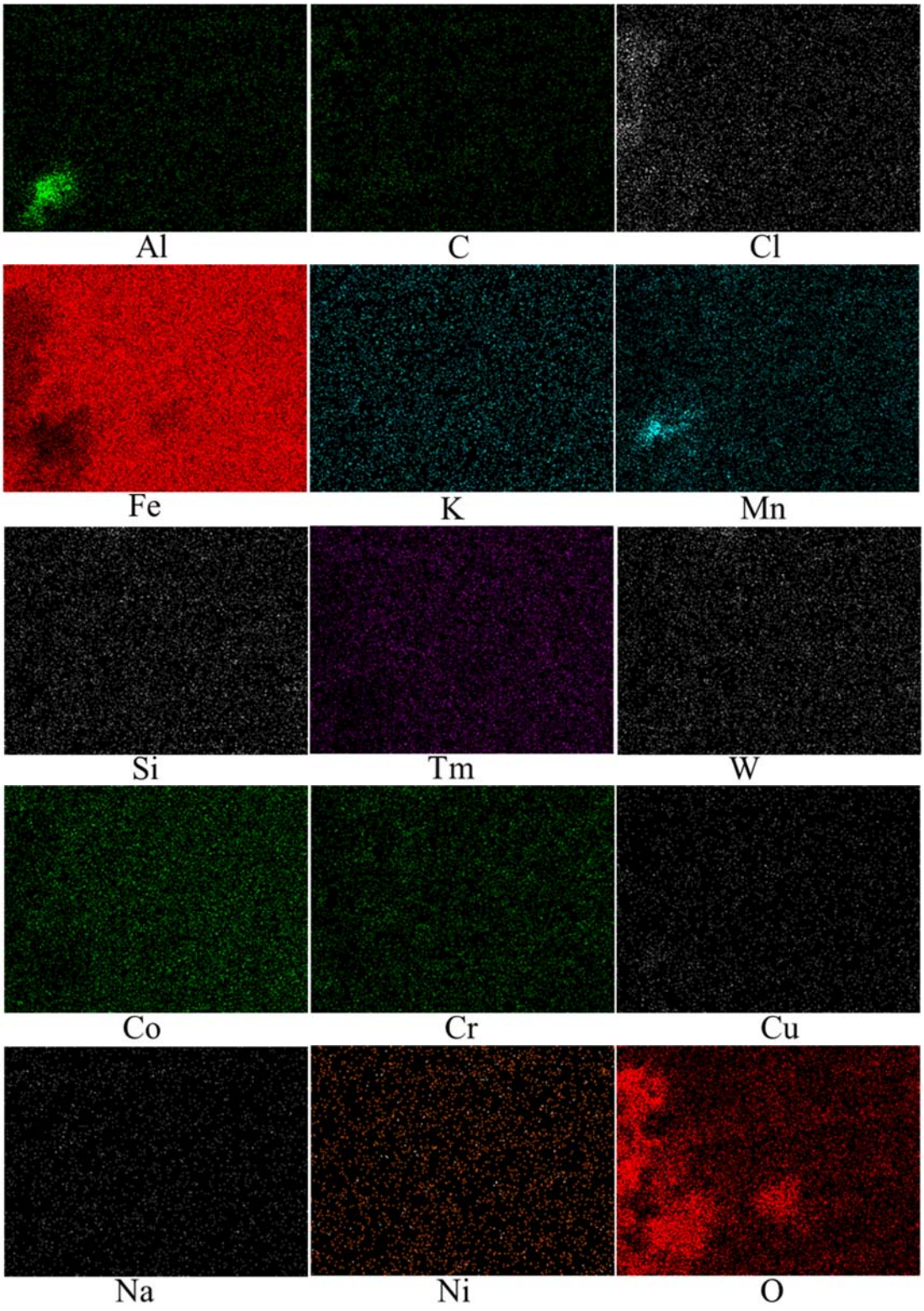


Figure 57. EDS analysis on wear track of O1 ss disks tested in KCl polymer mud + Amphiphile S.

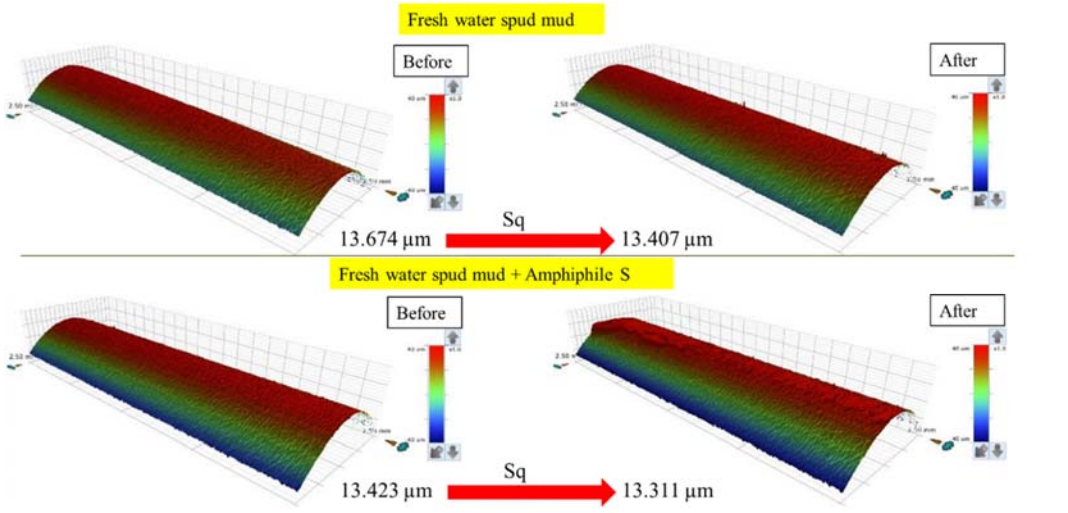


Figure 58. 3-D profilometry of hardbanded pins tested in fresh water spud mud and its altered version loaded with Amphiphile S.

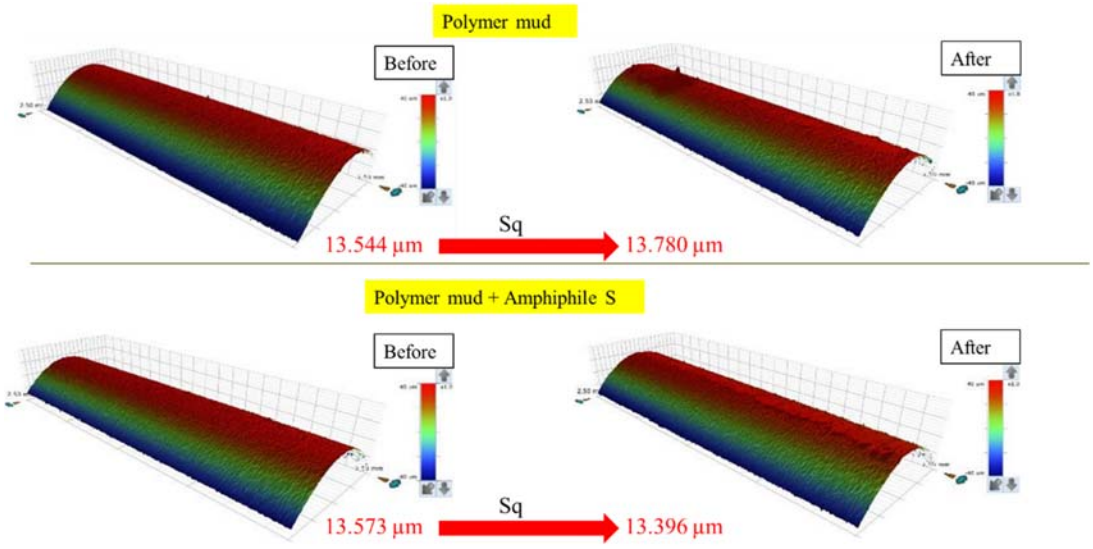


Figure 59. 3-D profilometry of hardbanded pins tested in polymer mud and its altered version loaded with Amphiphile S.

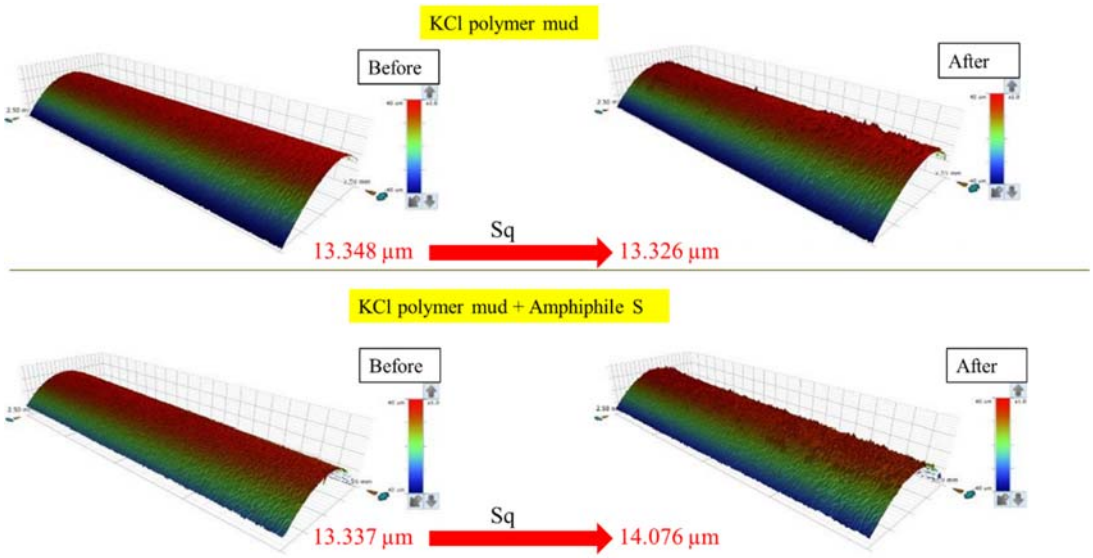


Figure 60. 3-D profilometry of hardbanded pins tested in KCl polymer mud and its altered version loaded with Amphiphile S.

### 6.5 Self-Welding in Drilling Applications for Oil & Gas Industry

In downhole drilling environment, as the heat generated due to friction between drill bit accumulates, the temperature of the drilling mud between the drill bit and the drill pipe keeps increasing. To a certain point, the temperature may be high enough to initiate vaporization of the drilling mud, gradually transforming from saturated lubrication towards boundary lubrication, even starved lubrication. When this occurs, metal-on-metal contact between the drill bit and the drill pipe becomes inevitable, consequently leading to excessive heat generation, which further aggravate the anti-friction and anti-wear performance of the drilling mud, and eventually result in system failure due to seizure between the drill bit and drill pipe, which could also be interpreted as self-welding between the drill bit and drill pipe. To this end, three preliminary concept proof experiments were performed to verify the tendency of self-welding for drilling applications, simulating starved lubrication (drilling mud completely vaporized). To better simulate the drilling application, sample pairs used for these preliminary tests were machined out of O1 ss disks, the

same material used for above tribological experiments reported in sections 6.1 ~ 6.4. The dimensions of the samples were not controlled (not neat), but the load pressure for all 3 tests was controlled at ~0.166 MPa.

Figure 73 (see Appendix) shows photographs of O1 ss sample pairs after preliminary concept proof self-welding experiments in air atmosphere under a nominal pressure of 0.166 MPa for drilling applications. Figure 73 (a)-(b) show the tested sample after 1-hour aging at 950 °C; Figure 73 (c) shows the sample pairs after 1-hour aging at 300 °C.

The experiments were done with 1-hour aging in air, at a temperature of 950 °C, 300 °C, and 200 °C, respectively. After 1-hour aging at 950 °C, the appearance of tested sample pairs changed from silver into completely grey and became very strongly self-welded, though the bonding strength measurement was not feasible due to the available sample preparing method and the sample dimensions obtained were not fully controlled. The appearance of samples aged at 300 °C changed from silver to dark blue, but not self-welded. The samples tested at 200 °C also did not demonstrate self-welding, and the sample appearance remained exactly the same as before aging.

These concept-proof tests proved that self-welding did can occur with a strong bonding at a high temperature when the aging period is short (1 hour), suggesting that a threshold of temperature exists for the self-welding in oil & gas applications to take place if the aging/ overhaul of drilling system due to seizure is short.

On the other hand, in case of a longer aging time/ overhaul of the drilling system, the threshold in temperature may be much lower for the tribopair to experience self-welding.

Further, in case of a higher loading pressure (>0.166 MPa), the sample pairs aged at 300 °C and 200 °C, are likely to experience self-welding even though the aging period is short as only 1-hour.

## 6.6 Summary

The primary purpose of this study was to further explore the lubricating performance of KCl polymer water-based mud (referred to as WBM) and three novel aqueous (water-based) drilling fluids under high-pressure high temperature (HPHT) conditions with increasing normal load, better simulating the downhole environment challenges for extended reach drilling, as well as their potential in continuous performance-improving with the aid of a selected additive. An Ultra-High Pressure Tribometer was used to realize simulation of the downhole HPHT drilling conditions and evaluate the tribological performance of pure aqueous muds with and without the influence of Amphiphile S.

With immersed lubrication, pure WBM (average overall COF 0.199) and KCl polymer mud (average overall COF 0.175) both demonstrated excellent lubricity highly competitive against oil-based muds, which typically deliver a COF about ~0.20. Under the influence of Amphiphile S selected for this study, the anti-wear and anti-friction performance of WBM, fresh water spud mud and polymer mud all demonstrated drastic improvement, with an overall average COF of 0.069, 0.103 and 0.111, respectively, all of which further outperform the COF range of OBMs.

When the tribopair was updated from O1 ss pairs into hardbanded pin against O1 ss disk, the overall lubricating performance of all drilling fluids, pure and loaded, all considerably degraded. Specifically, the performance-improving effect by Amphiphile S was remarkably weakened or even completed eliminated, this suggests a synergistic effect exists between the tribopair hardness and the effectiveness of selected additive. In other words, when the base fluids is the same, additive proven to benefit the tribological performance of relatively softer tribopairs does not necessarily guarantee the same effectiveness in performance promotion.

Also, it was observed through tribological experiments and further confirmed via hardness measurement that the same additive applied in this study imposed completely different influence over the surface hardness. With base fluids being fresh water spud mud and polymer mud, loading Amphiphile S resulted in softer contact surface, while loading the same additive into KCl polymer mud made the pin surface hardened, for both tested pin and fresh untested pin soaked in loaded drilling fluids for the period of time.

Different wear mechanisms were found to dominate for each drilling fluid. SEM images showed significant three-body abrasive and erosive wear on the metal surfaces due to silica particles, which are present in the drilling fluid.

# CHAPTER 7

## SELF-WELDING BEHAVIOUR OF NICKEL ALLOYS UNDER HPHT CONDITIONS

To investigate the potential self-welding tendency of nickel alloys at high temperatures, as well as to evaluate the strength of bonding within a tribopairs, which demonstrates self-welding behavior, a series of aging tests were performed inside a controlled atmosphere furnace at high temperature with nickel alloys Inconel 617® (950 °C) and 800 HT® (750 °C). The experiments involved usage of two atmosphere gases (helium and air, separately) and three different normal nominal load pressures (0.166 MPa, 0.248 MPa, and 0.341 MPa). The duration of aging of the samples inside the furnace ranged from 1~100 hours. After each experiment, a mechanical tensile stage was used to measure the bonding strength of the sample pairs that experienced self-welding. Figure 61 shows the schematic for aging test set-up and a photograph of the in-situ mechanical tensile stage used for bonding strength measurements upon completion of the aging experiments with nickel alloys. Figure 61 shows a photograph of Inconel 617® after 50-hour aging in helium and air, respectively.

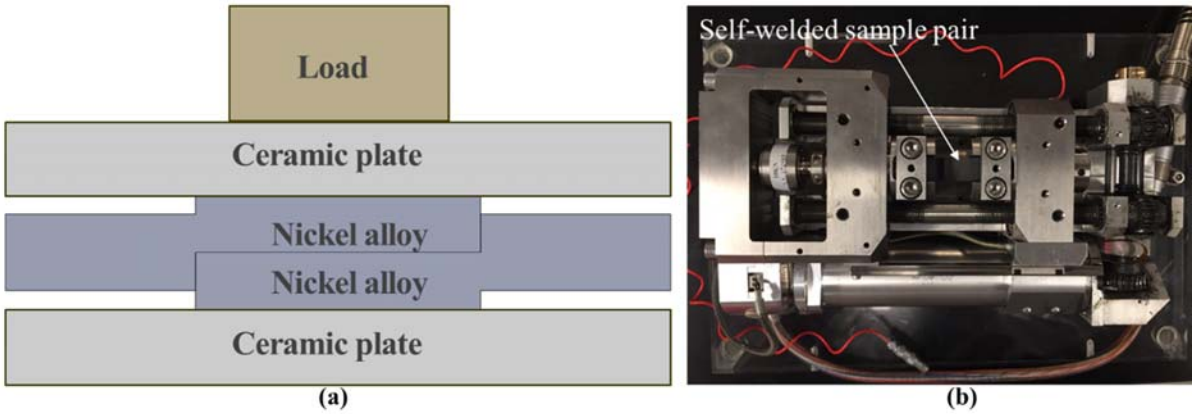


Figure 61. (a) Schematic for aging test set-up; (b) Photograph of tensile stage measuring the bonding strength of self-welded nickel alloy sample pairs.

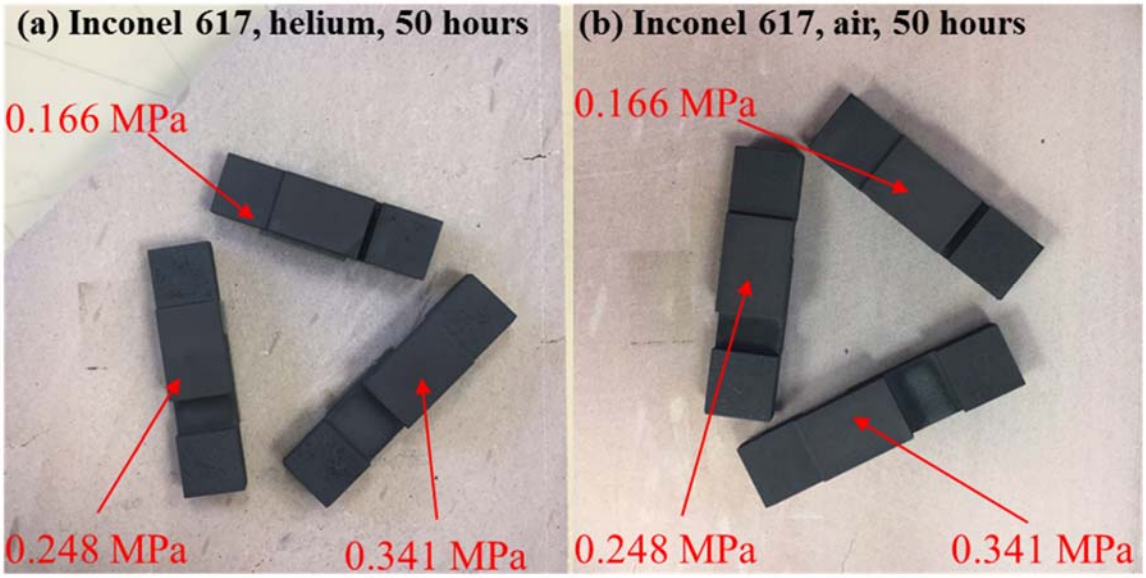

Figure 62. Self-welded Inconel 617® after 50-hour aging in: (a) helium; (b) air.

### 7.1 Self-welding of Inconel 617® in Helium Atmosphere

Figure 63 shows the measured breaking force (bonding strength) versus normalized bonding area, as well as the relationship between the apparent load pressure and the bonding force, obtained upon tests with Inconel 617® aged in helium environment for 50 and 100 hours, respectively. The normalized bonding area refers to the ratio of the surface area that experienced self-welding over the apparent contact area as preset before each experiment proceeded. The surface area that experienced self-welding is determined using image processing software Image J by detecting the areas that demonstrate abrasion/adhesion wear during the bonding strength measurement with a mechanical tensile stage (see Chapter 3). For each aging experiment, fresh nickel alloy samples were used inside fresh gas atmosphere.

As indicated in Figure 63 (a), for both aging durations, the breaking force (the force required to pull apart horizontally two pieces of Inconel 617® sample that self-welded with each other) increased dramatically along with increase in the normalized bonding area, suggesting an

exponential growth trend along with the normalized bonding area. For the same aging period, consistency has been observed for the potential relationship between normalized bonding area and breaking force. Extending the aging period from 50 to 100 hours resulted in a much steeper growth trend between the breaking force and the normalized bonding area.

With the same normalized bonding area, 100-hour aging in helium resulted in much stronger bonding than that obtained after 50-hour aging under exactly the same conditions. Also, for the sample pairs to obtain the same bonding strength, a longer duration of aging would require much less normalized bonding area.

Figure 63 (b) shows the relationship between the apparent loading pressure and the measured breaking force. For aging tests with a duration of 50 hours, the trend is very similar to that shown in Figure 63 (a).

The test data reported in Figure 63 was obtained through a series of simple experiments, not based on verified repeatability. Even with the apparent load and apparent contact area being the same, obtaining exactly the same effectively loaded area requires extremely fine control over the roughness of the contact surface, which is not available at this moment. Earlier experiments were performed under exactly the same conditions, i.e., experimental setup, normal loads, apparent contact areas, apparent contact pressures, aging durations and gas atmosphere. However, due to unexpected difficulty in obtaining effective loading for each sample pair during the test setup, most tested samples experienced self-welding to a rather limited extent. Consequently, the majority of those weakly self-welded sample pairs de-bonded easily when being secured on the tensile stage, before the measurement of bonding strength could proceed.

With exactly the same test setup and test conditions, self-welding experiments with Inconel 617® in aged for 10 hours in helium atmosphere were also performed. However, due to above explained

reasons, sample pairs under an apparent loading pressure of 0.248 MPa and 0.341 MPa both experienced de-bonding during the setup for tensile stage measurement. Sample pair under an apparent loading pressure of 0.166 MPa demonstrated a bonding strength of 89.5 N, with a normalized bonding area of 4.59%.

The breaking force increased along with the apparent loading pressure, which suggests that the three pairs of samples were all effectively loaded and evenly supporting the normal load applied on the top. When the aging duration was extended from 50 to 100 hours with fresh Inconel 617® samples under the same conditions and in the same environment, the case was not exactly as expected but instead slightly different. As the apparent loading pressure increased from 0.166 to 0.241 MPa, the bonding strength increased sharply from 340.6 to 3812.7 N. However, under a higher apparent loading pressure of 0.341 MPa, the bonding strength measured was lower at ~2000 N. The subsequent measurement for normalized bonding area was also lower with a value of ~30%, which aligns well with the lower bonding strength. Figure 64 shows the surface areas that experienced self-welding under different apparent loading pressures, for the measurement of normalized bonding area.

Table 21 summarizes the self-welding test results with Inconel 617® in helium environment after 50 and 100-hour aging (reported in Figure 63), as well as for all other tested aging durations ranging from 1 hour to 100 hours.

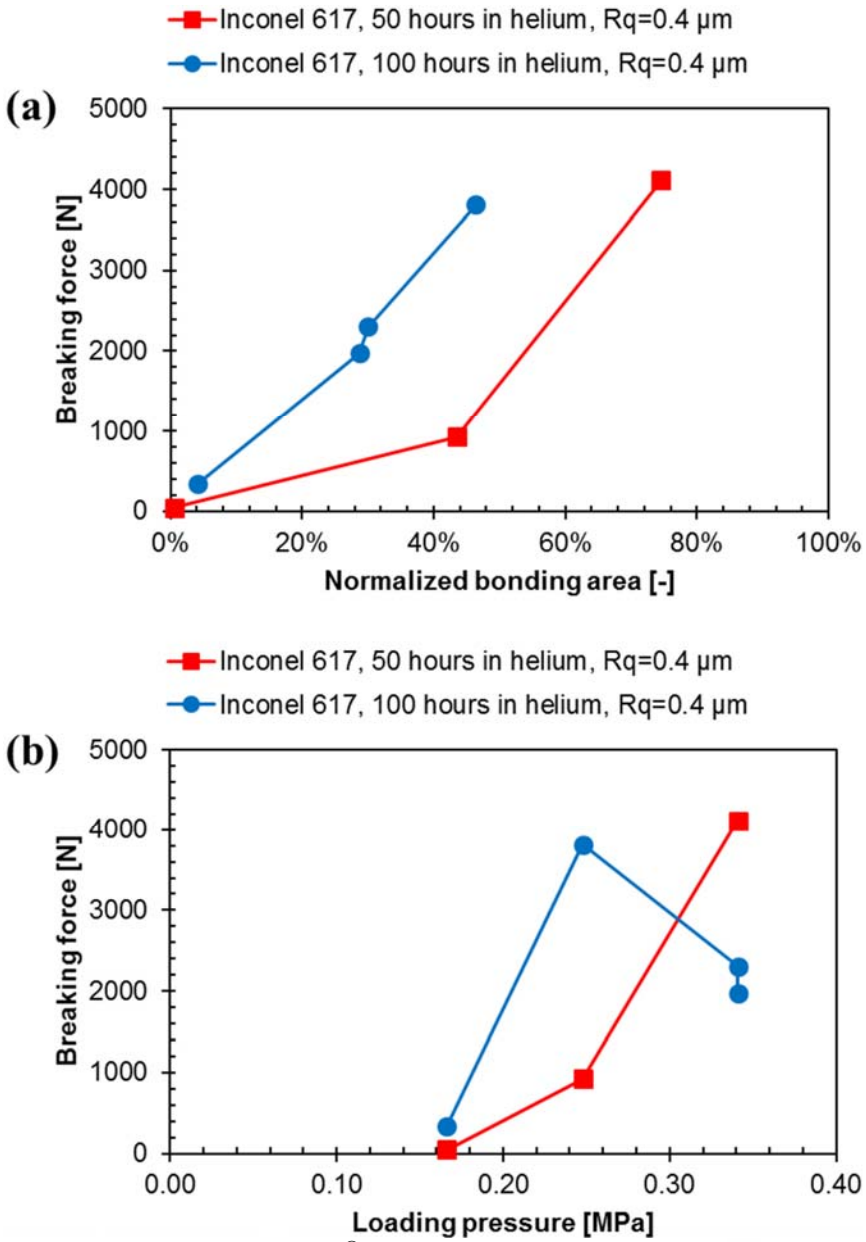


Figure 63. Breaking force of Inconel 617® after aging in helium at 950 °C for 50 and 100 hours. (a) Breaking force versus normalized bonding area; (b) breaking force versus apparent contact pressure.

In general, the nominally flat (universally ground with same grinding disks of the same grade) surfaces experience variation in their effective contacting areas.

As listed in Table 21, self-welding experiments with a nominal pressure of 0.166 MPa were also performed with an aging duration of 1 and 10 hours, respectively. For these two experiments, the apparent contact area was maintained the same as those samples pairs tested under a nominal pressure of 0.166 MPa for longer aging durations (50-hour and 100-hour). As indicated, the sample pair after 1-hour aging in helium atmosphere did not experience self-welding, while 10-hour aging in the same atmosphere under the same nominal pressure demonstrated bonding strength up to 200 N, suggesting that a threshold of aging duration exists for the self-welding of Inconel 617® to occur in helium atmosphere.

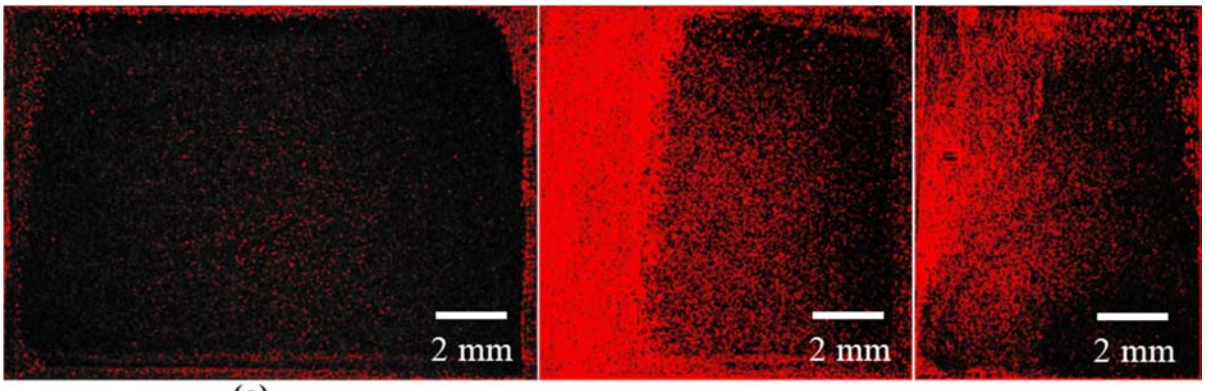


Figure 64. Measurement of normalized bonding area for Inconel 617® after 100-hour aging in helium at 950 °C under an apparent normal loading pressure of: (a) 0.166 MPa; (b) 0.248 MPa and (c) 0.341 MPa

**Table 21. Summary of self-welding test results for Inconel 617® in helium atmosphere.**

| Alloy | Surface Finish | Aging Time [hour] | Nominal Pressure [MPa] | Measured Force [N] | Bonding Ratio |
|---|---|---|---|---|---|
| Inconel 617® | Rq = 0.4 µm | 1 | 0.166 | 0 | 0% |
| | | 10 | 0.166 | 200.0 | 11.7% |
| | | 10 | 0.166 | 89.5 | 4.6% |
| | | | 0.248 | De-bonded | N/A |
| | | | 0.341 | De-bonded | N/A |
| | Rq = 0.2 µm | 50 | 0.166 | De-bonded | N/A |
| | | | 0.248 | De-bonded | N/A |
| | | | 0.341 | 117.3 | 12. 7% |
| | Rq = 0.4 µm | 50 | 0.166 | De-bonded | N/A |
| | | | 0.248 | 21.9 | 8.4% |
| | | | 0.341 | 324.1 | 20.7% |
| | | 50 | 0.166 | 48.2 | 0.6% |
| | | | 0.248 | 925.1 | 43.5% |
| | | | 0.341 | 4114.4 | 74.5% |
| | | 100 | 0.166 | 340.6 | 4.1% |
| | | | 0.248 | 3812.7 | 46.4% |
| | | | 0.341 | 2306.0 | 30.0% |
| | | | 0.341 | 1975.9 | 28.7% |

### 7.2 SEM and EDS Analysis of Inconel 617® Self-Welded in Helium Atmosphere

Figure 65 shows scanning electron microscopy images of the cross sections of Inconel 617® after 100 hours of aging at 950 °C, under a contact pressure of 0.166 MPa, 0.248 MPa and 0.341 MPa, respectively. Under all tested contact pressures, a special ‘glazed’ layer clearly distinguishable from the bulk materials was observed. As the contact pressure increased from 0.166 MPa to 0.341 MPa, the boundary lines between this layer and the bulk substrate became less and less distinguishable, indicating material creep at such high temperatures.

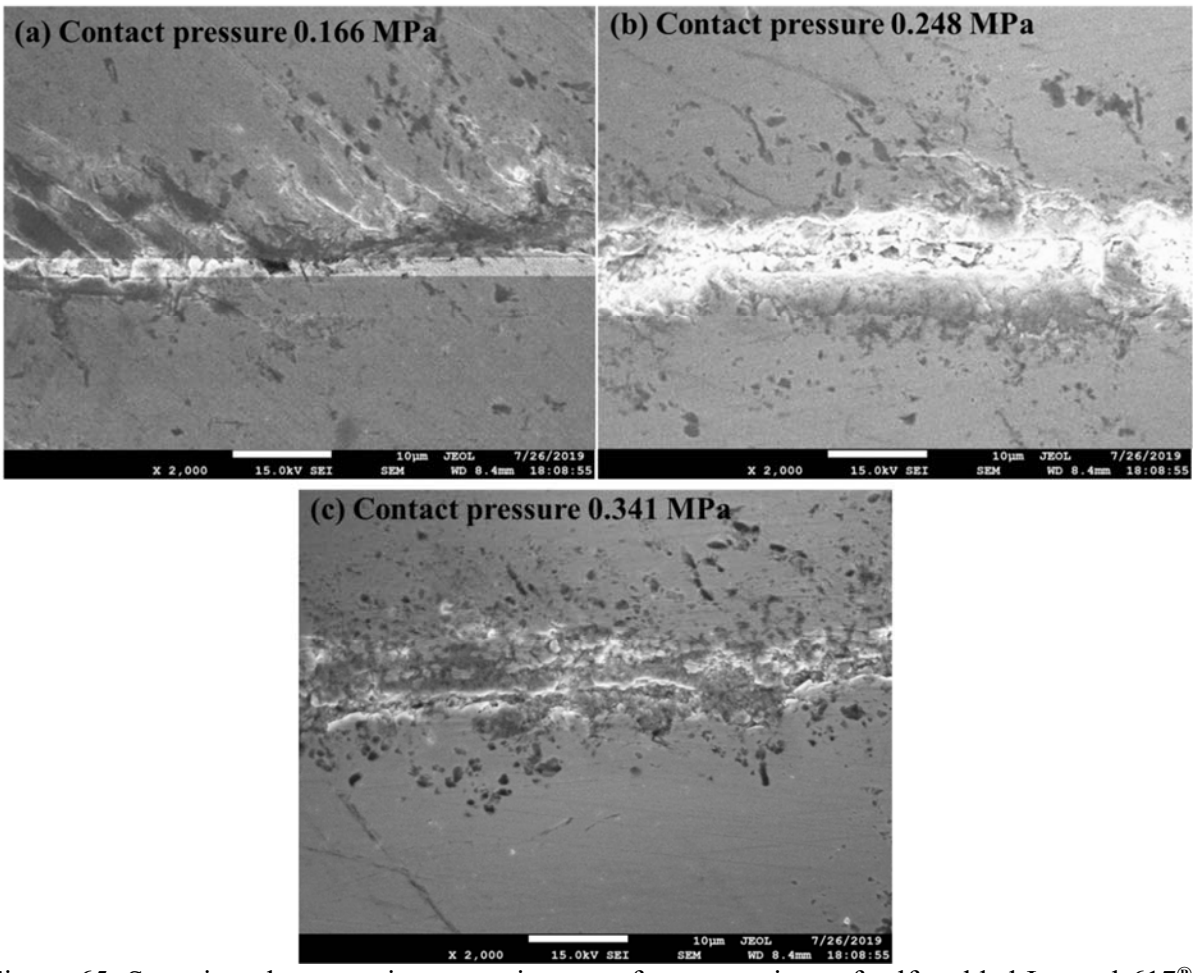

Figure 65. Scanning electron microscope images of cross sections of self-welded Inconel 617®. Aging period for 100 hours in Helium at 950 °C.

Figure 66, Figure 67 and Figure 68 show the elemental mapping for the cross sections obtained via Energy-dispersive X-ray spectroscopy. At the interface where self-welding occurred, elements of $O_2$, and Cr showed higher intensities, than the region of bulk material that is farther away from the interface. Elements Al, Fe, Co, Ni and Mo all showed lower intensities than the region of bulk material that is farther away from the interface. As the contact pressure increased from 0.166 MPa to 0.341 MPa, the concentration/migration of the above elements became more significant. The intensity increase of $O_2$ comes from the impurities of oxygen contained in the helium atmosphere,

while changes of intensity for Cr, Al, Fe, Co, Ni and Mo resulted from elemental diffusion/ migration through the interface of the contacting sample pairs. The special 'glazed' layers shown in Figure 65 are likely chromium oxides ($Cr_xO_y$), to which the self-welding is mainly attributable.

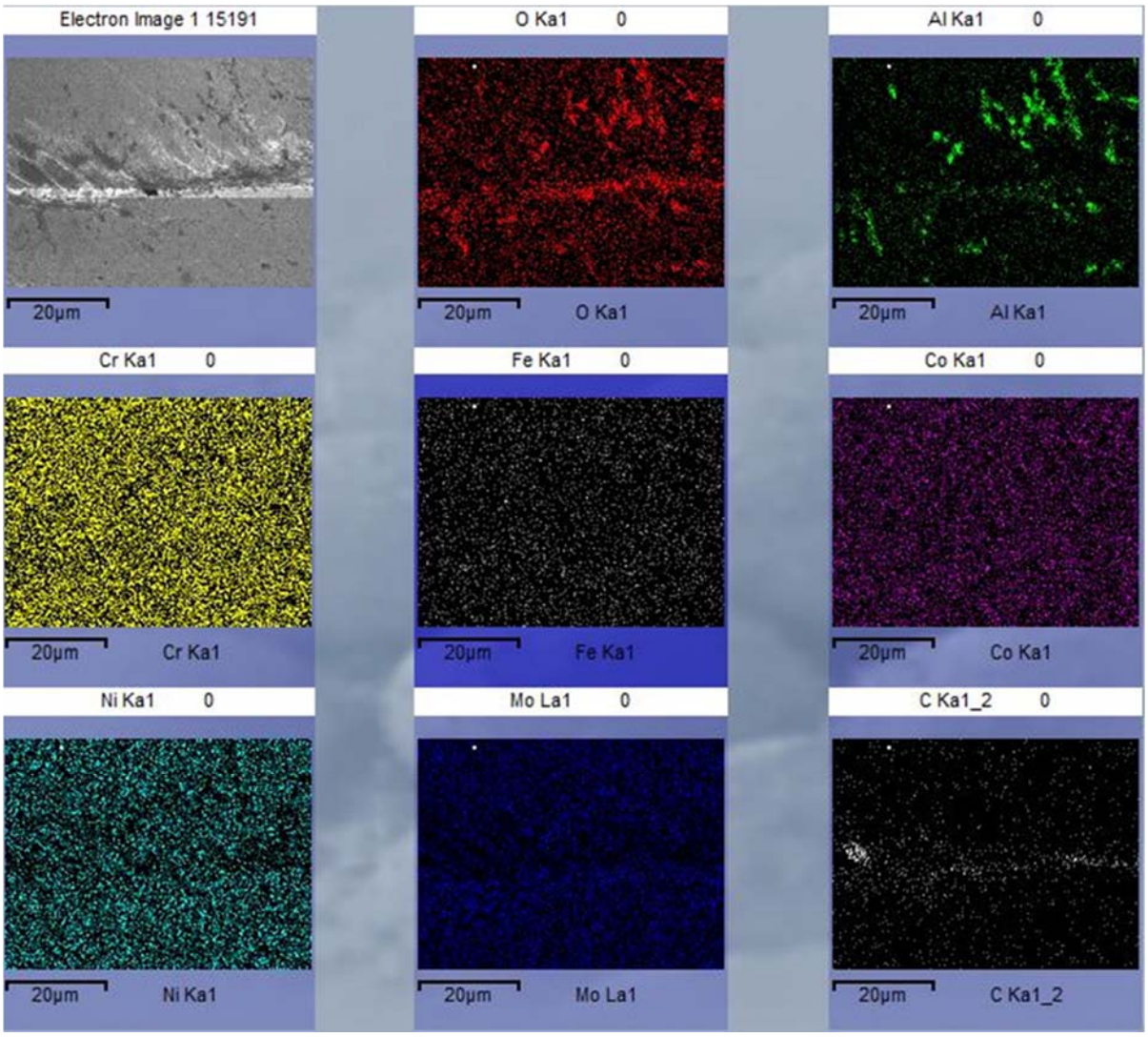

Figure 66. Energy-dispersive X-ray spectroscopic elemental mapping for cross section of self-welded Inconel 617® under contact pressure 0.166 MPa and after 100 hours aging in helium at 950 °C.

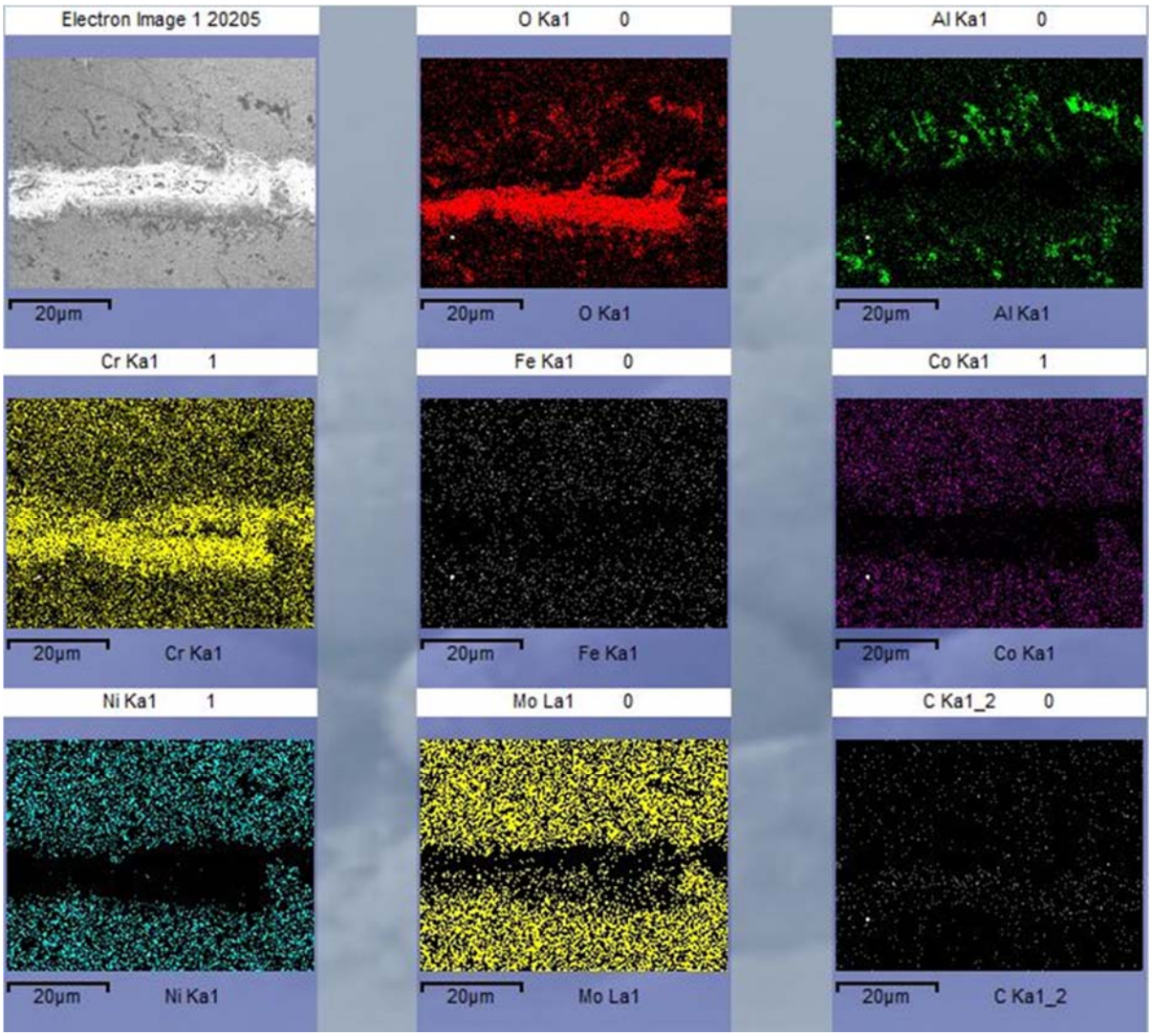

Figure 67. Energy-dispersive X-ray spectroscopic elemental mapping for cross section of self-welded Inconel 617® under contact pressure 0.248 MPa and after 100 hours aging in helium at 950 °C.

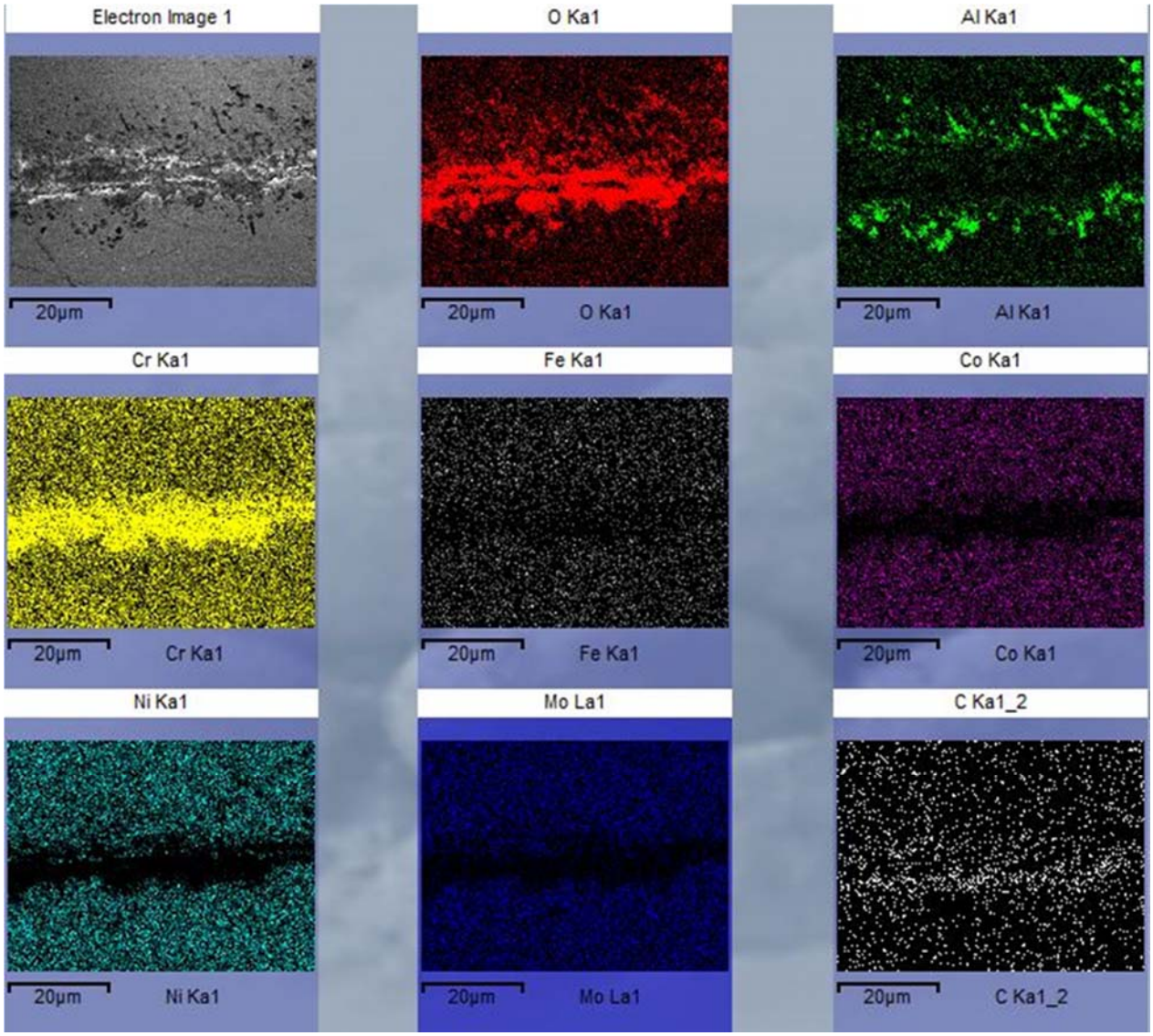


Figure 68. Energy-dispersive X-ray spectroscopic elemental mapping for cross section of self-welded Inconel 617® under contact pressure 0.341 MPa and after 100 hours aging in helium at 950 °C.

### 7.3 Self-welding of Inconel 617® in Air Atmosphere

When two surfaces are mated and come into close contact under a certain normal load, strong interatomic forces and weak intermolecular forces together promote intense adhesion between contacting metal surfaces. For nuclear reactor applications, the components and sub-systems all operate at extremely high temperatures, i.e., ≥ 1000 °C for VHTR. This high operating temperature further accelerates elemental diffusion/ migration across the contacting interface, and hence resulting in a stronger adhesion or self-welding. Therefore, maintaining an inert atmosphere serving as oxide film barrier, such as high purity helium, during normal operation is necessary. However, in scenarios where the system overhauls due to malfunctioning of components or subsystems, the inert atmosphere will be replaced by ambient air gradually, while the components of the system are still at extremely high temperatures. When this occurs, the risk of self-welding phenomena among components significantly rises, as the ~20% concentration of $O_2$ included in the ambient air would serve as a source of oxygen needed for the formation of oxides that are responsible for the self-welding, i.e., chromium oxides. Therefore, self-welding experiments following the same test protocol were also performed in air atmosphere.

Figure 69 shows the measured breaking force versus normalized bonding area, as well as the relationship between the apparent load pressure and the bonding force, obtained upon tests with Inconel 617 aged in air environment for 50 and 100 hours, respectively.

As shown in Figure 69 (a), the breaking force required to pull apart the bonded pair of Inconel 617® increases nearly exponentially along with the normalized bonding area, which is consistent with the previous test results performed in helium environment (see Figure 63). Similar to the tests in helium, the bonding strength of self-welded samples demonstrates an exponential trend in growth along with the normalized bonding area. Further, assuming the loading pressure is

effectively applied, a longer aging duration in air also suggests a steeper slope of the increase of bonding strength versus the normalized bonding area. The reason for this is that a longer aging time allows continuous formation and accumulation of oxides (the 'glazed' layer) at the interface, which is the plays a critical role in the occurrence self-welding and subsequent bonding strength. Figure 69 (b) further confirms that ineffective real contact area loading, the actual loading pressure is lower than apparent value, could result in a lower normalized bonding area even when the apparent loading pressure was increased, accompanied with a weakened bonding strength. Table 22 summarizes the self-welding test results with Inconel 617® in air after 50 and 100-hour aging, respectively. This further confirms that the complexity of macro rough surface finish renders the strength of self-welding difficult to predict. Similar to tests with Inconel 617 in helium atmosphere, the bonding strength of 0 N (absence of self-welding) and 302 N after 1-hour and 10-hour aging, respectively, suggests that a minimum aging time is required for the samples to experience self-welding when the nominal pressure is the same at 0.166 MPa.

**Table 22. Summary of self-welding test results for Inconel 617® in air atmosphere.**

| Alloy | Surface Finish | Aging Time [hour] | Nominal Pressure [MPa] | Measured Force [N] | Bonding Ratio |
|---|---|---|---|---|---|
| Inconel 617® | Rq = 0.4 µm | 1 | 0.166 | 0 | 0% |
| | | 10 | 0.166 | 302.0 | 1.91% |
| | | 50 | 0.166 | 1177.2 | 29.1% |
| | | | 0.248 | 1315.4 | 32.8% |
| | | | 0.341 | 4337.8 | 51.4% |
| | | 100 | 0.248 | 711.5 | 4.0% |
| | | | 0.166 | 798.9 | 5.0% |
| | | | 0.341 | 3394 | 11.5% |

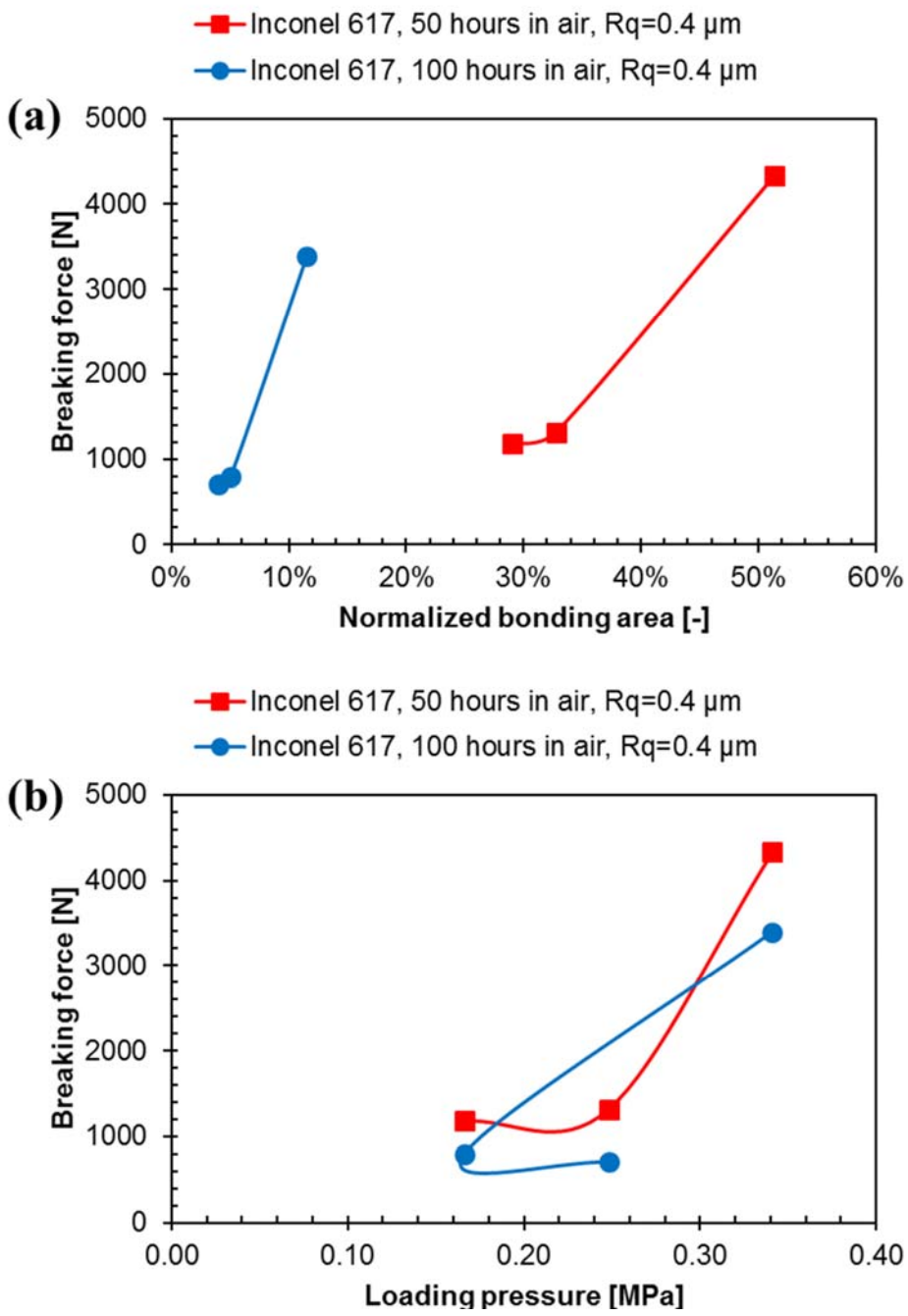


Figure 69. Breaking force of Inconel 617® after aging in air at 950 °C for 50 and 100 hours. (a) Breaking force versus normalized bonding area; (b) breaking force versus apparent contact pressure.

### 7.4 Self-welding of 800 HT® in Helium Atmosphere

Figure 70 shows the measured breaking force versus normalized bonding area, as well as the relationship between the apparent load pressure and the bonding force, obtained upon tests with 800 HT® aged in helium environment for 10 hours, with a surface finish of 0.4 and 0.2 μm, respectively.

These aging tests with 800 HT® were performed at the beginning of the study in this chapter, without extra measures to ensure each pair of samples were effectively loaded. Upon completion of an aging experiment in helium with 800 HT® samples at 750 °C, all the 800 HT® samples originally were self-welded within each of the tribopairs. However, two out of three pairs later de-bonded during the bonding strength measurement on the mechanical tensile stage, as the sample pairs were being secured onto the tensile stage via a locking mechanism. This suggests that a rather weak bonding had been formed during the aging period. One possible reason for this was due to insufficient duration of aging, but it is more likely a consequence of ineffective loading due to the microscale complexity due to the nature of nominally flat surfaces. Nevertheless, for 800 HT® samples polished with a surface finish of Rq = 0.2 μm, a nearly exponential trend for the bonding strength growth along with the normalized bonding area was observed, which is consistent with the obtained Inconel 617® results. Figure 70 (b) confirms that effective loading is of critical importance to the occurrence of self-welding phenomenon.

Based on observations and analysis for the possible root causes that resulted in weak bonding strength in tests with 800 HT®, the test procedure for alloy pairs setup and loading mechanism was reviewed and redesigned for help improve effective loading, though still difficult to control due to the nature of macro flat surfaces. Consequently, test results demonstrating significantly stronger self-welding were obtained for Inconel 617, as reported in sections 7.1~7.3.

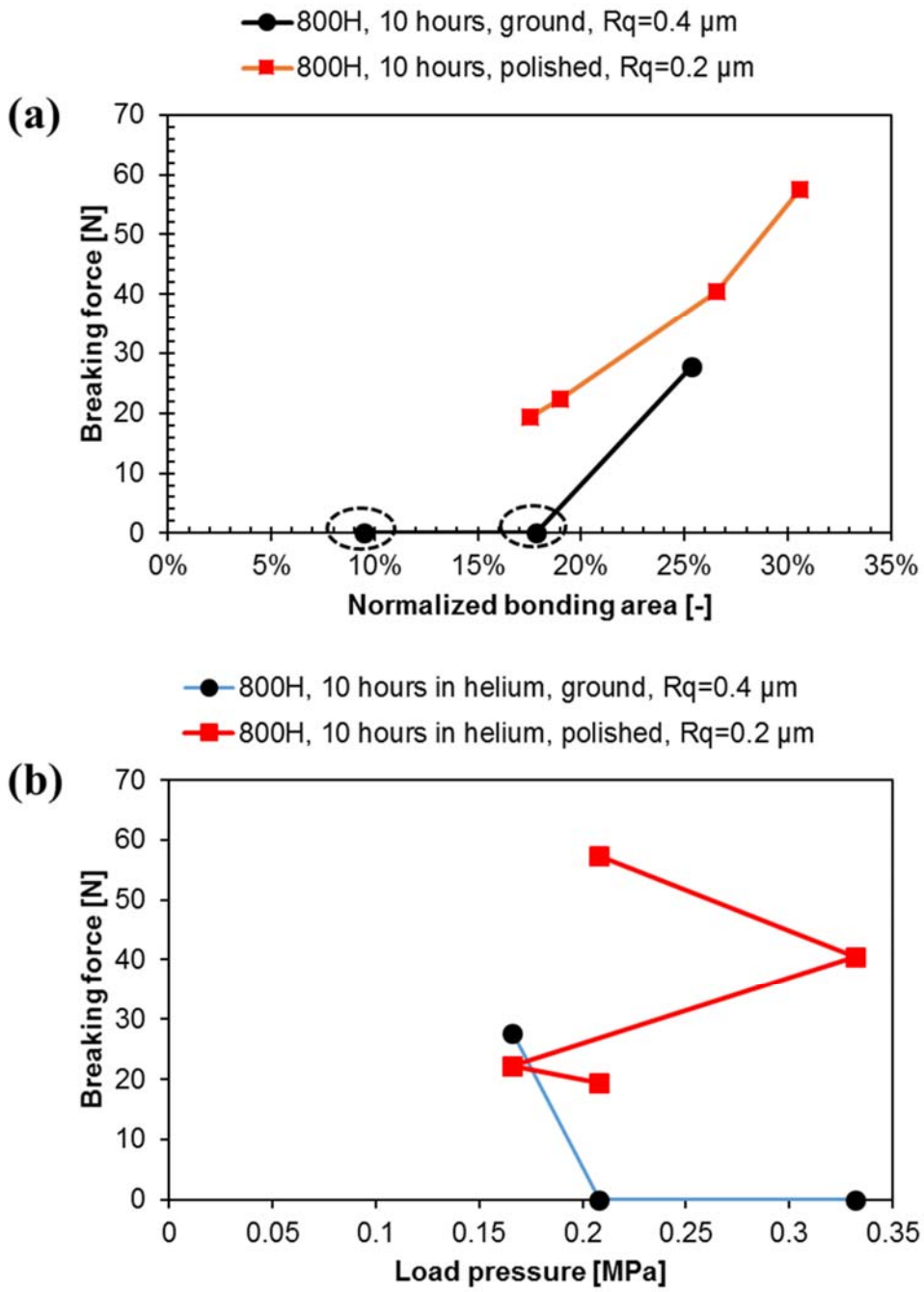


Figure 70. Breaking force of 800 HT® after aging in helium at 750 °C for 10 hours. (a) Breaking force versus normalized bonding area; (b) breaking force versus apparent contact pressure.

**Table 23. Summary of self-welding test results for 800 HT® in helium atmosphere.**

| Alloy | Surface Finish | Aging Time [hour] | Nominal Pressure [MPa] | Measured Force [N] | Bonding Ratio |
|---|---|---|---|---|---|
| 800 HT® | Rq = 0.2 μm | 10 | 0.166 | 22.3 | 19.0% |
| | | | 0.208 | 57.4 | 18.3% |
| | | | 0.332 | De-bonded | N/A |
| | | 10 | 0.166 | De-bonded | N/A |
| | | | 0.208 | 19.4 | 17.5% |
| | | | 0.332 | 40.4 | 26.6% |
| | Rq = 0.4 μm | 10 | 0.166 | 27.7 | 25.3% |
| | | | 0.208 | De-bonded | 9.5% |
| | | | 0.332 | De-bonded | 17.8% |
| | | 10 | 0.166 | De-bonded | N/A |
| | | | 0.208 | De-bonded | N/A |
| | | | 0.332 | De-bonded | N/A |
| | | 50 | 0.166 | 23.0 | 26.6% |
| | | | 0.208 | De-bonded | N/A |
| | | | 0.332 | De-bonded | N/A |

### 7.5 Summary

To investigate the tendency of potential self-welding behavior, as well as to measure the bonding strength of self-welded nickel alloys operating under extreme conditions, which can be of critical importance for the reliability and operability of mechanical components and systems in nuclear reactor applications, a series of aging experiments were performed at high temperature under applied normal load with nickel alloy Inconel 617® (950 °C) and 800 HT® (750 °C). Test results show that, under an applied normal load, self-welding behavior does occur between Inconel 617® vs. Inconel 617® and 800 HT® vs. 800 HT® tribopairs at high temperatures within air and helium environment, respectively. The bonding strength due to self-welding could be remarkably strong, i.e., 4114.4 N and 4337.8 N after 50-hour aging under an apparent loading pressure of 0.341 MP, inside helium and air atmosphere, respectively.

With effective loading applied on each pair of samples, a longer aging duration would result in much stronger bonding, as evidenced by a larger normalized bonding area after pulling apart two pieces of samples that experienced self-welding with each other upon completion of the aging tests. Also, provided with application of effective loading pressure, a higher apparent loading pressure would result in a significant higher normalized bonding area and accordingly a much higher bonding strength. However, during the tests performed with both Inconel 617® and 800 HT®, it has been observed that the actual loading pressure applied on each pair of samples may be much lower than the apparent value, as a result of imperfect surface finish, i.e., high spots or uneven surfaces, which is the nature of nominally flat rough surfaces.

# CHAPTER 8

# CONCLUSIONS AND RECOMMENDATIONS

## 8.1 Conclusions

### 8.1.1 Influence of Friction Modifying Additives on Tribological Performance of Water-based and Oil-based Muds

A series of tribological experiments were performed with E52100 stainless steel balls with a 4-ball tester to investigate the performance of water-based drilling fluids with a focus on anti-friction and anti-wear. Four different commercial additives were added into each of the water-based drilling fluids to evaluate the additives' potential influence on the tribological performance of the drilling fluids. A reference oil-based drilling fluid was tested with and without the presence of the same four additives, as a baseline for comparison.

Without interference of additives, the COF of pure WBM (0.493) and KCl (0.617) were significantly higher than that of pure OBM (0.264), by 86.7% and 133.7%, respectively. However, with the aid of certain additives, the tribological performance of both WBM and KCl was significantly improved to a level where they were fully competitive against, or even superior, to OBM and its mixtures. Particularly, WBM/ Vikinol® 18 (0.275) and WBM/ EvoLube® G (0.261) demonstrated lubricating performance very close to that of pure OBM. Further, with the aid of Ultra Lube® II and EvoLube® G, artificial sea water (KCl brine) showed superior COF (0.190 and 0.209, respectively), lower than pure OBM by 28.0% and 20.1%. Chemical analysis showed the formation of a thin tribolayer of $Fe_3O_4$ in the presence of WBM/ Vikinol® 18 and a layer composed of $FeCl_2/Fe_3O_4$ in KCl/Ultra Lube® II. The $FeCl_2/Fe_3O_4$ layer is an effective tribofilm and reduces both COF and wear. Taking into account both wear and COF results, it was found that with the aid

of selected friction modifying additives, the tribological performance of environmentally friendly alternatives such as artificial sea water (KCl brine) could be promoted to a level where they are completely qualified replacement for conventional OBM for oil & gas industry.

### 8.1.2 Influence of Graphene on the Tribological Performance of Water-Based and Oil-Based Muds

Similar to friction-modifying additives, wear test results showed that graphene could also benefit the tribological performance of drilling fluids, both water-based and oil-based.

For OBM and distilled water, a higher concentration of graphene added into the base fluid resulted in further improvement in the lubricant's anti-friction and anti-wear properties. Increasing the concentration of graphene from 2.5 wt. % to 5.0 wt. % resulted in further reduction in COF, and wear scar size. On the other hand, adding graphene of higher concentration did not further improve the tribological performance of the lubricant when the base fluid was WBM or KCl brine. Specifically, adding 2.5 wt. % graphene into KCl brine reduced the COF and wear diameter by 60.1% and 16.7%, while adding 5.0 wt.% graphene reduced the COF and wear diameter by 56.9% and 6.3% instead.

Unlike commercial additives tested in Chapter 4, adding graphene benefited the tribological performance of WBM to a rather limited extent, with a COF and wear rate that were still inferior to those of OBM.

In general, the presence of graphene significantly improved the tribological performance of OBM, KCl brine and distilled water, and graphene-loaded KCl brine and distilled water both showed lubricity comparable with and even better than OBM, though at the sacrifice of slightly higher

wear. The test results suggests that an optimum concentration of graphene exists for the tested base drilling fluids for maximum performance improvement, especially WBM and KCl brine.

### 8.1.3 Tribological Performance of Water-Based/Aqueous Muds in HPHT Downhole Environment

Under the influence of a proprietary additive Amphiphile S, the anti-wear and anti-friction performance of WBM, fresh water spud mud and polymer mud all demonstrated remarkable improvement, with an overall average COF of 0.069, 0.103 and 0.111, respectively, all of which completely outperform OBMs. Elevated hardness of tribopairs (with the intention of improved wear-resistance) may impose adverse influence on the friction-modifying benefit of the same additive when loaded into the same base fluid, showing degraded or even eliminated improvement in anti-friction and anti-wear performance.

Further, Amphiphile S applied in this study imposed varying influence over the surface hardness. Depending on the base fluid, introducing Amphihpile S resulted in increase and decrease in the surface hardness of the tribopairs. Note that the tribopairs were all of the same material for all the tribological tests performed.

### 8.1.4 Self-Welding Behavior of Nickel Alloys

Self-welding behavior does occur between Inconel 617® vs. Inconel 617® and 800 HT® vs. 800 HT® tribopairs at high temperatures within air and helium environments, respectively, under an applied normal load. Once occurred, the bonding strength due to self-welding could be remarkably strong. Inconel tribopairs demonstrated a bonding strength of 4114.4 N and 4337.8 N after 50-

hour aging under an apparent loading pressure of 0.341 MP, inside helium and air atmosphere, respectively.

The apparent loading pressure is not necessarily the same as the actual or real contact pressure, which means the tribopairs are not effectively loaded. Possible reasons for this include uneven surface finish on the top surface which is in direct contact with the ceramic plate atop, through which the normal load was applied.

Test results consistently indicate an exponential growing trend of the bonding strength along with the normalized bonding area. Further, assuming the loading pressure is effectively applied, a longer aging duration is expected to results in a much stronger bonding shown as a steeper slope of the increase of bonding strength versus the normalized bonding area. Also, with the same normalized bonding area, a higher bonding strength is expected after a longer duration of aging.

### 8.2 Recommendations for Future Work

1. Evaluate the influence of graphene with concentrations lower than 2.5 wt. % on the tribological performance of the tested drilling fluids, especially for WBM, considering the fact that the 2.5 wt. % graphene failed to improve the performance of WBM to a level comparable to OBM. Further, both WBM and KCl brine showed that a higher (5.0 wt. %) concentration of graphene resulted in less performance improvement than a lower (2.5 wt. %) concentration. It is highly likely that graphene with a concentration lower than 2.5 wt. % may improve the performance of WBM to a level competitive against OBM.
2. Given that the test protocol with UHPT represents operating conditions better simulating the downhole drilling environment, and that a proprietary additive Amphiphile S demonstrated that the performance of water-based and aqueous muds could be promoted to a level where

they are fully promising as replacement for conventional OBMs, it would be of practical value to evaluate the potential of performance capability of commercial additives, i.e., the four additives tested with the four-ball configuration.

3. Self-welding test results suggests that effective loading on top of nickel alloy tribopairs plays a critical role in the occurrence of self-welding and the bonding strength. Therefore, for further investigation, it is recommended that measures such as improving the quality of the contacting surface finish and/or applying universal textures/ patterns are necessary. Further, improving the finish of surfaces which will be in direct contact with the loading mechanism would also be beneficial.

## REFERENCES


[1] W.C. Lyons, G.J. Plisga, M.D. Lorenz, Standard Handbook of Petroleum and Natural Gas Engineering, 2015. https://doi.org/10.1016/C2010-0-64695-5.

[2] M. Humood, M.H. Ghamary, P. Lan, L.L. Iaccino, X. Bao, A.A. Polycarpou, Influence of additives on the friction and wear reduction of oil-based drilling fluid, Wear. 422–423 (2019) 151–160. https://doi.org/10.1016/j.wear.2019.01.028.

[3] P. V Kotvis, W.T. Tysoe, The surface chemistry of chlorinated hydrocarbon lubrication additives, Tribol. Lett. 3 (1997) 303–309. https://doi.org/10.1023/A:1019162028761.

[4] P. V Kotvis, L. Huezo, W.S. Millman, W.T. Tysoe, The surface decomposition and extreme-pressure tribological properties of highly chlorinated methanes and ethanes on ferrous surfaces, Wear. 147 (1991) 401–419. https://doi.org/10.1016/0043-1648(91)90195-Z.

[5] P. V Kotvis, W.T. Tysoe, M.N. James, An investigation of film removal in extreme pressure lubrication using chlorinated hydrocarbon additives, Wear. 153 (1992) 305–314. https://doi.org/10.1016/0043-1648(92)90171-4.

[6] P. V Kotvis, L.A. Huezo, W.T. Tysoe, Surface Chemistry of Methylene Chloride on Iron: A Model for Chlorinated Hydrocarbon Lubricant Additives, Langmuir. 9 (1993) 467–474. https://doi.org/10.1021/la00026a018.

[7] O. Beeck, J.W. Givens, A.E. Smith, On the mechanism of boundary lubrication I. The action of long-chain polar compounds, Proc. R. Soc. London. Ser. A. Math. Phys. Sci. 177 (1940) 90–102.

[8] O. Beeck, J.W. Givens, E.C. Williams, On the mechanism of boundary lubrication. II. Wear prevention by addition agents, Proc. R. Soc. London. Ser. A. Math. Phys. Sci. 177 (1940)

103–118. https://doi.org/10.1299/kikai1938.10.39-1_73.

[9] D.O. Leeser, R.C. Williams, Evaluation of Material Wear and Self-Welding in Sodium-Cooled Reactor Systems, in: JAtomic Power Dev. Assoc. Inc., Detroit, MI (United States), 1958. https://doi.org/10.1115/1.4008424.

[10] M.L. Payne, D.A. Cocking, A.J. Hatch, Critical technologies for success in extended reach drilling, in: Proc. - SPE Annu. Tech. Conf. Exhib., 1994: pp. 23–37. https://doi.org/10.2523/28293-ms.

[11] F. Allen, P. Tooms, G. Conran, B. Lesso, P. Van De Slijke, Extended-Reach Drilling : Breaking the 10-km Barrier, Oilf. Rev. Winter (1997) 32–47.

[12] M.L. Payne, D.A. Cocking, A.J. Hatch, Critical Technologies for Success in Extended Reach Drilling, in: SPE Annu. Tech. Conf. Exhib., 1994. https://doi.org/10.2118/28293-MS.

[13] P. Chilingarian, G.V. ; Vorabutr, Drilling and Drilling Fluids, Elsevier Scientific, Amsterdam, 1981.

[14] R. Caenn, H.C.H. Darley, G.R. Gray, Composition and Properties of Drilling and Completion Fluids, 2011. https://doi.org/10.1016/C2009-0-64504-9.

[15] R. Caenn, G. V. Chillingar, Drilling fluids: State of the art, J. Pet. Sci. Eng. 14 (1996) 221–230. https://doi.org/10.1016/0920-4105(95)00051-8.

[16] SPE, Drilling fluid types, (2001).

[17] P. et al., Oil Based Synthetic Hydrocarbon Drilling Fluid, 5189012, 1993.

[18] Noria Corporation, Lubricant Additives - A Practical Guide, (n.d.).

[19] H. Spikes, Friction Modifier Additives, Tribol. Lett. 60 (2015) 1–26. https://doi.org/10.1007/s11249-015-0589-z.

[20] B.U.B. Bray, C.C. Moore, D.R. Merrill, Improvements in Diesel-Engine Lubricating Oils, (2017) 35–42. https://doi.org/10.4271/390125.

[21] C.F. Prutton, D.R. Frey, D. Turnbull, G. Dlouhy, Corrosion of Metals by Organic Acids in Hydrocarbon Solvents, Ind. Eng. Chem. 37 (1945) 90–100. https://doi.org/10.1021/ie50421a020.

[22] and J.G.P. Herschel G. Smith, Wallingford, and Troy L. Cantrell, Drexel Hill, Pa., Mineral Oil Compositions Containing Amidic Acids or Salts Thereof, 1955.

[23] G.W. Eckert, Adducts of Aliphatic Monocarboxylic Acids and Aliphatic Amines in Gasoline, 1962, 1962.

[24] J.W. Schick, J.M. Kaminski, Lubricant Composition for Reduction of Fuel Consumption in Internal Combustion Engines, 4304678, 1981.

[25] A.F. Sirianni, I.E. Puddington, Friction Reducing Additives for Lubricants, 2689224, 1954.

[26] S.M. Hsu, J. Zhang, Z. Yin, The nature and origin of tribochemistry, in: Tribol. Lett., 2002. https://doi.org/10.1023/A:1020112901674.

[27] H. Okabe, M. Masuko, K. Sakurai, Dynamic behavior of surface-adsorbed molecules under boundary lubrication, ASLE Trans. (1981). https://doi.org/10.1080/05698198108983044.

[28] S. Jahanmir, M. Beltzer, Effect of Additive Molecular Structure on Friction Coefficient and Adsorption, J. Tribol. (1986). https://doi.org/10.1115/1.3261129.

[29] S.M. Campen, Fundamentals Of Organic Friction Modifier Behaviour, 2012.

[30] A. Tomala, A. Karpinska, W.S.M. Werner, A. Olver, H. Störi, Tribological properties of additives for water-based lubricants, Wear. 269 (2010) 804–810. https://doi.org/10.1016/j.wear.2010.08.008.

[31] J.W. Menter, D. Tabor, Orientation of fatty acid and soap films on metal surfaces, Proc. R.

Soc. London. Ser. A. Math. Phys. Sci. 204 (1951) 514–524.

[32] F.P. Bowden, The mechanism of boundary lubrication, World Pet. Congr. Proc. 1951-May (1951) 328–342.

[33] J.W. Hoyt, The effect of additives on fluid friction, J. Fluids Eng. Trans. ASME. 94 (1972) 258–285. https://doi.org/10.1115/1.3425401.

[34] A.G. Fabula, The Toms phenomenon in the turbulent flow of very dilute polymer solutions, in: Proc. 4th Int. Congr. Rheol., 1965: pp. 455–479. https://ntrs.nasa.gov/search.jsp?R=19670005218 (accessed December 6, 2019).

[35] J. Hoyt, W.D. White, High-Polymer Additive Effect on Turbulent Flow of Dextran, Saline Solution, and Plasma, Proc. Thé Annu. Conf. Eng. Med. Biol. 8 (1966).

[36] G.T. Pruitt, B. Rosen, H.R. Crawford, Effect of Polymer Coiling on Drag Reduction, West. Co. Rep. No. DTMB-2,. 2 (1966). https://doi.org/10.1080/00222348008241866.

[37] W. Zhang, W. Liu, L. Yu, Friction and wear behaviors of a (Ca, Mg)-sialon/SAE 52100 steel pair under the lubrication of various polyols as water-based lubricating additives, Tribol. Int. 33 (2000) 769–775. https://doi.org/10.1016/S0301-679X(00)00120-1.

[38] R. Caenn, G. V. Chillingar, Drilling fluids: State of the art, J. Pet. Sci. Eng. 14 (1996) 221–230. https://doi.org/10.1016/0920-4105(95)00051-8.

[39] W. Yong, X. Qunji, C. Lili, Tribological properties of some water-based lubricants containing polyethylene glycol under boundary lubrication conditions, J. Synth. Lubr. 13 (1997) 375–380. https://doi.org/10.1002/jsl.3000130405.

[40] D.W. Morecroft, Reply to comments on “reactions of octadecane and decoic acid with clean iron surfaces,” Wear. 18 (1971) 479–480. https://doi.org/10.1016/0043-1648(71)90173-6.

[41] H. Ma, J. Li, H. Chen, G. Zuo, Y. Yu, T. Ren, Y. Zhao, XPS and XANES characteristics of

tribofilms and thermal films generated by two P- and/or S-containing additives in water-based lubricant, Tribol. Int. 42 (2009) 940–945. https://doi.org/10.1016/j.triboint.2009.01.004.

[42] L.A. Huezo, P. V Kotvis, C. Crumer, C. Soto, W.T. Tysoe, Surface chemistry and extreme pressure lubricant additive properties of chloroform on iron, Appl. Surf. Sci. 78 (1994) 113–122. https://doi.org/10.1016/0169-4332(94)90039-6.

[43] S. Plaza, L. Margielewski, G. Celichowski, R.W. Wesolowski, R. Stanecka, Tribological performance of some polyoxyethylene dithiophosphate derivatives water solutions, Wear. 249 (2001) 1077–1089. https://doi.org/10.1016/S0043-1648(01)00847-X.

[44] F. Lin, D.H. Tao, Z.C. Wang, C.L. Li, Synthesis and hydrolytic stability of aqueous antiwear agents of organic phosphate and organic thiophosphate, J. Synth. Lubr. 14 (1997) 259–266.

[45] M.A.A. Alvi, M. Belayneh, A. Saasen, B.S. AadnØy, The effect of micro-sized boron nitride BN and iron trioxide Fe 2 O 3 nanoparticles on the properties of laboratory bentonite drilling fluid, in: SPE Norw. One Day Semin. Soc. Pet. Eng., 2018: pp. 478–491. https://doi.org/10.2118/191307-ms.

[46] J. Pu, S. Wan, W. Zhao, Y. Mo, X. Zhang, L. Wang, Q. Xue, Preparation and tribological study of functionalized graphene-IL nanocomposite ultrathin lubrication films on si substrates, J. Phys. Chem. C. 115 (2011) 13275–13284. https://doi.org/10.1021/jp111804a.

[47] S. Choudhary, H.P. Mungse, O.P. Khatri, Dispersion of alkylated graphene in organic solvents and its potential for lubrication applications, J. Mater. Chem. 22 (2012) 21032–21039. https://doi.org/10.1039/c2jm34741e.

[48] O. Elomaa, V.K. Singh, A. Iyer, T.J. Hakala, J. Koskinen, Graphene oxide in water lubrication on diamond-like carbon vs. stainless steel high-load contacts, Diam. Relat.

Mater. 52 (2015) 43–48. https://doi.org/10.1016/j.diamond.2014.12.003.

[49] H.P. Mungse, N. Kumar, O.P. Khatri, Synthesis, dispersion and lubrication potential of basal plane functionalized alkylated graphene nanosheets, RSC Adv. 5 (2015) 25565–25571. https://doi.org/10.1039/c4ra16975a.

[50] H.J. Kim, D.E. Kim, Water lubrication of stainless steel using reduced graphene oxide coating, Sci. Rep. 5 (2015) 1–13. https://doi.org/10.1038/srep17034.

[51] B. Gupta, N. Kumar, K. Panda, S. Dash, A.K. Tyagi, Energy efficient reduced graphene oxide additives: Mechanism of effective lubrication and antiwear properties, Sci. Rep. 6 (2016) 1–10. https://doi.org/10.1038/srep18372.

[52] W.H. King, W.A. Owczarski, Diffusion welding of commercially pure titanium, Weld J. 46 (1967) 289.

[53] K. Bendorf, Experimental Investigations of self-welding of structural materials under Sodium, Nucl. Eng. Des. (1970) 83–98.

[54] W. Freede, … L.N., Static and sliding contact behavior of materials in sodium environments at elevated temperatures, Liq. Met. Eng. Cent. (1967). https://scholar.google.com/scholar?hl=en&as_sdt=0%2C44&q=Static+and+sliding+contact+behavior+of+materials+in+sodium+environments+at+elevated+temperatures&btnG= (accessed July 23, 2019).

[55] F. Huber, K. Mattes, Investigations into the self-welding behavior of metallic materials exposed to sodium.pdf, (1976).

[56] N. Yokota, S. Shimoyashiki, Characteristics of self-welding of structural materials in liquid sodium, Liq. Met. Eng. Technol. 21 (1984) 99–103.

[57] S. Chander, C. Meikandamurthy, R.D. Kale, R. Krishnamurthy, Experimental study of self-

welding of materials in high temperature liquid sodium, Wear. 162–164 (1993) 458–465. https://doi.org/10.1016/0043-1648(93)90530-Y.

[58] R.N. Wright, Summary of Studies of Aging and Environmental Effects on Inconel 617 and Haynes 230, (2006) 27. https://doi.org/10.2172/911722.

[59] X. Li, D. Kininmont, R. Le Pierces, S.J. Dewson, Alloy 617 for the high temperature diffusion-bonded compact heat exchangers, Int. Conf. Adv. Nucl. Power Plants, ICAPP 2008. 1 (2008) 282–288.

[60] ASTM, Standard Test Method for Determination of the Coefficient of Friction of Lubricants Using the Four-Ball Wear Test Machine 1, Annu. B. ASTM Stand. 95 (2007) 1–5. https://doi.org/10.1520/D5183-05R11.2.

[61] P. Lan, A.A. Polycarpou, High temperature and high pressure tribological experiments of advanced polymeric coatings in the presence of drilling mud for oil & gas applications, Tribol. Int. 120 (2018) 218–225. https://doi.org/10.1016/j.triboint.2017.12.035.

[62] Across International, 1400 C Controlled Atmosphere Muffle Furnace UL/CSA/CE Certified, (n.d.). https://www.acrossinternational.com/1400C-Controlled-Atmosphere-Muffle-Furnace-UL-CSA-CE-Certified-GCF1400.htm.

[63] Arkema: Vikinol®, (n.d.).

[64] P. International, Friction Particle-6010®, (n.d.) 19474.

[65] Newpark Resources Inc., EvoLube® G, (n.d.).

[66] Integrity Industries, Ultra Lube® II, (n.d.).

[67] G. Gough, G. R., Offshore underbalanced drilling - The challenge at surface, in: SPE/IADC Drill. Conf. Proc., 2008: pp. 1285–1295.

[68] J.E. McCormick, C.D. Evans, J. Le, T.F. Chiu, The practice and evolution of torque and

drag reduction: Theory and field results, in: Int. Pet. Technol. Conf. 2011, IPTC 2011, European Association of Geoscientists & Engineers, 2011: p. cp-280-00196. https://doi.org/10.3997/2214-4609-PDB.280.IPTC14863_NOPW.

[69] J. Hosterman, S. Patterson, Bentonite and fuller's earth resources of the United States, U. S. Geol. Surv. Prof. Pap. 1522. 1522 (1992) 45.

[70] Schlumberger, Schlumberger Oilfield Glossary: Where the Oilfield Meets the Glossary, (n.d.).

[71] D.H. Larsen, Use of Clay in Drilling Fluids, Clays Clay Miner. 1 (1952) 269–281. https://doi.org/10.1346/CCMN.1952.0010124.

[72] Newpark Resources Inc., KCL Polymer Water-Based Drilling Fluid System, n.d.

[73] C. LibreText, Structure of Amides, (n.d.).

[74] M. Range, Special Metals: Inconel alloy 617, Spec. Met. (2016) 1–12. http://www.specialmetals.com/.

[75] SpecialMetals, Special Metals: Inconel alloy 800H & 800 HT, Www.Specialmetals.Com. (2004) 1–16. http://www.specialmetals.com/assets/smc/documents/alloys/incoloy/incoloy-alloys-800h-800ht.pdf.

[76] A. Shadravan, M. Amani, HPHT 101—What Petroleum Engineers and Geoscientists Should Know About High Pressure High Temperature Wells Environment, Energy Sci. Technol. 4 (2012) 36–60.

[77] M.I. Abduo, A.S. Dahab, H. Abuseda, A.M. AbdulAziz, M.S. Elhossieny, Comparative study of using Water-Based mud containing Multiwall Carbon Nanotubes versus Oil-Based mud in HPHT fields, Egypt. J. Pet. 25 (2016) 459–464. https://doi.org/10.1016/j.ejpe.2015.10.008.

[78] A. Patel, E. Stamatakis, S. Yong, J. Friedheim, M.-I. Swaco, Advances in Inhibitive Water-Based Drilling Fluids—Can They Replace Oil-Based Muds?, in: Int. Symp. Oilf. Chem. Soc. Pet. Eng., 2007.

[79] J. De Almeida Rodrigues, E.R. Lachter, C.H. De Sá, M. De Mello, R.S.V. Nascimento, New multifunctional polymeric additives for water-based muds, in: Proc. - SPE Annu. Tech. Conf. Exhib., 2006: pp. 5069–5074. https://doi.org/10.2523/106527-stu.

[80] P. Lan, L.L. Iaccino, X. Bao, A.A. Polycarpou, The effect of lubricant additives on the tribological performance of oil and gas drilling applications up to 200 °C, Tribol. Int. 141 (2020). https://doi.org/10.1016/j.triboint.2019.105896.

[81] L. Tokarzewski, J. Zakrzewski, J. Wachowicz, S. Szczepaniak, Phosphoryl tris(diethanolamide) (DAP) - A new additive for water-based and ethylene-glycol-based hydraulic fluids and lubricants, Wear. 50 (1978) 365–369. https://doi.org/10.1016/0043-1648(78)90081-9.

[82] J.K. Lancaster, A review of the influence of environmental humidity and water on friction, lubrication and wear, Tribol. Int. 23 (1990) 371–389. https://doi.org/10.1016/0301-679X(90)90053-R.

[83] F. Gao, G. Wu, D. Stacchiola, M. Kaltchev, P. V Kotvis, W.T. Tysoe, The tribological properties of monolayer KC1 films on iron in ultrahigh vacuum: Modeling the extreme-pressure lubricating interface, Tribol. Lett. 14 (2003) 99–104. https://doi.org/10.1023/A:1021752203606.

[84] F. Gao, P. V Kotvis, W.T. Tysoe, The friction, mobility and transfer of tribological films: Potassium chloride and ferrous chloride on iron, Wear. 256 (2004) 1005–1017. https://doi.org/10.1016/j.wear.2003.06.002.

[85] L. Huezo, C. Crumer, C. Soto, W.T. Tysoe, Growth Kinetics and Structure of Films Formed by the Thermal Decomposition of Methylene Chloride on Iron, Langmuir. 10 (1994) 3571–3576. https://doi.org/10.1021/la00022a033.

[86] P. V. Kotvis, J. Lara, K.K. Surerus, W.T. Tysoe, The nature of the lubricating films formed by carbon tetrachloride under conditions of extreme pressure, Wear. 201 (1996) 10–14. https://doi.org/10.1016/S0043-1648(95)06844-9.

[87] T.J. Blunt, P. V Kotvis, W.T. Tysoe, Surface chemistry of chlorinated hydrocarbon lubricant additives–-part ii: Modeling the tribological interface, Tribol. Trans. 41 (1998) 129–139. https://doi.org/10.1080/10402009808983731.

[88] V. An, Y. Irtegov, C. De Izarra, Study of tribological properties of nanolamellar WS2 and MoS2 as additives to lubricants, J. Nanomater. (2014). https://doi.org/10.1155/2014/865839.

[89] X. He, H. Xiao, H. Choi, A. Díaz, B. Mosby, A. Clearfield, H. Liang, α-Zirconium phosphate nanoplatelets as lubricant additives, Colloids Surfaces A Physicochem. Eng. Asp. 452 (2014) 32–38. https://doi.org/10.1016/j.colsurfa.2014.03.041.

[90] C. Zhang, S. Zhang, S. Song, G. Yang, L. Yu, Z. Wu, X. Li, P. Zhang, Preparation and tribological properties of surface-capped copper nanoparticle as a water-based lubricant additive, Tribol. Lett. 54 (2014) 25–33. https://doi.org/10.1007/s11249-014-0304-5.

[91] Shell Chemicals, Cargo Handling Sheet of ExxonMobil Escaid 110 Fluid, 2018.

[92] H. Zhong, Z. Qiu, Z. Tang, X. Zhang, D. Zhang, W. Huang, Minimization shale hydration with the combination of hydroxyl-terminated PAMAM dendrimers and KCl, J. Mater. Sci. 51 (2016) 8484–8501. https://doi.org/10.1007/s10853-016-0108-0.

[93] B. Joel, O. α, U. σ, N.C. ρ, Effect of KCL on Rheological Properties of Shale Contaminated

Water-Based MUD(WBM) Effect of KCL on Rheological Properties of Shale Contaminated Water-Based MUDWBM Effect of KCL on Rheological Properties of Shale Contaminated Water-Based MUD(WBM), Type Double Blind Peer Rev. Int. Res. J. Publ. Glob. Journals Inc. 12 (2012).

[94] S. Livescu, S. Craig, T. Watkins, Challenging the industry's understanding of the mechanical friction reduction for coiled tubing operations, in: Proc. - SPE Annu. Tech. Conf. Exhib., 2014: pp. 736–754. https://doi.org/10.2118/170635-ms.

[95] T. Yamashita, P. Hayes, Analysis of XPS spectra of Fe 2+ and Fe 3+ ions in oxide materials, Appl. Surf. Sci. 254 (2008) 2441–2449. https://doi.org/10.1016/j.apsusc.2007.09.063.

[96] A. Petran, T. Radu, B. Culic, R. Turcu, Tailoring the properties of magnetite nanoparticles clusters by coating with double inorganic layers, Appl. Surf. Sci. 390 (2016) 1–6. https://doi.org/10.1016/j.apsusc.2016.08.037.

[97] D. Tabor, Surface effects in adhesion, friction, wear and lubrication, Tribol. Int. 14 (1981) 368. https://doi.org/10.1016/0301-679x(81)90112-2.

[98] R.P. Morco, J.C. Wren, Effect of Gamma Radiation on the Interfacial Reactions and Transfer Processes of Phosphonium- based Ionic Liquids with Carbon Steel, 2014. https://ir.lib.uwo.ca/etd (accessed February 21, 2020).

[99] J. Landoulsi, M.J. Genet, S. Fleith, Y. Touré, I. Liascukiene, C. Méthivier, P.G. Rouxhet, Organic adlayer on inorganic materials: XPS analysis selectivity to cope with adventitious contamination, Appl. Surf. Sci. 383 (2016) 71–83. https://doi.org/10.1016/j.apsusc.2016.04.147.

[100] I. Frateur, A. Carnot, S. Zanna, P. Marcus, Role of pH and calcium ions in the adsorption of an alkyl N-aminodimethylphosphonate on steel: An XPS study, Appl. Surf. Sci. 252

(2006) 2757–2769. https://doi.org/10.1016/j.apsusc.2005.04.012.

[101] L. Wang, C. Guo, Y. Zhu, J. Zhou, L. Fan, Y. Qian, A FeCl2-graphite sandwich composite with Cl doping in graphite layers: a new anode material for high-performance Li-ion batteries, Nanoscale. 6 (2014) 14174–14179. https://doi.org/10.1039/c0xx00000x.

[102] D. Wei, Future directions of fundamental research in additive tribochemistry, Lubr. Sci. 7 (1995) 211–232. https://doi.org/10.1002/ls.3010070303.

[103] S. GW, ed., Wear: materials, mechanisms and practice, John Wiley & Sons, Ltd, 2006.

[104] Wikipedia, Graphene, Graphene. (2020). https://en.wikipedia.org/wiki/Graphene.

[105] F. Bonaccorso, L. Colombo, G. Yu, M. Stoller, V. Tozzini, A.C. Ferrari, R.S. Ruoff, V. Pellegrini, Graphene, related two-dimensional crystals, and hybrid systems for energy conversion and storage, Science (80-. ). 347 (2015). https://doi.org/10.1126/science.1246501.

## APPENDIX

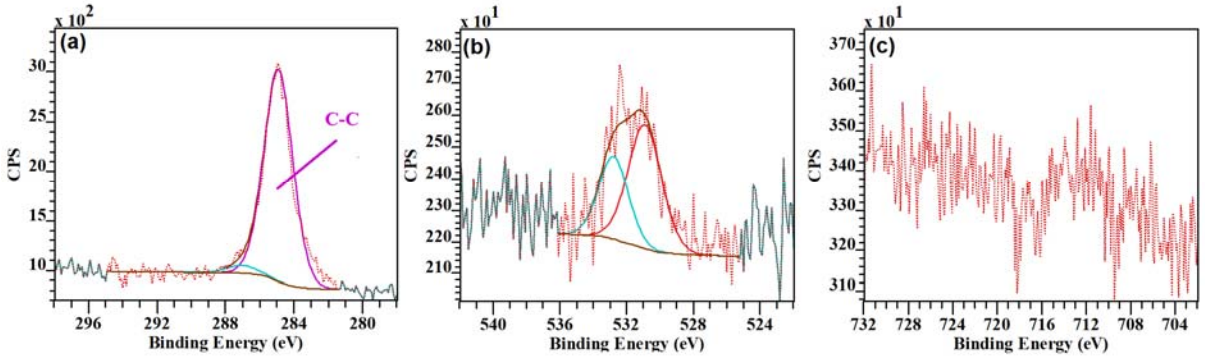


Figure 71. High resolution (a) C 1s, (b) O1s and (c) Fe 2 spectra of non-treated balls tested.

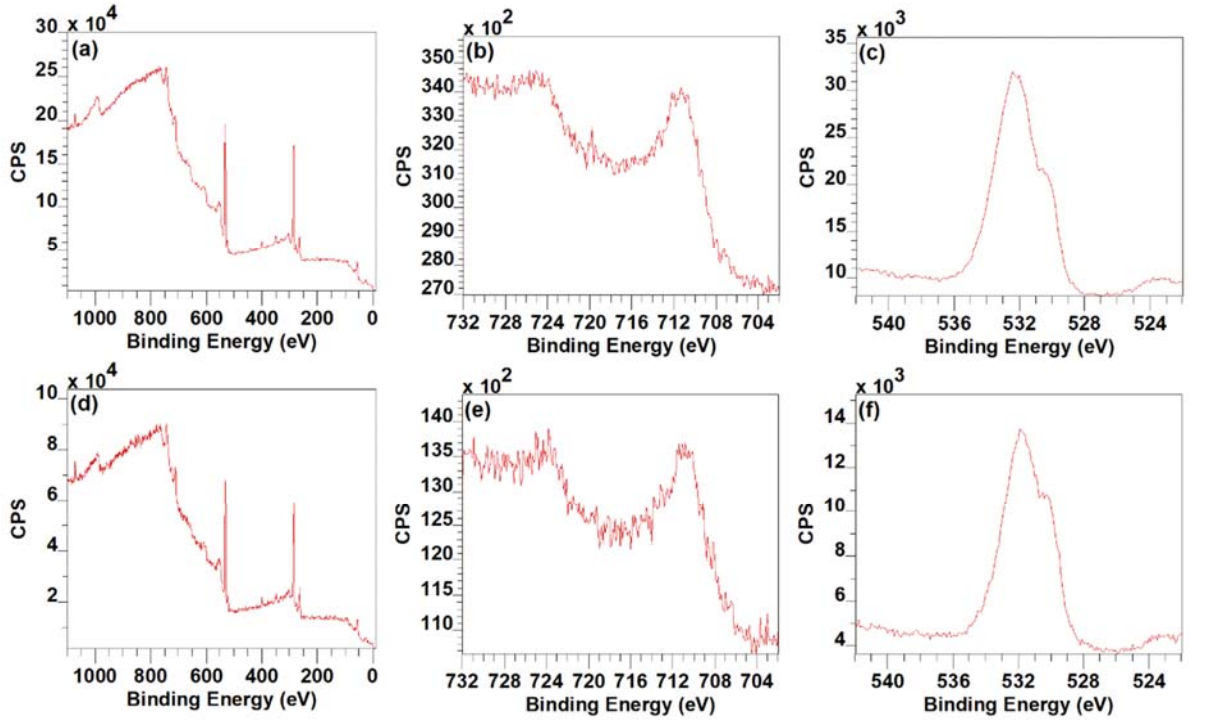


Figure 72. The XPS survey spectra of the inside wear track for balls tested in the presence of (a) pure OBM and (d) OBM/ Vikinol® 18. High resolution Fe 2p spectra of balls tested in the presence of (b) pure OBM and (e) OBM/ Vikinol® 18. High resolution O 1s spectra of balls tested in the presence of (c) pure OBM and (f) OBM/ Vikinol® 18.

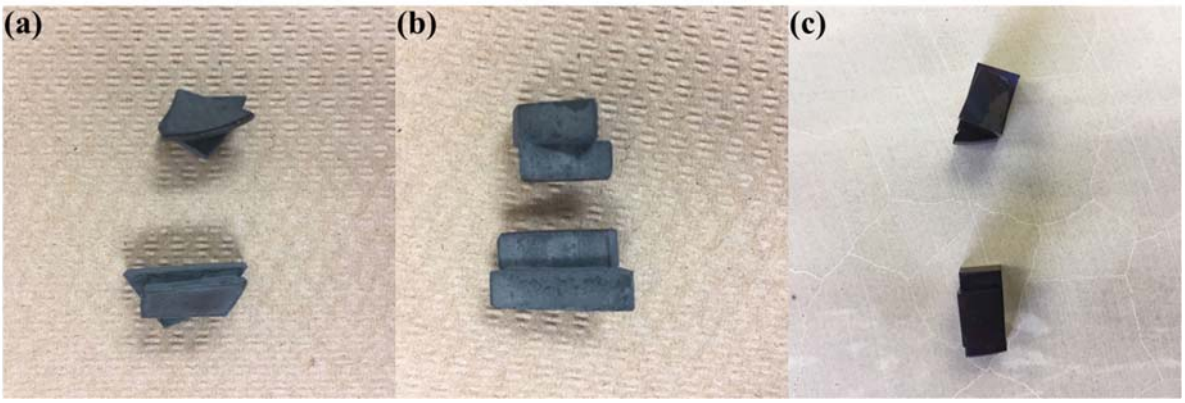

Figure 73. Photographs of O1 ss sample pairs after preliminary concept proof self-welding experiments in air atmosphere under a nominal pressure of 0.166 MPa for drilling applications: (a)-(b) samples experienced self-welding after 1-hour aging at 950 °C; (c) sample pairs did not experience self-welding after 1-hour aging at 300 °C.